EXAMINING THE REGULATION OF CONNEXIN EXPRESSION OVER THE COURSE OF THE ESTROUS CYCLE IN HIPPOCAMPUS AND SPINAL CORD

Ashleigh McLean

A thesis submitted to the Faculty of Graduate and Postdoctoral studies in partial fulfillment of the requirements for the degree of Masters of Science.

Department of Cellular and Molecular Medicine
University of Ottawa
Ottawa, ON, Canada

ABSTRACT

In this thesis, I explore the regulation of a highly homologous family of proteins, termed connexins. Connexins oligomerize to form gap junctions within the plasma membrane of cells allowing for communication between cells as well as functioning as hemichannels, which permit communication between the intracellular and extracellular environment of a cell. These gap junctions allow for the passage of ions, metabolites and second messengers, which have been shown to modulate proliferation, regeneration, and cell survival. Furthermore, following insult to the central nervous system, injured cells can propagate waves of toxic second messengers to adjacent coupled healthy cells thereby expanding secondary injury via gap junctions. Here, I asked whether expression of the functional subunits of these channels (connexins) was under hormonal control in the central nervous system. I conducted quantitative analysis of steady-state mRNA expression levels of seven crucial connexins in known neurogenic and gliogenic niches of the central nervous system during the mouse estrous cycle. To accomplish my overarching objective of identifying connexins of the hippocampus and spinal cord which may be under hormonal regulation, I identified technical limitations of quantifying expression of such a highly homologous gene family with commercially available reagents and I optimized an established protocol to minimize the invasiveness during the collection of estrous smears required to identify hormone status. Collectively, these steps permitted the quantification of connexin expression during various stages of the mouse estrous cycle and identified two connexins whose expression is under hormonal regulation in a tissue specific manner.

ACKNOWLEDGEMENTS

I would like to acknowledge my supervisor Dr. Steffany Bennett for providing me with the opportunity to perform my thesis research in her laboratory. I would also like to express my appreciation for her support and guidance. I would like to extend my gratitude to Dr. K. Willecke, Dr. D. Paul, Dr. D. Picketts, and Dr. R. Slack for generously providing breeding pairs of the mice used in this study. I would like to thank the members of my thesis advisory committee, Dr. Rashmi Kothary, Dr. Eve Tsai, Dr. Paul Albert, and Dr. Johnny Ngsee, for their support, constructive feedback and comments. I would like to acknowledge the members of the Neural Regeneration Laboratory at the University of Ottawa and Carleton Immersive Media Studio at Carleton University for their technical assistance, their encouragements and for the companionship with special thanks to Stephanie Fowler and Nico Valenzuela for their collaborative efforts and generous help. This research was funding by grants from Canadian Institutes of Health Research, Multiple Sclerosis Society of Canada, Ontario Graduate Scholarships in Science and Technology, and Scottish Rite Charitable Foundation of Canada to Ashleigh C. McLean and Canadian Institutes of Health Research to Dr. Steffany A.L. Bennett.

TABLE OF CONTENTS

LIST OF ABBREVIATIONS

3’ UTR	3’ untranslated region
5’ UTR	5’ untranslated region
AF-1	activation function 1
AF-2	activation function 2
AP-1	activator protein 1
ATP	adenosine triphosphate
BARN	blotting and removal of nitrocellulose
BME	β-mercaptoethanol
bp	base pair
CNS	central nervous system
CT	cycle threshold
CX	cerebral cortex
Cx	connexin
DCX	doublecortin
ddH_2O	double-distilled H_2O
DEPC	diethylpyrocarbonate
EAE	experimental autoimmune encephalomyelitis
Egr2/Knox20	early growth response gene 2
ERα	estrogen receptor alpha
ERβ	estrogen receptor beta
ERE	estrogen responsive element
FITC	fluorescein isothiocyanate
GAPDH	glyceraldehyde 3-phosphate dehydrogenase
GFAP	glial fibrillary acidic protein
GnRH	gonadotropin releasing hormone
GrDG	granular layer of the dentate gyrus
HNF-1	hepatocyte nuclear factor 1
Hprt	hypoxanthine-guanine phosphoribosyltransferase

HRE	hormone responsive element
HRP	horseradish peroxidase
IgG	immunoglobulin G
kb	kilobase
kDa	kiloDalton
KO	knockout
miRNAs	microRNAs
Nes-cre	nestin-cre recombinase
NFH_2O	nuclease-free H_2O
NG2	neuron-glial antigen 2
NPC	neural progenitor cell
NSC	neural stem cell
NTC	no template control
OL	oligodendrocyte
OPC	oligodendrocyte progenitor cell
OVX	ovariectomy
PCR	polymerase chain reaction
PBS	phosphate-buffered saline
PBST	phosphate-buffered saline with 0.1% Tween-20
PLP	proteolipid protein
PMD	Pelizaeus-Merzbacher disease
PMLD1	Pelizaeus-Merzbacher-like disease 1
POA	preoptic area
Ppib	peptidylprolyl isomerase B
PR	progestin receptor
PRE	progesterone responsive element
qRT-PCR	real-time quantitative reverse transcription polymerase chain reaction
Rn18s	18S ribosomal RNA
RT-PCR	reverse transcription polymerase chain reaction
SCI	spinal cord injury

SCN	suprachiasmatic nucleus
SDS	sodium dodecyl sulfate
SDS-PAGE	sodium dodecyl sulfate– polyacrylamide gel electrophoresis
Sp1	specificity protein 1
TSA	Trichostatin A
Tuj1	beta-tubulin 3
WT	wildtype

LIST OF FIGURES

LIST OF TABLES

CHAPTER 1: INTRODUCTION

1.1 The connexin family of gap junction proteins

Connexins (Cxs) are a highly conserved family of proteins that make up the structural units of gap junction channels at the plasma membrane of most cell types, allowing for the selective passage of molecules up to ~1-kiloDalton (kDa) in size (1). Six connexin proteins oligomerize to form a single trans-membrane pore or channel, termed a connexon (Figure 1.1A). These six connexins may be composed of identical family members or combinations thereof (Figure 1.1A). Connexons in non-junctional membranes form single membrane channels, often referred to as hemichannels, that allow for the spatial buffering of ions between cells and the extracellular environment (2). Gap junctions are composed of connexons elaborated by adjacent cells that align to form intercellular channels, allowing for passage of metabolites and secondary messengers between cells. When both connexons are composed of the same connexin the intercellular channel is considered a homotypic channel (Figure 1.1B_1). A channel composed of two homotypic connexons wherein each hemichannel is comprised of a different connexin is considered a heterotypic channel (Figure 1.1B_2). A channel comprised of at least one heterotypic connexon docking with either a homotypic or heterotypic connexon is considered a heteromeric channel (Figure 1.1B_3). Specificity of molecular passage through both connexons and gap junction intercellular channels is dictated by these differences in connexin combinations and composition.

Figure 1.1 Connexin proteins form gap junction channels allowing for cell-cell communication and pore formation in non-junctional membranes. Connexin proteins are the structural units of (A) connexons (hemichannels in non-junctional membranes) connecting cell cytoplasm with extracellular space and (B) intercellular channels that allow two adjacent cells to exchange molecules < 1-kDa. Collections of intercellular channels form the morphologically defined gap junction. (C) Connexins can also elicit channel-independent effects by interacting with protein partners at their C-terminal tail and thereby altering intracellular signaling as well as through promoting channel-independent adhesion between adjacent cells without exchange of small molecules. (D-H) Types of cell-cell connexin interactions formed between astrocytes and oligodendrocytes. Astrocytes form two classes of gap junctions with each other containing (D) only Cx26 or (E) a mixture of Cx30 and Cx43 homotypic channels. (F) It is not yet known whether Cx30 and Cx43 form heterotypic and heteromeric channels but these conformations are possible. Astrocytes and oligodendrocytes communicate through (G) heterotypic and possibly (H) heteromeric channels. Oligodendrocytes express Cx29, Cx32, and Cx47. Astrocytic Cx26 preferentially associates with oligodendrocytic Cx32. Astrocytic Cx30 and Cx43 preferentially associate with Cx47. Cx29 is believed to form hemichannels or interact with cytosolic proteins at its C-terminal tail to initiate signaling. (Adapted from Altevogt & Paul, 2004)

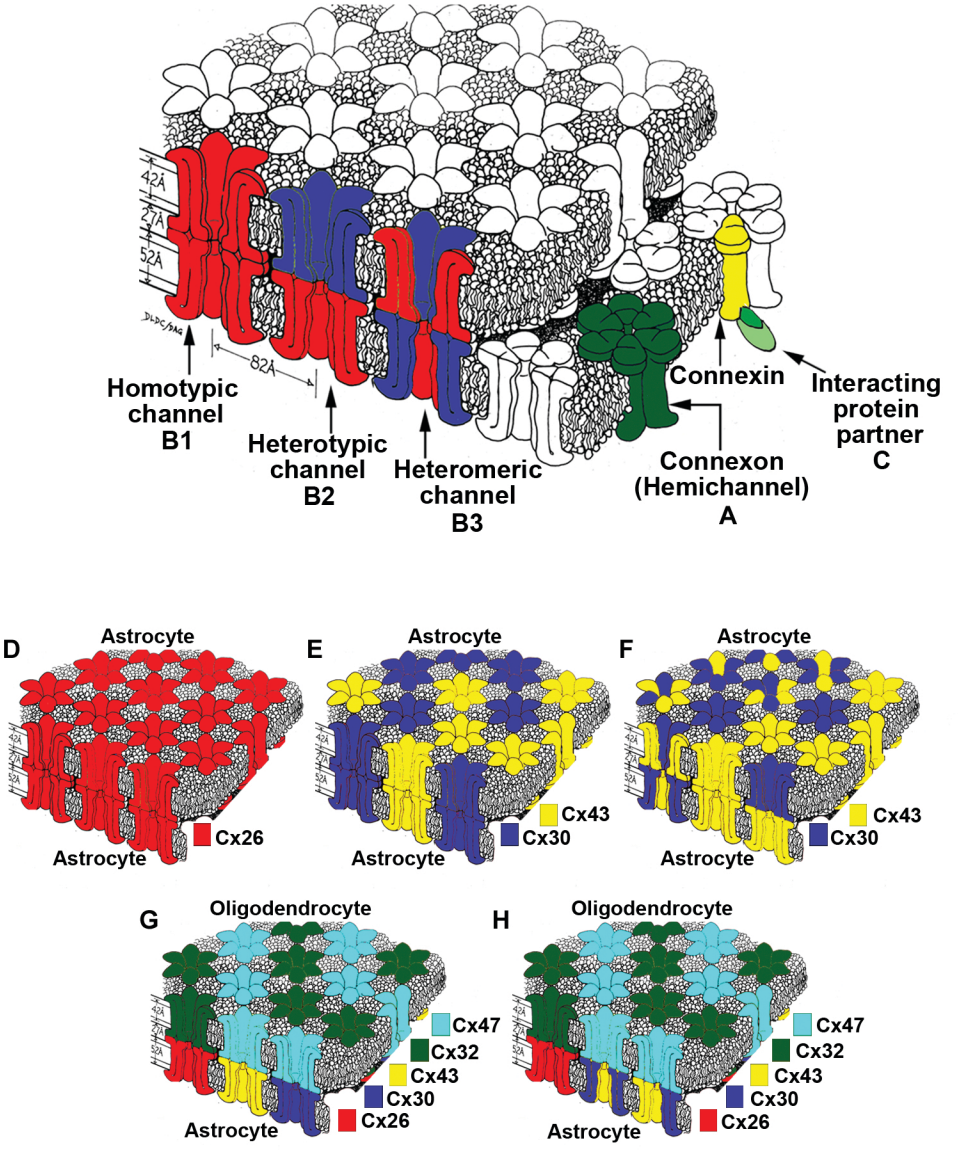
42Å
27Å
52Å
82Å
Homotypic channel B1
Heterotypic channel B2
Heteromeric channel B3
Connexin
Connexon (Hemichannel) A
Interacting protein partner C
D
Astrocyte
Cx26
Astrocyte
E
Astrocyte
Cx43
Cx30
Astrocyte
F
Astrocyte
Cx43
Cx30
Astrocyte
G
Oligodendrocyte
Cx47
Cx32
Cx43
Cx30
Cx26
Astrocyte
H
Oligodendrocyte
Cx47
Cx32
Cx43
Cx30
Cx26
Astrocyte

Figure 1.1

There are 20 different connexin proteins in mouse, 21 in humans (3). Fourteen (Cx26, Cx29, Cx30, Cx30.2, Cx31.1, Cx31.9, Cx32, Cx36, Cx37, Cx40, Cx43, Cx45, Cx47, Cx57) are detected in embryonic and/or adult central nervous system (CNS) (4-7). Specific connexins localize to specific cell types. Within the mature cell types of the murine CNS, Cx29, Cx32 and Cx47 are expressed by oligodendrocytes (OLs). Cx26, Cx30 and Cx43 are astrocytic connexins, whereas Cx30.2, Cx31.1, Cx36 and Cx45 localize to neurons (4-7). Cx37 and Cx40 are detected in endothelial cells of cerebral blood vessels and some leptomengial cells (8). Cx57 is restricted to retinal neurons (9).

During development or over the course of adult neurogenesis and gliogenesis, markers of cell lineage (10) and connexin expression are dynamically regulated in neural and glial stem cells (11) (Figure 1.2). Type 1 putative neural stem cells (NSC), which have the ability for self-renewal or further specification, express nestin and glial fibrillary acidic protein (GFAP), as well as Cx26, Cx30 and Cx43 (11). Upon loss of nestin expression, Type 1 putative NSCs can differentiate into a mature astrocyte, expressing GFAP and connexins 26 (12), 30 (13) and 43 (14). Upon specification of a Type 1 NSC to a Type 2a putative neural progenitor cell (NPC), loss of GFAP and Cx26/Cx43 expression occurs (11). These cells can self renew or differentiate into a) an $Cx32^{+}$ oligodendrocyte progenitor cell (OPC) or b) take on a more neuronal progenitor lineage as a Type 2b progenitor cell. OPCs will be committed to an OL cell fate, and upon differentiation to mature cells types, as previously mentioned, post-mitotic mature OLs express Cx29 (15), Cx32 (16), and Cx47 (17). Should the type 2a NPC take on a more neuronal progenitor lineage as a Type 2b progenitor cell, expression of nestin and doublecortin (DCX) is present (11). This cell is now committed to a neuronal lineage and can self renew or differentiate into a DCX^{+} type 3 neuroblast. When

Figure 1.2 Connexin expression during neurogenesis and gliogenesis in the adult hippocampus. Connexin expression in each cell type is denoted in red. In the hippocampus, new neurons are generated in step-wise fashion from nestin+ Type 2a NPCs. These cells are derived from nestin+/GFAP+ Type 1 cells. Type 1 cells are multipotential with capacity to generate neurons and glia. A subset of Type 1 cells may transiently express neuron-glial antigen 2 (NG2) and commit to an OL lineage. The majority of adult OLs are derived from NG2+ cells that are "born" embryonically in the SVZ, migrate to terminal locations throughout the brain, and activate to generate new OLs when needed (Ivanova et. al., 2003). Our lab has shown that Type 1 cells cultured in vitro from P0-2 neonates in the SGZ express Cx26, Cx30, and Cx43 (Imbeault et. al., 2009) Type 2a cells express Cx30 in vitro and in vivo (Imbeault et. al., 2009). Cx36 is transiently expressed when Type 3 NPCs step out of the cell cycle to become post-mitotic immature neurons (Imbeault et. al., 2009). Cx32 is expressed when a subset of NG2+ progenitor cells commit to and OL lineage (Melanson-Drapeau et. al., 2003). Cx36 is expressed by mature interneurons (Belluardo et. al., 2000). During oligodendrogenesis, PDGFαR+ early OLs express Cx29 (Imbeault et. al., 2009), while Cx29 and Cx47 by mature OLs (Altevogt et. al., 2002, Odermatt et. al. 2003).

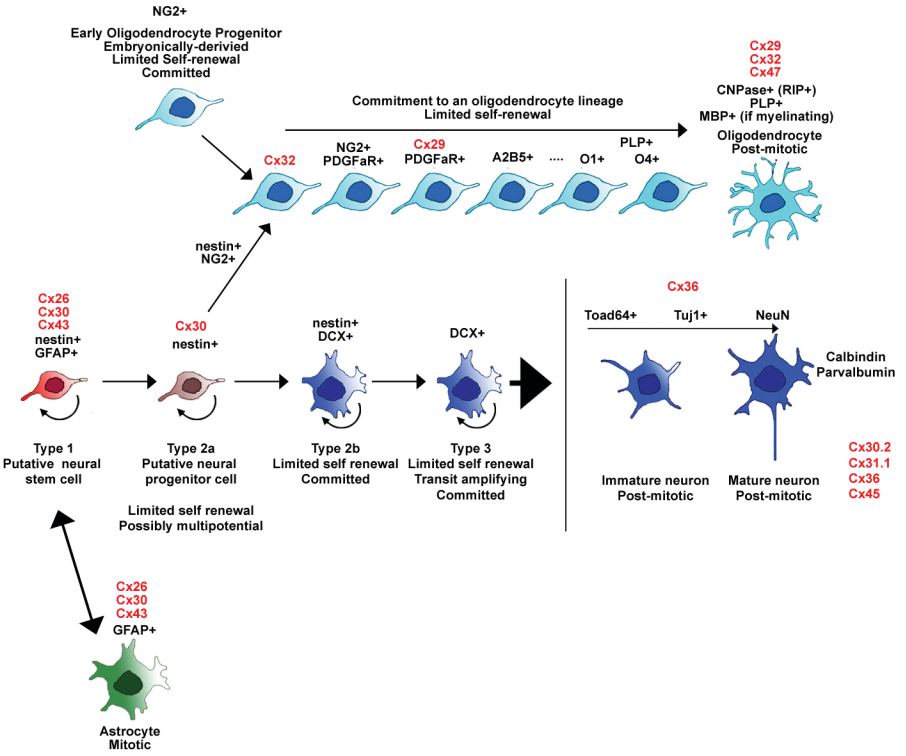
NG2+
Early Oligodendrocyte Progenitor
Embryonically-derived
Limited Self-renewal
Committed
Commitment to an oligodendrocyte lineage
Limited self-renewal
Cx29
Cx32
Cx47
CNPase+ (RIP+)
PLP+
MBP+ (if myelinating)
Oligodendrocyte
Post-mitotic
Cx32
NG2+
PDGFaR+
Cx29
PDGFaR+
A2B5+
....
O1+
PLP+
O4+
nestin+
NG2+
Cx26
Cx30
Cx43
nestin+
GFAP+
Cx30
nestin+
nestin+
DCX+
DCX+
Cx36
Toad64+
Tuj1+
NeuN
Calbindin
Parvalbumin
Type 1
Putative neural
stem cell
Type 2a
Putative neural
progenitor cell
Type 2b
Limited self renewal
Committed
Type 3
Limited self renewal
Transit amplifying
Committed
Immature neuron
Post-mitotic
Mature neuron
Post-mitotic
Cx30.2
Cx31.1
Cx36
Cx45
Limited self renewal
Possibly multipotential
Cx26
Cx30
Cx43
GFAP+
Astrocyte
Mitotic

Figure 1.2

Cx36 is expressed, type 3 neuroblasts have differentiated into post-mitotic immature neurons expressing Toad64, and later beta-tubulin 3 (Tuj1) (11). Mature GABAergic interneurons of the hippocampus lose expression of Tuj1 and retain expression Cx36 (18).

1.2 Connexin compatibility dictates capacity for cell-cell channel-dependent and channel-independent communication

Only select connexin combinations are capable of oligomerization, cell-cell docking, and functional gap junctional communication. Channels comprised of Cx30/Cx43 (heterotypic and heteromeric) or Cx26 (homotypic) permit astrocyte-to-astrocyte communication (19) (Figure 1.1D-F). It should be noted, however, that Cx26-containing connexons likely do not align with connexons composed of Cx30 and Cx43 (19). The specificity of connexin "partnering" dictates which cells can communicate through gap junctions (Figure 1.3A). For example, intracellular heterotypic channels composed of Cx26, homomeric connexons docking with Cx32 homomeric connexons, or heterotypic channels composed of Cx30/Cx43, and heteromeric connexons docking with Cx47 homomeric connexons allow for gap junctional communication between astrocytes and OLs (19) (Figure 1.1G, H).

Connexin-mediated communication is not restricted to gap junctional intercellular communication. Functional hemichannel activity in non-junctional membranes also enables adjacent cells to coordinate their responses (Figure 1.3B). Cx26 hemichannels on horizontal cells have been shown to modulate Ca^{2+} channels of retinal cone cells and subsequent

Figure 1.3 Mechanisms of gap junctional communication. Small ions and metabolites acting as signaling molecules can pass (A) between adjacent cells or (B) through hemichannels. Alternatively, (C) protein-protein interactions can occur whereby a signaling molecule will act as a binding partner causing downstream signaling effects. Images created by Crystal Hanley, Carleton Immersive Media Studio, Carleton University as part of our CIHR Training Program in Neurodegenerative Lipidomics.

A

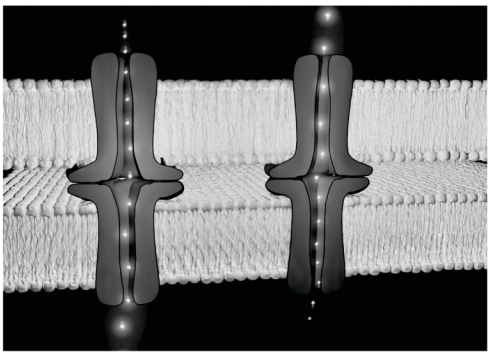

B

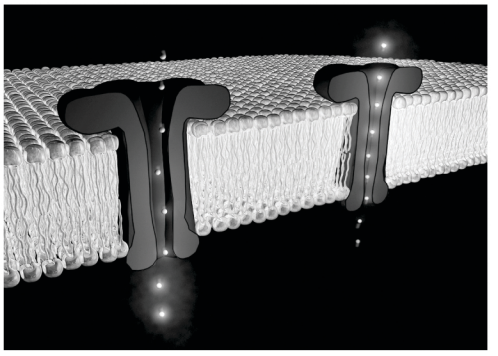

C

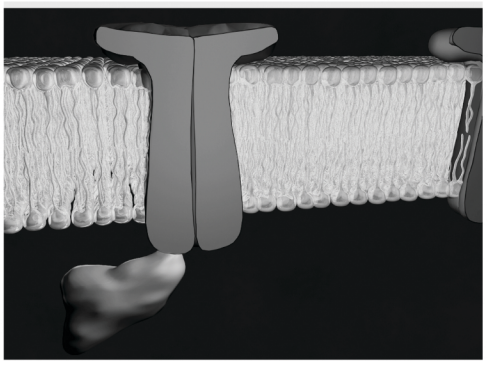

Figure 1.3

glutamate release (20). The passage of adenosine triphosphate (ATP) through hemichannels in radial glia of the neocortex has been shown to stimulate waves of intracellular Ca^{2+} release that shape neural development (21). As well, astrocytic Ca^{2+} waves triggered by photoconductive stimulation in hippocampal cultures was shown to regulate growth cone guidance (22). Together, these data highlight an important role for hemichannel formation in the control of CNS development and cell survival. It is interesting that Cx29, exclusively expressed by cells in the OL lineage, likely forms hemichannels and not gap junction channels since it rarely colocalizes with any other known connexin of the CNS, and is not expressed at junctional membranes (19). While the impact of these hemichannels on OL function and survival have yet to be assessed, colleagues in my lab have shown that Cx29 expression restricts NPC-derived neuron-glial antigen 2^+ ($NG2^+$) cells to an OL lineage *in vitro*. In Cx29 null-mutant mice, $NG2^+$ cells present in neurosphere culture adopt an astrocytic fate when exposed to gliogenic stimuli, while in the presence of Cx29 they specify to OLs (11). It remains to be elucidated how fate determination is signaled by Cx29.

Channel-independent signaling may also be mediated by interaction with a cytosolic binding partner at the C-terminus to initiate intracellular signaling (Figure 1.1C, 1.3C). Moreover, the adhesive properties of adjacent connexons have been implicated in the control on NPC migration. Previous studies have shown Cx26 and Cx43 form adhesive contacts between cells with the cytoplasmic C-terminal tails of these docked connexins interacting with the cytoskeleton to provide stabilization for embryonic neurons migrating along radial glia towards the cortical plate during development (23). These data demonstrate key regulatory activities of connexins mediated independently of functional channel formation.

1.3 The critical role of connexins in proper myelination over the course of development

Cx29, Cx32 and Cx47 are expressed in mature OLs. Cx32 and Cx47 form functional gap junctions with Cx30 and Cx43 in astrocytes (19) creating a panglial network, with communication being essential for proper myelination (24) and buffering of ions following neuronal activity (25). Distinct channel pairing exists, formed by Cx32-Cx30 and Cx47-Cx43 between OL-astrocytes (26). It was previously assumed that OLs are not coupled, however, recent studies suggest this may not be the case given evidence of gap junctional communication between OLs in the corpus callosum (27). It still remains unclear whether OL coupling in the corpus callosum is mediated by Cx32 or Cx47 homomeric gap junction channels (27, 28). Lastly, reflexive junctions between layers of the myelin sheath are formed exclusively by Cx32 (29, 30).

Cx47 is a myelin related gene, as determined by Cx47 RNA expression in white matter tracts in corpus callosum and spinal cord, which follow a similar temporal pattern during development as proteolipid protein (PLP) expression in the cerebrum and cerebellum (24). Furthermore, Cx32 and Cx47 RNA levels were significantly reduced in the brain of a myelin deficient rat model, which contains a PLP point mutation (24). PLP mutations in humans cause Pelizaeus-Merzbacher disease (PMD) (31), characterized by impaired motor development, progressive spasticity and ataxia. Interestingly, Cx47 autosomal recessive missense mutation causes Pelizaeus-Merzbacher-like disease 1 (PMLD1) in humans. The symptoms of PMLD1 are analogous to PMD, and cause reductions in glial network communication, decreased myelin basic protein expression, astrogliosis, hypomyelination, impaired motor behavior, and early death in rodent disease models (32).

A severe neuropathic demyelinating disease, X-linked Charcot-Marie-Tooth disease has been mapped to mutations in the human Cx32 gene (33), whereas Cx32 null mutant mice have normal CNS myelin sheath and similar nerve conductance as wildtype (WT) mouse (34). Discrepancies between human and mouse disease may lie in the expression and compensation abilities of Cx47 and/or missense mutant protein gain of function (35). Within rodent studies, Cx32 and Cx47 appear to display functional redundancy and are vital for proper myelination. For example, the double null mutant mouse lacking both Cx32 and Cx47, displays a tremor at three weeks, with pathology being confined to myelinated fiber tracts, followed by death at 6 weeks of age (24). The vacuolation and demyelination present in this mouse are likely mediated by an inability to redistribute ions and H_2O following neuronal activity (25).

Disruption of OL-astrocytic communication via astrocytic gap junctions can also affect CNS tissue and cause the formation of vacuoles within the CNS (36). Double Cx30 and Cx43 null-mutation affects not only astrocytes, but mature OLs as well. Edematous astrocytes are found in the CA1 region of the hippocampus, although spatial memory is not impaired in conditional double null mutants (36). Edematous astrocytes are also present in white matter of the spinal cord, as well as an increase in apoptosis and reduction in mature OL markers. These pathologies coincide with impaired motor skills, although there is no change in proliferation, microglial activation, or myelination per axon (36). The localization of large vacuoles around OL nuclei (36) in these double Cx30/43 null mutant mice appears to reflect a difference in potassium ion accumulation, in comparison to the Cx32/47 knockout (KO) mice, wherein vacuoles are present between the axon and the sheath (24, 25), and coincide with the cellular localization of channels and lack thereof. Cx32/43KO causes

sensorimotor impairment and seizures, leading to premature death. Intriguingly, Cx47/43KO mice do not show vacuolation or behavioural impairments, suggesting the function of reflexive junctions formed by Cx32 are critical in myelination (37). Eliminating the OL-astrocytic communication would occur in both models, but reflexive junctions between layers of the myelin sheath would also be abolished in the Cx32/43 and Cx32/47 double null mutants. Taken together, these studies suggest OL-astrocytic communication, in conjunction with Cx32 reflexive junctions, are essential for proper myelination. Furthermore, the buffering of potassium appears to be a viable cause of vacuolation and demyelination, since mice lacking the K^+ channel Kir4.1, show no gross behavioural abnormalities, yet present with vacuoles associated with outer aspect of the sheath (38), comparable to the Cx30/43 double null mutant (25).

A third gap junction protein, Cx29, is expressed in OLs (39), yet localization does not recapitulate that seen for Cx32 or Cx47 (24). Cx29 is present along the paranode and exists exclusively in hemichannel formation (15, 30), which may account for its inability to compensate for the loss of Cx32 and Cx47. In OLs, functional redundancy exists between Cx32 and Cx47, since a double null mutant lacking either Cx32 or Cx47 in conjunction with Cx29 shows no demyelination, unlike the extremely deleterious phenotype of the Cx32/47 null mutants (24).

Taken together, these studies provide evidence for functional redundancy between connexin proteins. However, given the complexity of combinatorial pairing, and the findings from individual and multiple missense/null mutant studies, it is clear that the OL gap junction proteins (Cx29, Cx32 and Cx47), together with the astrocytic gap junctions (Cx30

and Cx43), and the OL-astrocyte pairings, are essential to the panglial network, and for the formation and maintenance of myelination.

1.4 Connexin dysregulation following CNS insult

Injury alters the repertoire of connexins expressed in damaged tissue (40). These changes may be attributed to an influx of inflammatory cell types expressing different connexins, the activation and expansion of mitotic CNS cells in response to injury (i.e., astrocytes and $NG2^{+}$ early OPCs), and by specific changes in connexin expression in post-mitotic OLs and neurons. For example, following ischemic injury *in vivo,* a positive correlation has been observed between infarct size and increased connexin-mediated metabolic and electrical coupling (40). Gap junctional communication has been shown to propagate secondary damage from astrocytes to coupled neuronal and OL cell populations, by allowing for movement of toxins and other metabolic stress factors to uninjured cells, triggering a 'bystander effect' *in vitro* (41-43). Through open astrocytic Cx43 hemichannels, glutamate toxicity can be propagated to neuronal co-cultures, resulting in excitotoxic cell death (44, 45). Cell death can be reduced by antisense inhibition of Cx26, Cx32 or Cx43, or by impeding connexin channels with the *in vitro* use of pharmacological blockades such as rotenone (46) and carbenoxolone (46, 47).

While *in vitro* data suggest connexin overexpression is cytotoxic, *in vivo* studies paint a more complex picture. Astrocyte-specific Cx43 conditional KO mice and constitutive $Cx43^{+/-}$ mice subjected to ischemic insult demonstrate increased apoptosis and a larger stroke volume when compared to WT mice (48, 49). These findings can be reconciled by data suggesting that Cx30 and Cx43 are reciprocally regulated following injury. A decrease

in Cx43 expression coinciding with an increase in Cx30 was found to propagate neuronal loss, while neuroprotective effects are seen by the restoration of Cx43 and reduction of Cx30 (50, 51). These findings are further validated by the protection exhibited via ectopic expression of Cx43 from calcium overload, oxidative stress, metabolic inhibition, tamoxifen, and UV irradiation to a comparable efficiency as anti-apoptotic protein Bcl-2 (52). Thus, restoring connexin balance may prove to be a more effective therapeutic strategy than blocking channel activity. In support of this conclusion, pharmacological channel inhibitors have yet to demonstrate therapeutic benefit in injury models, are often toxic, and will inhibit astrocytic signaling of P2X7 receptors in addition to connexin-mediated communication (53-55). Post-traumatic ATP release during secondary injury is also modulated by gap junctional communication. Recently, promising studies have shown that mice lacking both Cx30 and Cx43 in the CNS demonstrated a reduction in ATP release following spinal cord injury (SCI), that corresponded to a reduction in lesion size, microglial activation and improvement in functional recovery (56). Furthermore, regulating Cx43 channel function by mimetic peptides has proven useful in reducing secondary damage in an *ex vivo* model of SCI (57) and may represent a new therapeutic approach to targeting connexin cell-cell communication.

Dysregulation of glial connexins has been shown to occur in spinal cord following experimental autoimmune encephalomyelitis (EAE). Not only were Cx32 and Cx47 plaques reduced in lesions seen 14 days post immunization, healthy white matter tracts were also decreased in abundance (58). Further investigation revealed a redistribution of gap junctional proteins, with Cx47 being located intracellularly (58) and a decrease in Cx43 expression in astrocytes (58, 59). During remyelination, levels of Cx32 and Cx47 in WT mouse (58) and Cx43 in guinea pig (60) have been shown to increase. Loss of function studies with Cx null

mutants subjected to EAE have been performed and produced intriguing results (58, 61). Although previous findings demonstrate mice lacking in both Cx30 and Cx43 display hypomyelination and vacuolation in white matter (36), inducing EAE in the double null mutant has no significant pathology or clinical difference than WT (61). WT and Cx32 null mutant mice subjected to EAE display a comparable degree of inflammation, however, an increase in demyelination and neuronal loss is present in the Cx32 null mutant cohort. This result suggests that an impairment in gap junctional communication via lack of Cx32 is detrimental during EAE (58). Learning and memory dysfunction is a common symptom in multiple sclerosis patients (62), and interestingly, EAE has also been shown to induce atrophy and neuronal loss in hippocampus (63). The hippocampus is a neurogenic niche richly populated with progenitor cells, and it will be extremely important to determine how EAE dysregulates connexin expression, and what effect this has on resident progenitor cell proliferation, specification and differentiation.

In EAE and SCI, OL survival is compromised, leading to neuronal loss. During development, OL survival is dependent upon expression of Cx32 and Cx47 (24). Although null mutants for either Cx32 or Cx47 display only minimal impairment in myelination, mice lacking both Cx32 and Cx47 show major myelination deficits, OL cell death, and axonal loss (24). Further, connexins have been linked to regulation of oligodendrogenesis. Our laboratory has shown that expression of Cx32 by $NG2^+$ early OPCs promotes their differentiation to mature OLs in adult mice, and that subsets of OPCs in null-mutant mice fail to terminally differentiate and are deleted by apoptosis (64). As well, Cx29 is expressed in both a subset of OPCs and mature OLs with expression restricting $NG2^+$ OPCs to an OL lineage. However, Cx29 is expressed by only a subset of NPC-derived $NG2^+$ cells (11).

Relevant to these studies, Cx32 and Cx29 are expressed in mutually exclusive OPC populations (unpublished data from our laboratory). Whether OPC or OL and/or astrocytic connexins are dysregulated following SCI and whether potential dysregulation impacts upon the demyelination and remyelination or oligodendrogenesis induced by the secondary damage that follows acute trauma is still unknown. To date, few studies (56, 57) have investigated the possibility of reducing demyelination or promoting OL replacement of the hippocampus and spinal cord following injury by targeting the cell death mediated by connexin mediated communication.

1.5 Hormonal regulation, classical mechanism of action

Steroid hormones are highly lipophilic compounds which permeate membranes and act as endogenous modulators of many cellular processes including transcription (65), translation (66), protein trafficking (67), and/or post-translational modification (68). In a classical manner, hormonal regulation is dictated by the presence or absence of the specific steroid ligands, intracellular receptor expression, hormone responsive elements (HREs) and other regulatory elements within gene promoter regions, as well as co-activators/co-repressors (69), all which may be cell, tissue, and regionally specific and may exist in a sexually dimorphic manner (65, 66). Downstream effects can occur as soon as 10 minutes (70), or within hours to days following hormone exposure (71).

Multiple intracellular hormone receptors such as estrogen receptor alpha (ERα), estrogen receptor beta (ERβ) and progestin receptor (PR) have been found with various isoforms possible, each binding multiple ligands with varying affinities (72-76). Following

the binding of a ligand to the C-terminal ligand binding domain, hormone receptors undergo conformational change, dimerize and are internalized into the nucleus (77-79). In conjunction with highly conserved transactivation domains within the receptor which permit binding of co-activators (80, 81), ligand-activated dimers expose their DNA binding sequence surrounded by two zinc-finger DNA binding motifs, permitting binding to nucleic sequences of a palindromic nature and act as a transcription factor (82). Modulation by interaction with regulatory elements such as other transcription factors along the promoter region can be further enhanced or suppressed by co-activators or co-repressors (81, 83-85). Due to the multifactorial nature of classical hormonal signaling, the multitude of receptors, ligands, co-activators/repressors, and varying expression levels of all components involved (including hormones and receptors) results in a highly dynamic, tightly regulated mechanism that may be cell, regional, sex and steroid specific (65, 66, 86). Furthermore, downstream effects of hormonal regulation has been shown to proceed as rapidly as seconds to less than 10 minutes (70, 87), suggesting a second hormonal mechanism that would not be explained by classical genomic modulation of transcription/translation. This has led to discovery of a rapid non-classical manner of hormonal modulation involving membrane mediated signal transduction cascades, as estradiol can cause the rapid activation of the mitogen-activated protein kinase pathway (88, 89) and increases phosphorlyation of cAMP response element binding protein (90, 91). There is a growing body of literature indicating that expression of connexins are under control of hormonal steroids in various tissues by both genomic and non-genomic modulation (65, 67, 68, 92-94).

1.6 Gene organization and hormonal regulation of connexins

The basic organization for connexin genes remains relatively conserved throughout the family, with the 5' UTR (5' untranslated region) located within exon 1 and the coding sequence and 3' UTR (3' untranslated region) located within exon 2 as is the case with Cx29 (Figure 1.4A) (95), although multiple variations to this structure in many connexins has been identified (96, 97). Also relatively conserved is the canonical promoter, regulating basal transcription and located within exon 1 approximately 300 base pair (bp) upstream of the transcription initiation site (96, 98). Cell-type independent putative binding sites are also located within the promoter region and 5' UTR of connexin genes, including specificity protein 1 (Sp1) (99) and activator protein 1 (AP-1) (100) as well as binding sites such as hepatocyte nuclear factor 1 (HNF-1) (101) and HREs (82), which permit cell-type dependent connexin expression. More recently, evidence suggests alternative splicing and multiple promoters are present in a subset of connexin genes allowing for further transcriptional activity refinement and cell-type specific transcripts (102, 103). Although multiple transcript isoforms exist in a subset of connexins, the coding sequence remains the same, with main sequence alterations being present in the 5'UTR (96, 98).

The human Cx30 gene has been shown to have six exons, with exon 6 containing the coding region in all transcripts, whereas exon 1-5 can be alternatively spliced producing multiple isoforms of Cx30 transcript, all varying in the 5' UTR (104), although mouse Cx30 gene has only four exons (Figure 1.4B) (96).

The Cx32 gene was originally believed to contain two exons, with 5' UTR found within exon 1, and the uninterrupted coding sequence contained within exon 2 (105). Within the mouse, it is now known that Cx32 contains at least four exons (1, 1A, 1B, and 2) (Figure

Figure 1.4 Genomic structure of connexin genes and alternative splicing. Cx29 consists of two exons with the coding sequence (blue) located within exon 2 (A). Cx30 and Cx32 contain four exons (1A, 1B, 1C and 2) with the coding sequence located in exon 2 (B, C). Cx36 contains two exons with regions of the coding sequence located within both exon 1 and exon 2 (D). Cx43 contains six exons (1A, 1B, 1C, 1D, 1E and 2) with complex alternative splicing (E) producing multiple transcripts. Cx45 contains five exons (1A, 1B, 1C, 2 and 3) with the coding sequence within exon 3 (F). Cx47 has five exons (1A, 1B, 1C, 1D and 2) with the coding sequence within exon 2 (G). Adapted from Sohl 2003, Anderson et. al. 2004, and Sohl et. al. 2013.

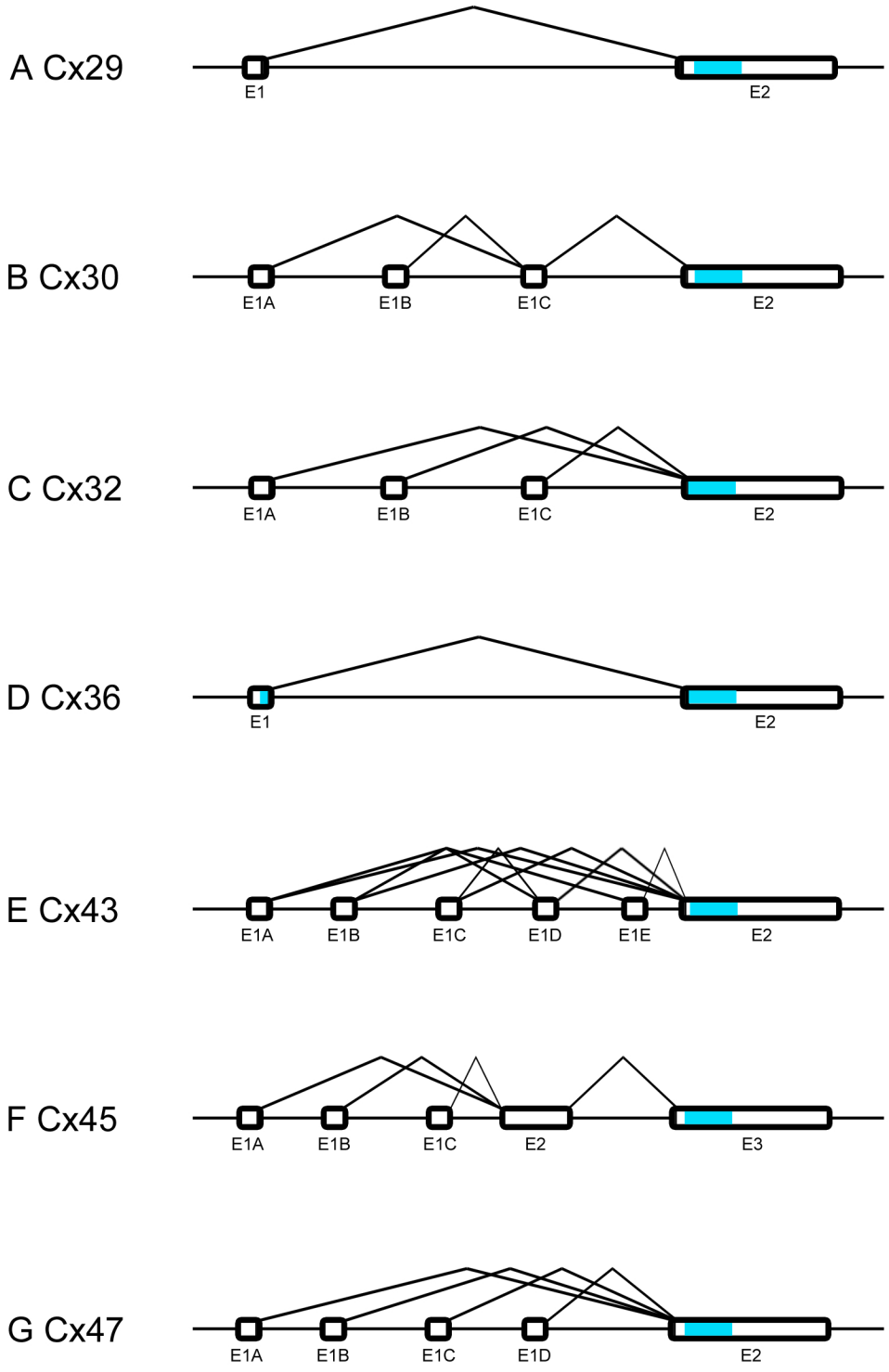
A Cx29
E1
E2
B Cx30
E1A
E1B
E1C
E2
C Cx32
E1A
E1B
E1C
E2
D Cx36
E1
E2
E Cx43
E1A
E1B
E1C
E1D
E1E
E2
F Cx45
E1A
E1B
E1C
E2
E3
G Cx47
E1A
E1B
E1C
E1D
E2

Figure 1.4

1.4C), with multiple transcripts driven from three promoters in a cell type specific manner (103). The splice variant expressed within hepatocytes (E1/E2), contains a 5' UTR with a consensus sequence for HNF-1 (101) and expression of Cx32 mRNA is driven by promoter P1 (103), whereas promoter P2 includes regulatory elements such as Sox10 and early growth response gene 2 (Egr2/Knox20) (106, 107) and the isoform (E1B/E2) is considered nerve-specific, found in schwann cells (103). Mice lacking Egr2/Knox20 display abnormal nervous system development and peripheral neuropathy (108, 109). Furthermore, mutations in human Sox10 and Egr2/Knox20 has been found in patients with peripheral myelin defects (106). Within these patients, mutants are unable to transactivate the promoter P2-driven gene expression of Cx32 (106). Isoform E1A/E2 is found in liver, embryonic cells and oocytes (103). These transcription factors work in a synergistic manner and appear to be under direct (Krox20) and indirect (Sox10) hormonal regulation (110). Sox10 has been shown to be highly expressed in myelinating cells (111). Using cultured rat schwann cells, an increase in Krox20 was found 1 hour following treatment with progesterone, as well as a subsequent rise in Sox10 at 2 hours (110). Following investigation of the potential presence of HREs within the gene structure of Sox10 and Krox20, it was determined that Krox20 contained progesterone responsive element (PRE) sequences whereas Sox10 did not (110). The increased expression levels of Sox10 at 2 hours were attributed to regulation by the preceeding Krox20 expression increase at 1 hour (110).

The Cx36 coding sequence is interrupted by an intron 1.14 kb in length, with the initial 71 bp located within exon 1 and the remainder of coding sequence within exon 2 (Figure 1.4D) (112). The separated coding sequence was found in both rat and mouse Cx36

genes, which were highly homologous between species, differing in only one amino acid (112).

The conservation of sequence homology and organization between rat and mouse, is seen in Cx43 gene expression as well (102). Cx43 was initially described to consist of two exons and one canonical promoter P1 (97), but more recently it has been shown that a further four exons and two promoters exist (Figure 1.4E), with nine alternative transcript isoforms expressed in a regionally specific manner (102). As well, relative abundance differs between tissue sources (102). When examining cardiac tissue, transcripts derived from promoter P1 are located throughout the heart, whereas promoter P2 transcript isoforms are found in the atria and septum, and promoter P3 transcripts are located solely in the ventricles (102). In conjunction with the alternative promoters, tissue source specificity can be mediated by variable 5' UTRs which contain unique gene regulatory elements in a tissue specific manner (102). For example, expression by the promoter P2 has been shown to be modulated by the Ras signaling pathway and consensus sequence AGT TC(A/C) A(T/C)C A, which acts as a binding site for a c-Myc/HSP90 complex (113).

The 5' UTR of the Cx45 gene has been shown to contain regulatory elements such as AP-1 sites and a TATA-box (114). Five exons are present (exons 1A, 1B, 1C, 2 and 3) (Figure 1.4F), with the initial four containing 5' UTR sequences and the last (exon 3) containing the remainder of 5' UTR, the coding sequence and the 3' UTR (115, 116). Multiple isoforms of transcript can be formed by 1A, 1B, or 1C spliced to the sequence of exon 2 and 3, or exon 2 and 3 spliced together (115, 116). Again, the expression of these various transcripts differ in abundance and tissue location, with the isoforms containing 1A

ubiquitous, 1B in colon (trace amounts), 1C in colon, bladder, lung, ovary and heart (115, 116).

The Cx47 gene contains five exons (1A, 1B, 1C 1D and 2) (Figure 1.4G) (115). The transcript isoform containing E1B/E2 is highly expressed in myelinating cells of the mouse CNS (115, 117). Like Cx32, the 5' UTR of Cx47 has been shown to contain Sox10 binding sites within the promoter located on exon 1B (118). Furthermore, mutations within exon 1 has been found in 29% of patients with PMLD1 which is suggested to impair Sox10 binding and is attributed to the cerebral hypomyelination seen within these patients (119).

Classically, HREs are 16 bp palindromic sequences (Estrogen Responsive Element, ERE: AGGTCANNNTGACCT, PRE: AGAACANNNTGTTCT), yet prior functional promoter studies of the Cx43 promoter sequence determined that three half palindromic estrogen response elements are sufficient to drive an upregulation of luciferase expression *in vitro* when cotransfected with estrogen receptor cDNA in HeLA cells in an estradiol-concentration dependent manner (82). Along with HREs, transcriptional regulatory elements, such as activation function 1 and 2 (AF-1 and AF-2) sites affect expression of connexin expression (81). *In vitro*, the estrogen induced co-activator protein Ini causes an increase of Cx43 mRNA expression through its action of binding to AF-1 sites (81). Following overexpression of ERα cDNA in HeLa cells, upregulation of Ini expression leads to further upregulation of Cx43 mRNA in a concentration-dependent manner (81).

Steroid hormone levels have been directly correlated to changes in connexin expression and communication in various tissues. Comparison between genders has shown gap junctional expression can be regulated in a sexually dimorphic manner, specifically Cx43 protein in the rat preoptic area (POA) and the hypothalamus (66). *In vitro*,

progesterone secretion has been directly correlated to the increased mRNA expression of Cx43 and subsequent gap junctional communication in cultured ovine luteal cells with effects being abolished using siRNA directed specifically at Cx43 (92). *In vivo*, Cx43 mRNA expression is relatively low within myometrial tissue, but has been shown to increase during gestation and peak during labour (120). To elucidate the actions of fluctuating hormones, surgical removal of ovaries or ovariectomy (OVX), which are the main endogenous source of estradiol and progesterone, followed by exogenous hormonal treatment with estradiol was found to increase Cx43 transcription, yet expression levels were not altered when treating with both estradiol and progesterone (121). Furthermore, treatment with progesterone during late gestation decreased Cx43 mRNA expression (86). The hormone specific regulation of gap junctional communication within the myometrium plays a critical role during the onset of labour by producing synchronous uterine contractions and is directly affected by the endogenous ratio of estradiol to progesterone (122). Hormones can alter gap junctional communication within myometrial tissue by means other than transcriptional regulation. Using pregnant intact or OVX rats, treatment with progesterone in late stages of gestation inhibited labour but did not alter the translation of Cx43 protein in myometrial tissue (121). Further evaluation of the localization of Cx43 found progesterone treatment suppressed the trafficking of Cx43 from the golgi apparatus to the plasma membrane in myometrial tissue (67).

As seen in various reproductive tissues (86, 92), steroid hormones play a direct role in connexin expression in a tissue-specific manner. Within the rodent brain, hormone receptor expression is regionally specific (123, 124) and may account for the tissue specific effects of hormones on connexin levels. Using OVX female rats, exogenous estradiol

administration significantly increases Cx36 mRNA expression within the suprachiasmatic nucleus (SCN), but not the cerebral cortex (CX), an effect specific to estradiol treatment, as progesterone does not induce the upregulation of Cx43 expression (65). Furthermore, transcriptional induction within the SCN did not occur when estrogen treatment was followed by progesterone treatment, demonstrating the suppressive effects of hormonal regulation (65).

As exogenous hormonal treatment using OVX females have been shown to alter connexin expression (86, 121), endogenous hormonal fluctuations of cycling females have been implicated in the regulation of connexins as well (122). During the luteal phase of the porcine reproductive cycle, high levels of circulating progesterone levels correlate to a significant decrease in Cx43 immunoreactivity within myometrium, as well as a decrease in phosphorylation of Cx43 protein (122). During the late-luteal and pre-ovulatory stages with low progesterone levels, Cx43 protein immunoreactivity and phosphorylation are increased (122). Connexin modulation by hormones in specific CNS regions (i.e., hippocampus, spinal cord) over the course of estrous has yet to be determined.

1.7 Hormone receptors and the hippocampus

Hormone receptors are expressed dynamically within the rodent hippocampus (124, 125). High levels of ER were initially localized to the rat hippocampus by audioradiography (126) and further validated by *in situ* hybridization (124). Specifically, within OVX female rat hippocampus, ERβ mRNA labeling was seen throughout the CA regions and bordering the hilus within the dentate gyrus, increasing from a) the rostral to caudal and b) dorsal to

ventral regions of the hippocampus overall, whereas ERα mRNA labeling was very weak, with signal found strongest within the more ventral regions of hippocampus (124).

Receptor levels have been shown to fluctuate over the course of the female mouse estrous cycle (125). During the estrous cycle, circulating progesterone levels peak during the late-luteal diestrus stage, followed by a surge in 17-β-estradiol which peaks during the pre-ovulatory stage of proestrus (127). Following ovulation, the female mouse enters estrus where 17-β-estradiol levels decrease and progesterone remains relatively low (127). During the luteal metestrus stage, progesterone levels are on the rise until reaching a maximum during subsequent diestrus (127). Within the hippocampus of cycling female mice, ERβ expression peaks during both the estrus and diestrus stages, then decreases during proestrus, at which point, expression is comparable to males (125). ERα peaks during diestrus, following a decrease in the proestrus and estrus stages, with expression at all estrous stages more elevated than males (125). Peak levels of PR expression are seen during proestrus while lowest during diestrus, with levels expressed at an intermediate level during estrus, at which point they are comparable to PR male expression (125). These changes are of interest given that the hippocampus has been described as a neurogenic niche rich with multipotent NSCs (10) and connexin expression plays a key role in the cell proliferation and fate determination within (11, 64). Examining potential modulators (i.e, 17-β-estradiol, progesterone) of connexin expression within the CNS may prove useful in targeting endogenous cellular replacement as treatment for neurodegenerative/regenerative conditions.

1.8 Rationale, Hypothesis and Objectives

The relationship between connexins within the CNS and hormonal regulation is significant although not fully understood. Based on evidence described previously with respect to the modulation of Cx36 mRNA (65) and Cx43 protein (66) in a tissue specific and hormone specific manner, I hypothesized that connexin expression, whether it be mRNA or protein expression, is modulated by hormonal fluctuations in the female mouse CNS. To test this hypothesis, I optimized detection methodologies for Cx32 detection (Chapter 2) and accurate assessment of hormonal status with minimal invasive procedures (Chapter 3) then quantitatively assessed mRNA expression levels of seven different CNS connexin (Cx29, Cx30, Cx32, Cx36, Cx43, Cx45, and Cx47) in both the hippocampus and spinal cord over the course of the estrous cycle (Chapter 4). Throughout this thesis, I used Cx null mice to verify and ensure the specificity of protein and mRNA assessments.

CHAPTER 2: TISSUE-SPECIFIC CROSS-REACTIVITY OF CONNEXIN32 ANTIBODIES: PROBLEMS AND SOLUTIONS UNIQUE TO THE CENTRAL NERVOUS SYSTEM

2.1 Objective of this study

Due to the homologous nature of the connexin protein family, there has been much controversy as to which cell types express specific connexins (19, 128, 129). Accurate labeling must be assessed in the hippocampus and spinal cord. As such, a comprehensive evaluation of existing commercial and "in-house" generated antibodies was required using null-mutant controls. **This study was published in the journal of Cell Communication and Adhesion** as Fowler, S.L.*, McLean, A.C.* & Bennett, S.A.L. Tissue-specific cross-reactivity of connexin32 antibodies: problems and solutions unique to the central nervous system. *Cell Communication & Adhesion* 16, 117-130 (2009)**.** *Both authors contributed equally.

2.2 Statement of author contributions

The colony maintenance, tissue collection, immunofluorescence, microscopy and genetic analysis data was performed by A.C. McLean. S.L. Fowler performed the immunoblotting, fractionation and mass spectrometry content of this study. Both authors contributed equally to the experimental design and writing of the manuscript and antigenic epitope identification. This study was performed under the supervision of Dr S. Bennett who

designed the experiments, analyzed the data, and wrote the manuscript with S.L. Fowler and A.C. McLean.

2.3 Summary

To ensure success of this research, myself and another colleague in the Bennett laboratory have collaborated in the assessment of a large panel of connexin antibodies for specificity by western blotting, immunoprecipitation, and immunofluorescence comparing WT brain samples to congenic null-mutant controls. We found a surprising lack of specificity for existing Cx32 antibodies and have determined that a CNS-specific cross-reactivity with a protein with similar mobility to Cx32 exists for most of these reagents upon protein denaturation. Through bioinformatic analyses, tested by sucrose gradient fractionation and immunoblotting of lysates from connexin null-mutant mice, we show that the cross-reactive protein is not found in the same cellular compartments as Cx32 and is likely not a member of the connexin family. Through this work, I have identified and characterized the necessary reagents to realize my thesis research in the quantification of Cx32 protein should subsequent studies validate this examination (see Chapter 4).

2.4 Introduction

Connexin proteins are a highly conserved family of single and double-membrane channels characterized, in part, by four transmembrane-spanning domains. The connexin family consists of 21 members, 11 of which are expressed in the mammalian CNS (4, 50, 130). Hexamerization of compatible connexins form structures called connexons that

incorporate as hemichannels in nonjunctional membranes (single-membrane channels) or dock with compatible connexons donated from adjacent cells to form intercellular gap junction channels (double membrane channels) (131). Gap junctions are present in membranes as plaques composed of hundreds of channels of various connexin combinations that allow for the transfer of ions and metabolites less than 1-kDa in size between neighboring cells (132).

Cx32 is the predominant liver connexin, and was first isolated in 1986 from purified calf liver gap junctional preparations (133). Hydropathy analysis of the Cx32 cDNA clone predicted a protein with four transmembrane domains flanked by α-helical loops. Shortly thereafter, the cytoplasmic localization of both N- and C-termini, and a hydrophilic domain corresponding to the loop between the second and third transmembrane regions, were confirmed (Figure 2.1). It is generally accepted that these cytoplasmic regions are the least conserved amongst connexin family members, and thus provide the most attractive sites for connexin-specific antibody development (134, 135).

The first Cx32 antibodies were prepared from purified calf liver gap junction preparations (133, 136) or from peptides localized to the C-terminus, and the intracellular loop (134, 135). Each of these antibodies recognized a monomeric protein with a molecular weight of approximately 27-kDa, as well as the predicted Cx32 dimer migrating at approximately 54-kDa. Specificity was confirmed by peptide competition and by qualitative observations of target protein oligomerization upon heating in sodium dodecyl sulfate (SDS), a defining characteristic of connexin proteins (134, 135). However, the ultimate negative control for any immunogenic protein analysis lies in analysis of samples from a

Figure 2.1 Schematic of the transmembrane structure of Cx32, highlighting the position of the peptides used to generate each of the antibodies assessed. Additional details are provided in Table 2.1.

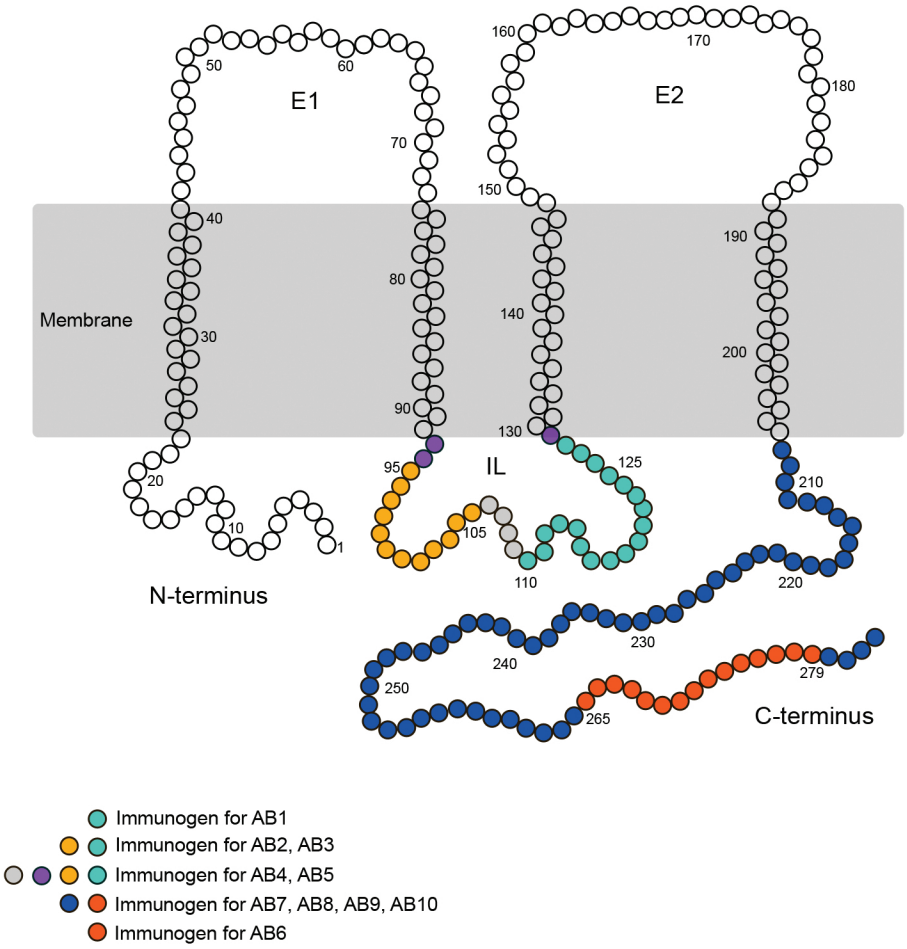
E1
E2
IL
Membrane
N-terminus
C-terminus
1
10
20
30
40
50
60
70
80
90
95
105
110
125
130
140
150
160
170
180
190
200
210
220
230
240
250
265
279
Immunogen for AB1
Immunogen for AB2, AB3
Immunogen for AB4, AB5
Immunogen for AB7, AB8, AB9, AB10
Immunogen for AB6

Figure 2.1

Code	Catalogue number	Source	Epitope location[a]	Type[b]	[Western]	[Immuno]
AB1	CX32C13-M	Alpha Diagnostics	IL 110-128	Monoclonal	0.5 µg/ml	1:200
AB2	Hybridoma	David Paul	IL 95-125	Monoclonal	No dilution	No dilution
AB3	MAB3069	Chemicon	IL 95-125	Monoclonal	1:1000	1:100
AB4	13-8200	Zymed	IL[c]	Monoclonal	1:250	1.0 µg/ml
AB5	71-0600	Zymed	IL[c]	Polyclonal	1:125	2.0 µg/ml
AB6	C3470	Sigma	C-term 265-279	Polyclonal	1:200	1:600
AB7	C7854-05E	USBiological	C-term 19 aa	Polyclonal	0.7 µg/ml	1:400
AB8	C7854-04	USBiological	C-term	Polyclonal	3.0 µg/ml	1:800
AB9	34-5700	Zymed	C-term[d]	Polyclonal	1:125	1.0 µg/ml
AB10	35-8900	Zymed	C-term[d]	Monoclonal	3.0 µg/ml	1:800
AB11	51-2800 (Cx26)	Zymed	C-term	Polyclonal	1:125	NA
AB12	71-2200 (Cx30)	Zymed	C-term	Polyclonal	1:200	NA

NA, not applicable.

[a]Peptides used to generate each antibody are listed by amino acid position where known (see Figure 2.1). Position and/or length of the peptides used to generate AB4, AB5, AB7-10 were not disclosed by the manufacturer. IL, intracellular loop; C-term, C-terminus.

[b]All monoclonal antibodies were raised in mouse. All polyclonal antibodies were raised in rabbit.

[c]AB4 and AB5 were raised against the same proprietary IL antigen.

[d]AB9 and AB10 were raised against the same proprietary C-term antigen.

Table 2.1 Connexin antibodies

null-mutant animal. The Cx32 null-mutant mouse, generated by the Willecke laboratory, has greatly facilitated the investigation of Cx32 localization and function (34). This control has confirmed that Cx32 is predominantly expressed in myelinating glia (OLs and Schwann cells) of the CNS and peripheral nervous system (16, 64, 137-140).

Although great care has been taken to ensure antibody specificity in tissues with high levels of target connexin expression (i.e., specific detection of Cx32 in liver, Cx45 in heart), few studies have assessed the potential for cross-reactivity in the CNS wherein an extensive repertoire of connexins is expressed in different cell types (141, 142). Unpublished data from our laboratory and anecdotal reports from other groups have detected a 27- to 32-kDa anti-Cx32 reactive band in murine brain and spinal cord homogenates of Cx32-null animals by Western blot analysis using antibodies that have been repeatedly verified for appropriate

immunofluorescent analyses (64, 140, 143). Because laboratories are understandably reticent to publish the appearance of spurious artifacts, these observations have not been systematically evaluated; however, the presence of a cross-reactive band, with the same approximate mobility in null-mutant animals, represents an important complication in the analysis of Cx32 by Western analysis following CNS injury.

To address this issue, we compared reactivity of 10 commonly used Cx32 antibodies in brain and liver using immunoblotting, immunofluorescence, and immunoprecipitation applications. Surprisingly, we found that eight antibodies cross-reacted with a protein present in $Cx32^{Y/-}$ brain but not liver. We show that this cross-reactivity is only observed when proteins were subjected to reducing/denaturing conditions prior to immunodetection. To further distinguish Cx32 from CNS-specific cross-reactive protein(s), we used sucrose gradient fractionation, demonstrating that Cx32 and the cross-reactive protein(s) localize to distinct subcellular compartments and exhibit a 4-kDa size difference. Finally, combined bioinformatics and molecular approaches provide converging evidence that the cross-reactive protein is likely not another connexin but rather an immature (Golgi-localized) or partially degraded (lysosome-localized) subunit of a larger unidentified protein complex. Together, these data highlight a key concern for the interpretation of changes in Cx32 protein expression in the CNS that can be easily controlled by the choice of methodology and the optimized reagents described in this study.

2.5 Experimental Procedure

Cx32 Antibodies

Table 2.1 describes the Cx32 antibodies employed, the peptides used to generate each antibody, the antigenic sites within these peptide sequences, the source of each antibody, and the concentrations employed.

$Cx32^{Y/+}$ and $Cx32^{Y/-}$ Animals

Cx32 null-mutant breeding pairs (34), kindly provided by Dr. Klaus Willecke (Universitat Bonn, Germany), were backcrossed for 13 generations onto a C57Bl/6 background in our laboratory. Congenic WT mice were derived from heterozygote matings. Male mice used in this study were 3 to 4 months of age at the time of sacrifice. A total of 15 $Cx32^{Y/+}$ and 15 $Cx32^{Y/-}$ mice were analyzed. Genotyping was confirmed at time of weaning and again at time of sacrifice (Figure 2.2). DNA isolated from tail snips was amplified using primers A, B, and C (A: 5'-TCA TTC TGC TTG TAT TCA GGT GAG AGG CGG-3'; B: 5'-ATA CAC CTT GCT CAG TGG CGT GAA TCG GCA-3'; C: 5'-TCT TAC TCC ACA CAG GCA TAG AGT GTC TGC-3'). A and B amplified a 750-bp fragment of the $Cx32^{Y/+}$ WT allele, whereas A and C produced a 1.3-kb fragment indicating the $Cx32^{Y/-}$ KO allele (Figure 2.2). Polymerase chain reaction (PCR) amplification was performed on a Whatman Biometra TGradient96 system. Cycling parameters were 95°C for 10 min, followed by 30 cycles of 95°C for 60 s, 67°C for 60 s, and 72°C for 60 s.

Immunoblotting

Brain tissue (encompassing either cerebrum and cerebellum or dissected hippocampus as indicated) was isolated from $Cx32^{Y/+}$, $Cx32^{Y/-}$, $Cx32^{Y/-}Cx29^{-/-}$, and $Cx30^{-/-}$

Figure 2.2 Genotyping for Cx32 WT or null-mutant KO allele. All mice were genotyped at both the time of weaning and time of sacrifice for (A) a 1300-bp KO amplicon and (B) a 750-bp WT amplicon. Representative genotyping from four null-mutant mice ($Cx32^{Y/-}$) and five WT mice ($Cx32^{Y/+}$) used in this study is shown. NT represents no template control, confirming lack of reagent contamination.

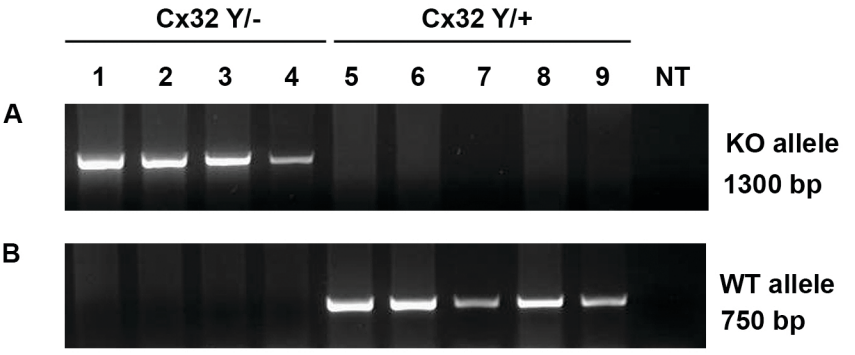
Cx32 Y/-
Cx32 Y/+
1
2
3
4
5
6
7
8
9
NT
A
KO allele
1300 bp
B
WT allele
750 bp

Figure 2.2

mice. $Cx29^{-/-}$ mice (137) were kindly provided by Dr. David Paul (Harvard Medical School) and crossed onto a Cx32 null-mutant background in our laboratory. $Cx30^{-/-}$ breeding pairs (144) were obtained through the European Mouse Mutant Archive with the kind assistance of Dr. Klaus Willecke. Liver was obtained from the same animals. Human brain from a 67-year-old female who suffered sudden death due to non-neurological complications was obtained from the Douglas Hospital Research Centre Brain Bank (Montreal, Canada). At autopsy, parahippocampal gyri were removed and flash-frozen in liquid nitrogen without fixation for protein extraction. Postmortem delay was 17 h. The hippocampus was dissected from this sample for Western analysis. All tissues were homogenized in fresh RIPA buffer (1% Nonidet P-40, 0.5% sodium deoxycholate, 0.1% SDS, 1 mM NaF, 50 g/mL aprotinin, 1 mM sodium orthovanadate, 1 mg/mL phenylmethylsulfonyl fluoride, 10 mM phosphate-buffered saline [PBS; 10 mM phosphate, 154 mM NaCl]) and assayed for protein concentration using a Bio-Rad DC protein assay kit (Bio-Rad, Hercules, CA). Brain and liver samples were diluted in 2 × SDS sample buffer (Tris-HCl/SDS pH 6.8, 5% glycerol, 1.67% SDS, 100 mM dithiothreitol, 0.002% bromophenol blue) with 10% β-mercaptoethanol (BME) and solubilized at room temperature for 30 min. All experiments were performed and repeated using 30 μg of hippocampal or whole-brain protein and 10 μg of liver protein to allow for comparable signal and exposure times given the differences in abundance of Cx32 protein between liver and brain tissue. Proteins were resolved under reducing/denaturing conditions on 12.5% or 15% (sucrose fractions only) Tris-HCl polyacrylamide gels and transferred onto Immobilon PSQ polyvinylidene fluoride membrane (Millipore, MA) at 100 V for 60 min. Membranes were blocked in 5% (*w/v*) skim milk powder–PBS with 0.1% Tween-20 (PBST; blocking buffer) for 1 to 3 h and incubated in

primary antibody diluted in the same buffer overnight at 4°C (see Table 2.1 for working concentrations of all connexin antibodies). Membranes were rinsed twice in 0.1% PBST and twice in blocking buffer for 10 min prior to a 1- to 3-h incubation in horseradish peroxidase (HRP)-conjugated anti-mouse or anti-rabbit (Jackson ImmunoResearch Laboratories, PA; 1:2000 and 1:5000) secondary antibody diluted in blocking buffer. Signal was detected on x-ray film using SuperSignal West Pico Chemiluminescent Substrate (Pierce, IL).

Immunofluorescence

Male mice ($Cx32^{Y/+}$ and $Cx32^{Y/-}$) were anesthetized with Euthansol (65 mg/mL) and intracardially perfused with 10 mM PBS (pH 7.2) followed by 3.7% molecular grade paraformaldehyde (Sigma) in 10 mM PBS diluted immediately prior to use. Brain and liver were removed and postfixed for 24 h at 4°C in the same fixative followed by 48 h of cryoprotection in 20% sucrose solution containing 0.001% sodium azide at 4°C. Serial cryostat sections (10 μm) were obtained (Leica Microsystems). Sections were immunoreacted with anti-Cx32 primary antibodies (Table 2.1) diluted in antibody buffer (10 mM PBS, 0.3% Triton-X100, 3% bovine serum albumin). Optimal concentrations were determined by serial dilution on both liver and brain sections with the antibody concentration giving the most robust signal employed for the rest of the study. Where antibodies were not reactive or showed cross-reactivity on brain tissue, the optimal concentration determined using liver cryosections was employed. Secondary antibodies used were Cy3- or fluorescein isothiocyanate (FITC)-conjugated anti-mouse immunoglobulin G (IgG) (diluted 1:800 and 1:400, respectively) and Cy3- or FITC-conjugated anti-rabbit IgG (1:600, 1:100; Jackson ImmunoResearch Laboratories, PA). Details are as described in Melanson-Drapeau et al.

(2003) (64). Sections were coverslipped in 0.05% *p*-phenylenediamine in PBS/glycerol, pH 8.0, and imaged by epifluorescent microscopy using OpenLab 5.0.2 (Improvision) on a DMXRA2 epifluorescent microscope (Leica Microsystems).

Immunoprecipitation

Cx32-coupled protein G agarose beads were prepared as follows: One milliliter of protein G agarose bead slurry (1:1 PBS; Roche, Germany) was incubated with 25 μg of AB1 (Table 2.1) overnight at 4°C. The beads were washed with 10 mL of 0.1 M borate buffer (pH 9.0) and resuspended in 10 mL of the same buffer. AB1 was chemically coupled to the protein G beads by the addition of solid dimethylpimelimidate (Pierce, IL) to a final concentration of 20 mM. Beads were incubated for 30 min at room temperature. The reaction was stopped by washing the beads twice with 0.2 M ethanolamine. Beads were resuspended in 10 mL of 0.2 M ethanolamine and incubated at room temperature for 2 h, followed by two washes with 10 mL of PBS. Beads were resuspended in 1 mL PBS and stored at 4°C. Human and mouse hippocampal and brain lysates as well as mouse liver lysates were prepared for Western analyses in RIPA buffer with fresh protease inhibitors and assayed for protein concentration. Protein lysates were diluted to 100 μg in 200-μL volumes for preclearing with 50 μL of uncoupled protein G agarose beads for 1 h at 4°C. Precleared lysates were added to 50 μL of prepared AB1-coupled beads and incubated overnight at 4°C. Beads were washed twice in RIPA buffer and three times in PBS. Proteins were eluted from the IgG molecules at room temperature for 30 min with inversion in 200 μL of ammonium hydroxide elution buffer (0.5 M NH4OH, 0.5 mM EDTA). Samples were lyophilized in a SpeedVac and solubilized in 45 μL 2 × SDS sample buffer and 5 μL BME at room temperature for 30 min.

The SDS solubilized proteins were resolved on 12.5% Tris-HCl polyacrylamide gels, transferred to PDVF membranes, and blotted with polyclonal AB6.

Sucrose Gradient Fractionation

Whole brain and whole liver were extracted from $Cx32^{Y/+}$ and $Cx32^{Y/-}$ mice and immediately frozen in liquid nitrogen. For each experiment, one brain hemisphere or one lobe of liver was homogenized in 1.5 mL PTN buffer (50 mM sodium phosphate, 1% Triton X-100, 50 mM NaCl, 30 μL protease inhibitor cocktail, pH 7.4) using a Teflon Potter-Elvehjem homogenizer fitted to a 30-mL glass tube. Homogenates were incubated on ice for 30 min and centrifuged at 16,000 × g for 10 min at 4°C. The Triton X-100 soluble supernatant was reserved on ice. One milliliter of supernatant was mixed with 1 mL 80% sucrose. Samples were carefully overlaid with 1.5 mL 30% sucrose followed by 1.5 mL of 5% sucrose. Prepared tubes were centrifuged at 130,000 × g in an SW-40 Ti swinging-bucket rotor overnight (18 h) at 4°C (Beckman 50 Ultra-Clear Tubes [14 × 95 mm]; catalog number 344060). Gradients were carefully aliquoted (10 fractions at 500 μL each), with fraction 1 being the uppermost, lightest fraction. Protein quantification was performed using the Bio-Rad DC protein assay kit, and samples were analyzed by immunoblotting using AB1 and the fractionation markers coxIV (Molecular Probes [A-21348] 0.4 μg/mL), caveolin-1 (Santa Cruz [SC-894] 1:500), flotillin-1 (BD Transduction Laboratories [610820] 1:1000), syntaxin-1 (Sigma [S0664] 1:2000), LAMP1 (Cell Signaling [C54H11] 1:1000), and golgin-97 (Molecular Probes [A-21270] 1:1000).

Mass Spectrometric Identification of Proteins after Western Analysis

Blotting and removal of nitrocellulose (BARN) methodology followed by tryptic digest and mass spectrometry analysis were performed as described in Luque-Garcia et al. (2008) (145) to identify the Cx32 cross-reactive protein under reducing/denaturing conditions. Briefly, 20 μg of liver fractions 4, 5, and 6 from a $Cx32^{Y/+}$ fractionation were resolved in each of eight lanes of a 12.5% sodium dodecyl sulfate– polyacrylamide gel electrophoresis (SDS-PAGE) gel and transferred to a nitrocellulose membrane (Triton-free, pore size 0.2 μm) at 400 mA for 1 h on ice in transfer buffer (25 mM Tris, 192 mM glycine, 0.1% SDS, 20% methanol). The membrane was blocked with PVP-40 buffer (0.5% *w/v* poly(vinylpyrrolidone) in 100 mM acetic acid) for 1 h at room temperature and rinsed with four changes of PBS (1 min each) before overnight incubation with AB1 diluted in PBS. Primary antibody was rinsed from the membrane with four changes of PBS (10 min each), incubated with anti-mouse IgG-HRP secondary antibody diluted in PBS for 1 h, followed by four rinses in PVP-40 blocking buffer. The membrane was rinsed with four changes of PBS (1 min each) to remove excess PVP-40 buffer. Chemiluminescent detection was performed as usual except that all surfaces coming into contact with the membrane were washed with 70% ethanol and rinsed with double-distilled H_2O (ddH_2O) to prevent keratin contamination. The developed film was aligned with the chemiluminescent stain on the membrane to facilitate accurate detection of the Cx32-containing region of the membrane. Each of the eight Cx32-containing bands were excised with no. 11 scalpel blades and washed three times with 1.5 mL 20 mM sodium bicarbonate buffer (pH 7.4) for 5 min each at room temperature. The membrane sections were then washed three times with 1.5 mL 100 mM glycine (pH 2.4) for 10 min to remove all traces of antibody before a final 5-min wash in 1.5 mL 20 mM

sodium bicarbonate buffer. The nonspecific sites on the membrane sections were blocked with 0.5 mL PVP-40 buffer for 30 min at 37°C and rinsed six times with ddH_2O. Trypsin (Promega) prepared in 50 mM NH_4HCO_3 buffer (pH 8) was added at 12.5 ng/μL to the membrane sections and incubated at 37°C overnight. The samples were dried under vacuum and dissolved by vortexing in acetone (90 μL acetone/4 mm^2 nitrocellulose) followed by a 30 min incubation at room temperature. The acetone containing the nitrocellulose was removed, and the peptides were air-dried and resuspended in 20 μL 2% acetonitrile in 0.1% formic acid. Nanoflow liquid chromatography tandem mass spectrometry was used to analyze peptide mixtures derived from these on-membrane digestions as described by Luque-Garcia et al. (2008) (145) and data were analyzed as in Lambert et al. (2009) (146).

2.6 Results

2.6.1 A cross-reactive protein with the same mobility as Cx32 is detected in null-mutant brain but not liver.

Protein lysates prepared from murine tissue (liver, brain, and isolated hippocampus) as well as human hippocampus were resolved by SDS-PAGE under reducing conditions. Western analysis was performed using 10 different Cx32 antibodies (Table 2.1, Figure 2.1). Five antibodies were directed against epitopes localizing to the intracellular loop (Figures 2.1, 2.3); five antibodies were directed against epitopes found within the C-terminal tail of Cx32 (Figures 2.1, 2.4). Because six of the antibodies tested were raised against proprietary peptide sequences (Table 2.1), three algorithms (147-149) were used to identify the peptides most likely to raise an immunogenic response within the targeted region using (1) Antigenic

Figure 2.3 Four of the five Cx32 antibodies directed against the intracellular loop cross-react with a protein exhibiting the same mobility as Cx32 in Cx32$^{Y/-}$ brain but not Cx32$^{Y/-}$ liver under reducing/denaturing conditions. (A–E, left panel) Transmembrane schematics of the peptides for each Cx32 antibody, with the colored circles representing available information about each immunizing peptide sequence. Black brackets indicate primary sequence with the highest antigenic potential (see Table 2.2). (A–E, right panel) Cx32 immunoblots were performed using 10 μg liver or 30 μg of human (Hu) and murine hippocampus or brain lysates. Lines indicate size markers. Black arrowheads point to Cx32 specifically detected by all antibodies in liver (A–E) and AB5 in brain (E). White arrowheads indicate isoform variations specific to human samples (D, E). Arrows indicate the cross-reactive protein(s) detected by AB1 to AB4 in both Cx32$^{Y/+}$ brain tissue and the Cx32$^{Y/-}$ control (A–D). Note that this particular cross-reactive protein(s) migrates with the same mobility as Cx32 when separated on 12.5% Tris-HCl polyacrylamide gels.

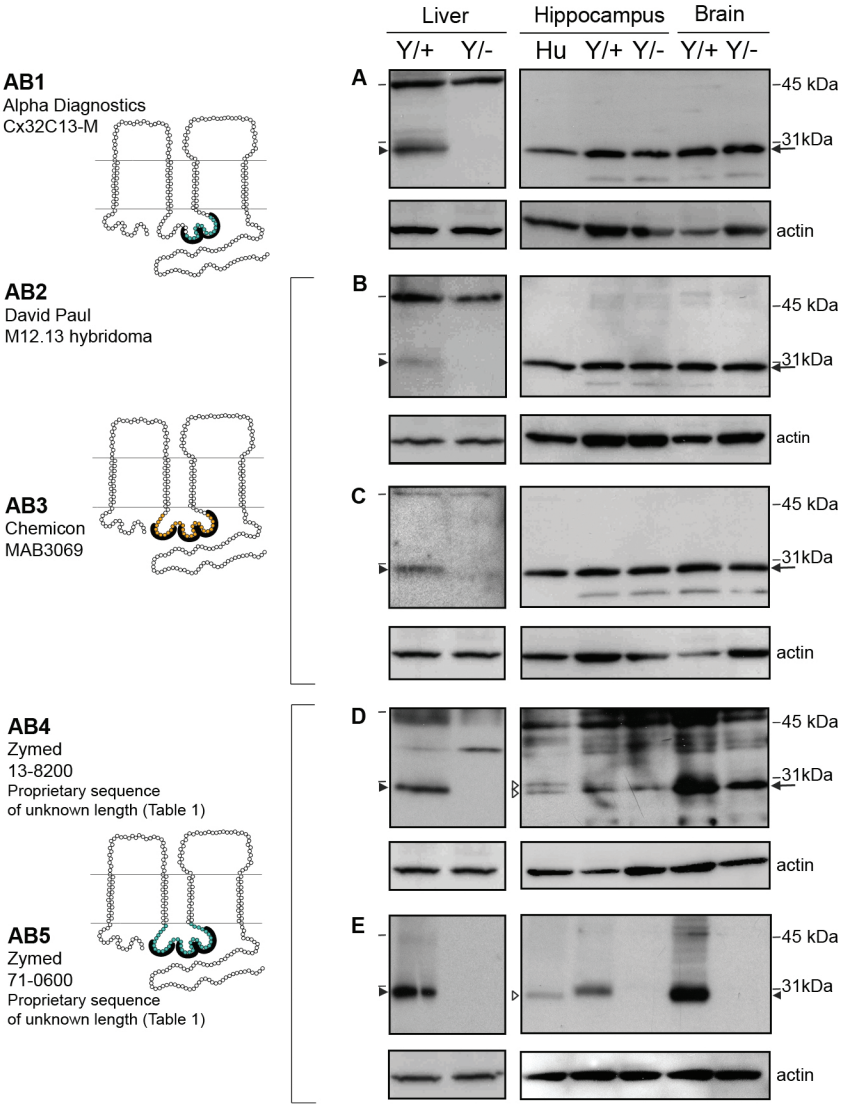
AB1
Alpha Diagnostics
Cx32C13-M
AB2
David Paul
M12.13 hybridoma
AB3
Chemicon
MAB3069
AB4
Zymed
13-8200
Proprietary sequence
of unknown length (Table 1)
AB5
Zymed
71-0600
Proprietary sequence
of unknown length (Table 1)
Liver
Hippocampus
Brain
Y/+
Y/-
Hu
Y/+
Y/-
Y/+
Y/-
A
B
C
D
E
45 kDa
31kDa
actin

Figure 2.3

Figure 2.4 Four of the five Cx32 antibodies directed against the C-terminal tail cross-react with a protein exhibiting the same mobility as Cx32 in Cx32$^{Y/-}$ brain but not Cx32$^{Y/-}$ liver under reducing/denaturing conditions. As in Figure 2.2, lines indicate size markers. Closed arrowheads point to Cx32 specifically detected by all antibodies in liver (A–E) and AB10 in brain (E). White arrowheads indicate isoform variations specific to human samples (C–E). Arrows indicate the cross-reactive protein(s) detected by AB6-9 in both Cx32$^{Y/+}$ brain tissue and the Cx32$^{Y/-}$ control (A–D). Note that this particular cross-reactive protein(s) migrates with the same mobility as Cx32 when separated on 12.5% Tris-HCl polyacrylamide gels. All other details are as in Figure 2.2.

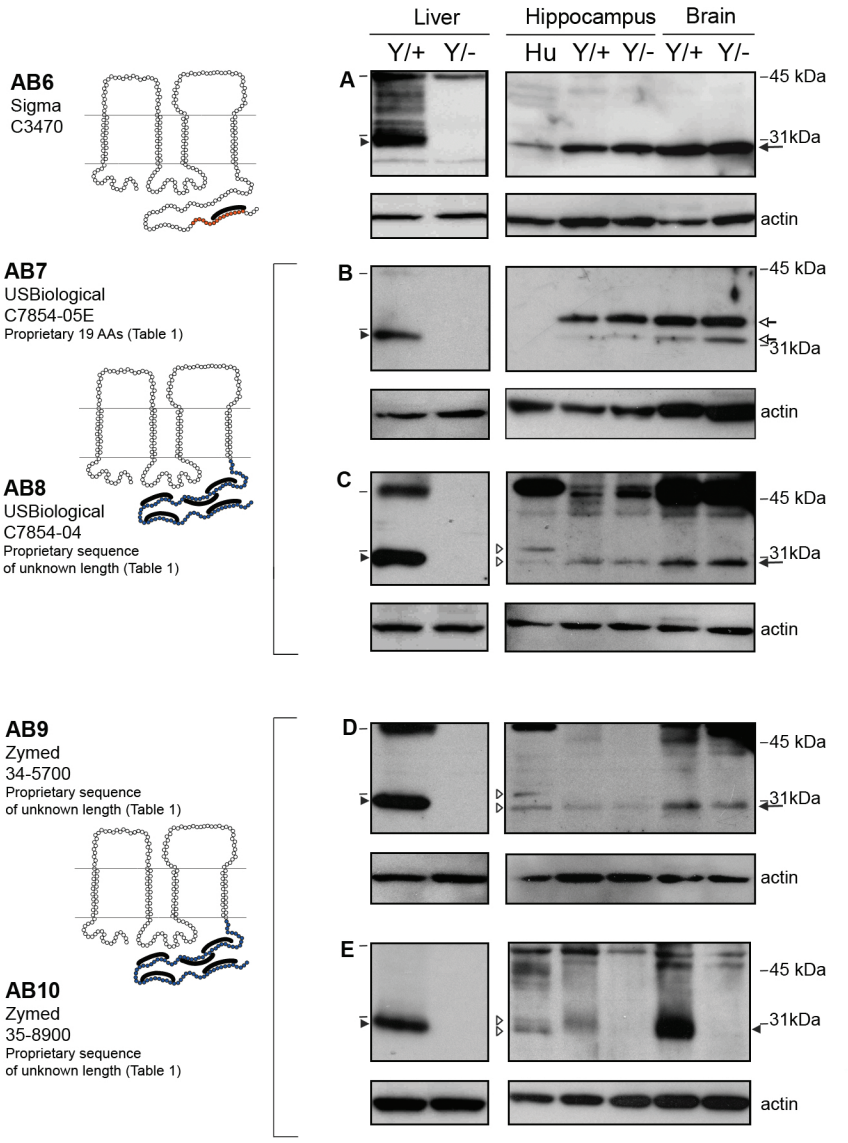
AB6
Sigma
C3470
AB7
USBiological
C7854-05E
Proprietary 19 AAs (Table 1)
AB8
USBiological
C7854-04
Proprietary sequence
of unknown length (Table 1)
AB9
Zymed
34-5700
Proprietary sequence
of unknown length (Table 1)
AB10
Zymed
35-8900
Proprietary sequence
of unknown length (Table 1)
Liver
Hippocampus
Brain
Y/+ Y/-
Hu Y/+ Y/- Y/+ Y/-
A
B
C
D
E
45 kDa
31kDa
actin

Figure 2.4

Peptide Tool (Immunomedicine group at Universidad Complutense de Madrid; Kolaskar and Tongaonkar method) and (2) Abie Pro 3.0 (Chang Biosciences; Hopp-Woods and Kyte-Doolittle hydrophillicities). For each prediction tool, the peptide size was set to 8. Results are presented in Table 2.2 and mapped in Figures 2.3 and 2.4.

	Site (amino acid position)[a]	Sequence	Hopp-Woods	Kyte-Doolittle	Kolaskar and Tongaonkar
IL epitopes	118-125	EEVKRHKV	✔	✔	
	98-105	QQHIEKKM	✔	✔	
	109-116 (112-119)	EGHGDPLH	✔	✔	✔ (GDPLHLEE)
C-term epitopes	220-227	AQRRSNPP	✔	✔	
	225-232	NPPSRKGS	✔	✔	
	239-246 (235-242)	SPEYKQNE	✔	✔	✔ (FGHRL SPE)
	252-259	SEQDGSLK	✔	✔	
	271-278	GLAEKSDR	✔	✔	

Abbreviations are as in Table 2.1.

[a]Sites are listed from most to least likely to raise an antibody response determined using three different bioinformatic tools: (1) Antigenic Peptide Tool (Immunomedicine group at Universidad Complutense de Madrid; Kolaskar and Tongaonkar method); (2) Abie Pro 3.0 (Chang Biosciences; Hopp-Woods and Kyte-Doolittle hydrophilicities).

Table 2.2 Antigenic sites along the IL and C-terminus of the Cx32 protein

In immunoblots of rat liver lysates, Cx32 migrates with a mobility of approximately 27-kDa under reducing/denaturing conditions (133). As expected, this same pattern was detected in murine liver (Figures 2.3, 2.4, Liver). All of the antibodies tested reacted specifically with a protein migrating just below the 31-kDa protein standard that was absent from the $Cx32^{Y/-}$ controls (Figures 2.3, 2.4, Liver, closed arrowhead). However, in lysates prepared from either whole brain or dissected hippocampus, seven of the antibodies (AB1 to AB4, AB6, AB8, AB9) detected a cross-reactive protein(s) with the same mobility as Cx32 in both $Cx32^{Y/+}$ and $Cx32^{Y/-}$ samples (Figures 2.3A to D, 2.4A, C, D, arrow). Some species

variation in reactivity was also observed. AB4 (Figure 2.3D, open arrowhead), AB8 (Figure 2.4C, open arrowhead), and AB9 (Figure 2.4D, open arrowhead) detected a doublet in human hippocampus, but only one species in murine brain/hippocampus. However, this single species was also evident in $Cx32^{Y/-}$ samples (Figures 2.3D, 2.4C, D, arrow). AB7 detected a doublet that migrated above the 31-kDa marker in all murine CNS samples (Figure 2.4B, open arrow) but failed to react with human protein (Figure 2.4B).

Only AB5 and AB10 detected Cx32 specifically in brain tissue (Figures 2.3E, 2.4E closed arrowhead). Some species variations were again observed in that the human protein appeared to migrate faster than murine Cx32 in hippocampal lysates (Figure 2.3E, open arrowhead), possibly as a doublet (Figure 2.4E, open arrowheads). The Cx32-specific signal detected using AB5 and AB10 was more abundant in lysates prepared from whole brain (and thus enriched in protein isolated from myelinated fiber tracts containing Cx32-expressing OLs) than in hippocampal lysates (Figures 2.3E, 2.4E, compare murine brain to hippocampus). This expression pattern is consistent with the expected localization of Cx32. Conversely, the signal intensity of the cross-reactive protein was comparable across samples (Figures 2.3A to D, 2.4A to D, arrow).

2.6.2 Cx32 immunofluorescent analysis is not confounded by cross-reactivity with other proteins in murine brain

To test whether this tissue-specific cross-reactivity is also detected in situ, immunofluorescent analysis of fixed 10 μm liver and brain cryosections was performed. As expected, all 10 of the antibodies detected Cx32 at hepatocyte plasma membrane in $Cx32^{Y/+}$ liver tissue, with minimal to no background reactivity in the $Cx32^{Y/-}$ controls (Figures 2.5A

Figure 2.5 Specific immunofluorescent detection of Cx32 in both liver and brain using intracellular loop-directed antibodies. (A–E) All five antibodies directed against epitopes localizing to the Cx32 intracellular loop detected Cx32 at hepatocyte plasma membrane in $Cx32^{Y/+}$ liver tissue (arrows, inset, Liver), with minimal to no background reactivity in the $Cx32^{Y/-}$ controls with the exception of some low level background staining of hepatocyte plasma membrane with AB5 (Liver). (A, B, D, E) Four antibodies detected fixed protein in situ in $Cx32^{Y/+}$ mouse hippocampal sections with (D) AB4 providing the most robust signal. Hippocampal immunostaining was evident at the plasma membrane of cells with expected OL and/or OPC morphology (arrows, inset, Hippocampus). None of the antibodies exhibited significant cross-reactivity with $Cx32^{Y/-}$ brain tissue. GrDG, granule cell layer of the dentate gyrus; PMNL, polymorphonuclear layer of the dentate gyrus; CA3c, CA pyramidal cell field 3c of the hippocampus. Scale bars, 50 μm.

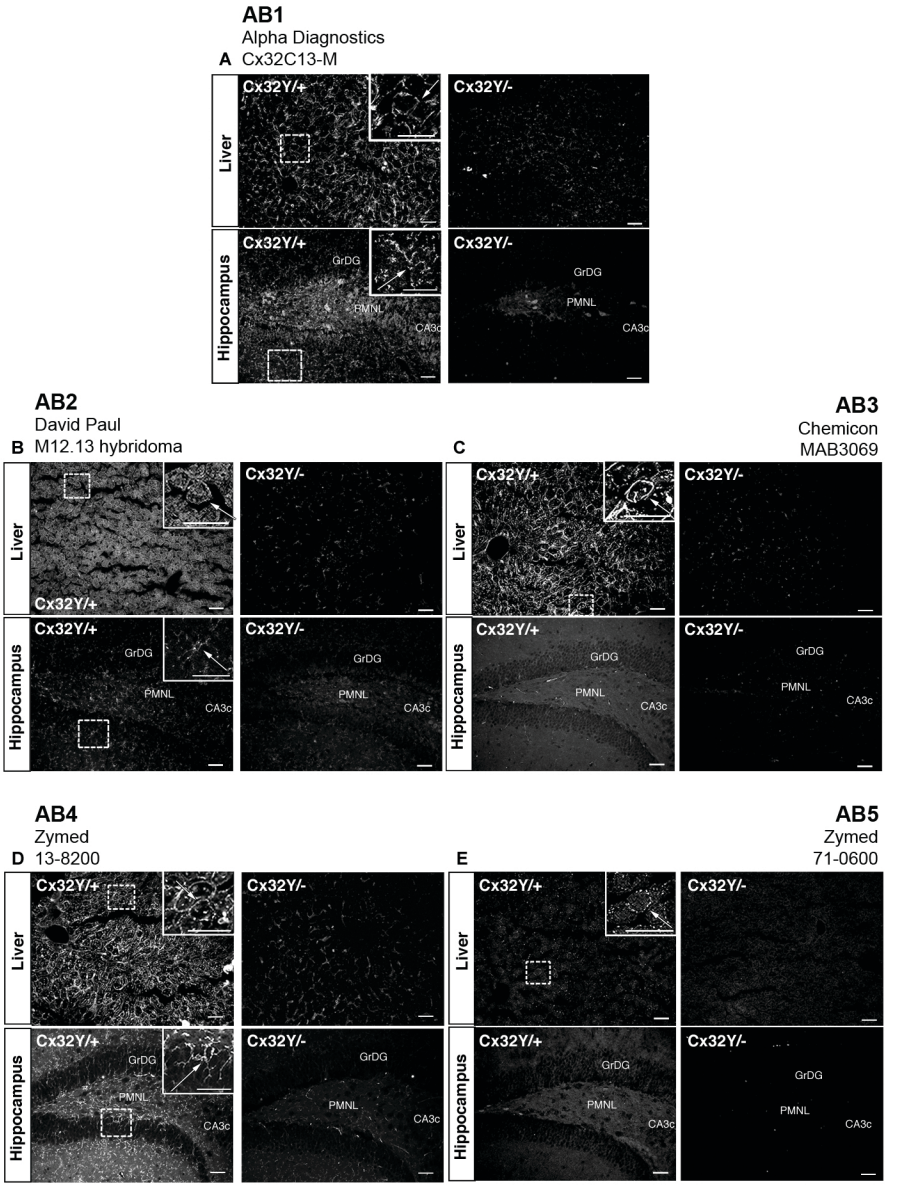
AB1
Alpha Diagnostics
A Cx32C13-M
Liver
Hippocampus
Cx32Y/+
Cx32Y/-
GrDG
PMNL
CA3c
AB2
David Paul
B M12.13 hybridoma
AB3
Chemicon
MAB3069
C
AB4
Zymed
D 13-8200
AB5
Zymed
71-0600
E

Figure 2.5

to E, 2.6A to E, Liver, arrows) with the exception of low level labeling of rare heptatocyte membranes with AB5 (Figure 2.6E, Liver). Some of the antibodies detected intracellular pools of Cx32 in addition to robust immunostaining at the membrane (AB2, AB7, and AB9) (Figures 2.5B, 2.6B, D, Liver). None of the antibodies exhibited significant cross-reactivity with $Cx32^{Y/-}$ brain tissue (Figures 2.5A to E, 2.6A to E, $Cx32^{Y/-}$ hippocampus), with the possible exception of AB6 at the highest concentration tested (Figure 2.6A). Each reagent was examined over a minimum of three concentrations. The dilution that gave optimal signal in brain sections is presented in Figure 2.5 and Table 2.1. Where specific signal was not detected in hippocampus (Figures 2.5C, 2.6) or corpus callosum (not shown), the dilution optimal for detection of Cx32 in liver sections is shown (Table 2.1, Figures 2.5, 2.6). Four of 10 antibodies tested (AB1, AB2, AB4, and AB5) reliably detected fixed protein in situ in mouse hippocampal sections (Figure 2.5A, B, D, E $Cx32^{Y/+}$ hippocampus) under the perfusion, postfixation, and cryoprotection protocol employed here, with AB4 providing the most robust signal (Figure 2.5D). All of these antibodies were directed against epitopes localizing to the intracellular loop of Cx32. Immunostaining was evident at the plasma membrane of cells with the expected OL and/or OPC morphology (Figures 2.5A, B, D, E $Cx32^{Y/+}$ hippocampus).

None of the C-terminal–directed antibodies produced a specific immunosignal under the fixation protocol defined in Materials and Methods (Figure 2.6A to E, $Cx32^{Y/+}$ hippocampus). Moreover, AB6 exhibited some artifactual labeling of neurons in both $Cx32^{Y/+}$ and $Cx32^{Y/-}$ sections (Figure 2.6A, compare labeling in the granular layer of the Dentate Gyrus, GrDG).

Figure 2.6 Specific immunofluorescent detection of Cx32 in liver but not brain using C-terminal tail-directed antibodies. (A–E) All five C-terminal antibodies detected Cx32 at hepatocyte plasma membrane in $Cx32^{Y/+}$ liver tissue (arrows, inset, Liver), with minimal to no background reactivity in the $Cx32^{Y/-}$ controls. No specific immunosignal was seen in the $Cx32^{Y/+}$ hippocampus under the specific fixation and processing conditions employed in this study. Abbreviations are as in Figure 2.4. Scale bars, 50 μm.

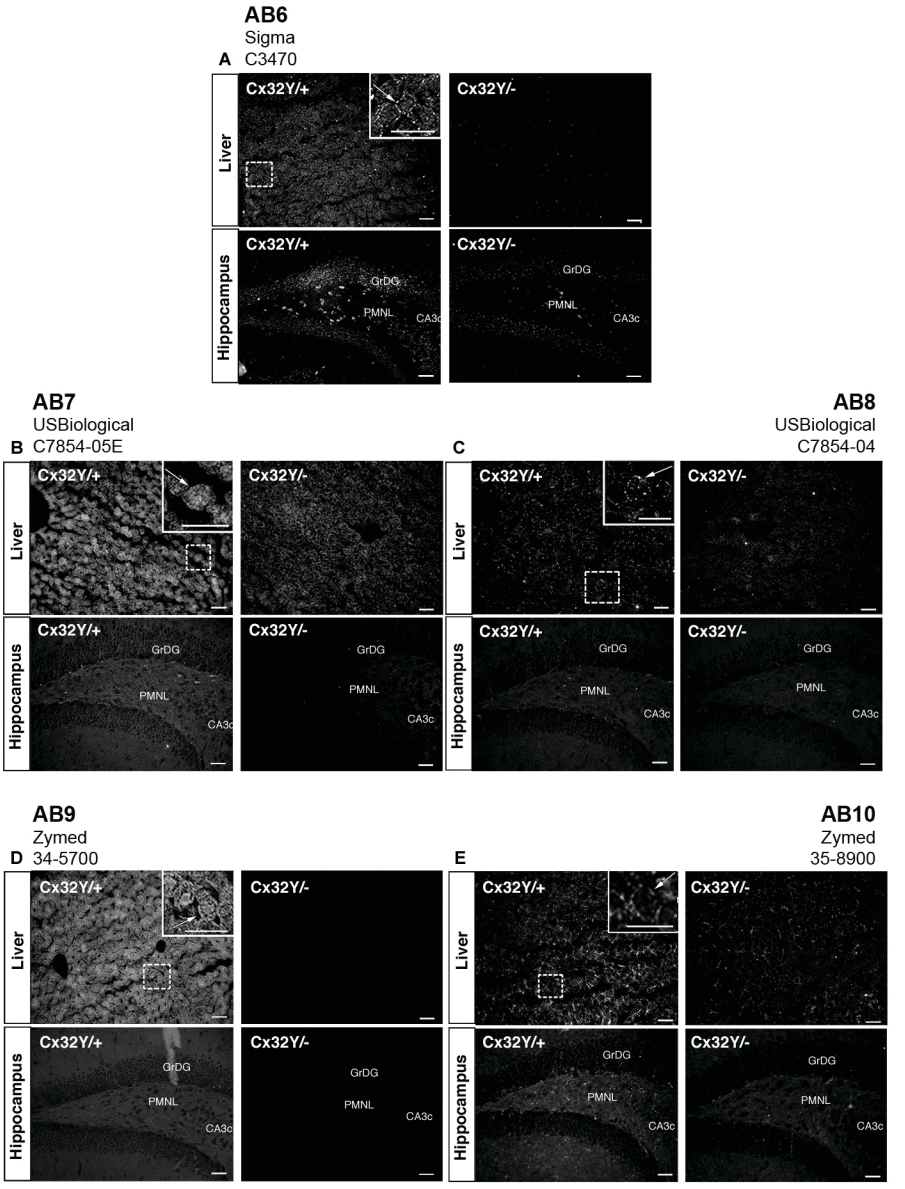
AB6
Sigma
A C3470
Cx32Y/+
Cx32Y/-
Liver
Hippocampus
GrDG
PMNL
CA3c
AB7
USBiological
B C7854-05E
AB8
USBiological
C C7854-04
AB9
Zymed
D 34-5700
AB10
Zymed
E 35-8900

Figure 2.6

2.6.3 Cross-reactivity is not observed when tertiary structure is maintained during initial detection.

Taken together, these results suggested that cross-reactivity is primarily detected in CNS tissue under reducing/denaturing conditions. These data led us to hypothesize that antibody cross-reactivity was dependent upon protein conformation. To test this hypothesis, the tertiary conformation of Cx32 was maintained during immunoprecipitation before being subjected to reducing/denaturing conditions in immunoblot detection. This approach restored specific detection of Cx32 in brain tissue (Figure 2.7A, Hippocampus and Brain, arrow). No cross-reactivity was observed in $Cx32^{Y/-}$ samples (Figure 2.7A). Mobility was consistent with that observed in liver lysate controls subjected to Western blotting only (Figure 2.7A, Liver, arrow). To further confirm that this specificity was conformation dependent, aliquots of the same protein samples used in the immunoprecipitations (Figure 2.7A) were analyzed by Western blotting (Figure 2.7B). Figure 2.7B reiterates the presence of a cross-reactive species in $Cx32^{Y/-}$ brain lysates immunoblotted under reducing/denaturing conditions.

2.6.4 The brain-specific cross-reactive protein(s) is expressed at higher levels than endogenous Cx32 and exhibits a distinct subcellular localization.

Although demonstrating that Cx32 can be detected specifically in brain tissue by immunoprecipitation, this finding also limited our capacity to identify cross-reactive CNS protein(s) by standard proteomic protocols. As an alternative, we attempted BARN to identify proteins present in the anti-Cx32–immunoreactive bands under reducing/denaturing conditions (145). We were, however, unable to detect Cx32 from on-membrane digestions of $Cx32^{Y/+}$ liver samples despite successful identification of other co-migrating proteins (data

Figure 2.7 Brain-specific cross-reactivity is not observed following immunoprecipitation. (A) Cx32 lysates were purified from native RIPA lysates using monoclonal AB1, resolved under denaturing conditions by SDS-PAGE, and immunoblotted using polyclonal AB6. In the first two lanes WT ($Cx32^{Y/+}$) and null-mutant ($Cx32^{Y/-}$) liver lysates were subjected to Western analysis under reducing/denaturing conditions. The following three lanes represent human hippocampus and murine brain samples from WT ($Cx32^{Y/+}$) and null-mutant ($Cx32^{Y/-}$) controls immunoprecipitated with AB1 under native conditions before denaturing/reducing SDS-PAGE separation and immunoblotting with AB6. Specific immunoaffinity purification of Cx32 is observed under these conditions. (B) Standard Western analysis with aliquots of the same samples used in (A) reiterate the cross-reactivity observed when protein is first detected under reducing/denaturing conditions.

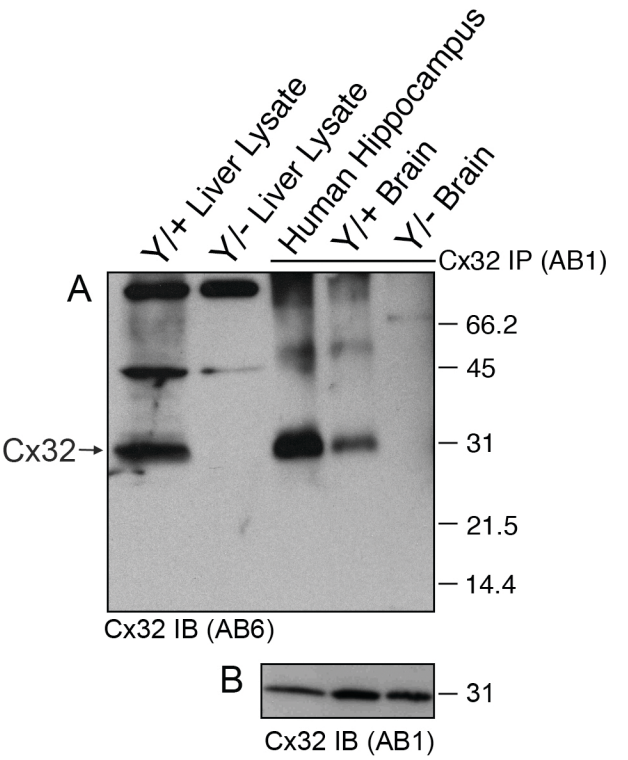
Y/+ Liver Lysate
Y/- Liver Lysate
Human Hippocampus
Y/+ Brain
Y/- Brain
Cx32 IP (AB1)
A
66.2
45
Cx32
31
21.5
14.4
Cx32 IB (AB6)
B
31
Cx32 IB (AB1)

Figure 2.7

not shown). As such, we lacked the appropriate positive control required to apply this profiling approach to identify the anti-Cx32–reactive proteins in $Cx32^{Y/+}$ and $Cx32^{Y/-}$ brain samples.

We turned to an analysis of AB1-reactive proteins under denaturing/reducing conditions using sucrose flotation gradients (Figure 2.8). In $Cx32^{Y/+}$ liver lysates, a single immunoreactive band was detected in the Triton X-100 insoluble pellet (Figure 2.8A, P) and fractions 4 to 6 (Figure 2.8A, fractions 4 to 6). This distribution reflected predominant localization to detergent-insoluble and detergent-soluble lipid raft and plasma membrane fractions and possibly to mitochondria. No reactivity was detected in any of the fractions derived from control $Cx32^{Y/-}$ lysates (Figure 2.8B). Artifactual labeling was evident in $Cx32^{Y/+}$ and $Cx32^{Y/-}$ brain samples, as demonstrated in Figures 2.3 and 2.4, but with a detectable difference that could be used to distinguish specific Cx32 signal. Using a 15% SDS-PAGE gel (as compared to 12.5% gels presented in Figures 2.3 and 2.4), a reproducible difference in mobility was evident between brain and liver samples (Figure 2.8A, B). A single AB1-immunoreactive band was present in brain lysates (Figure 2.8A, Brain) migrating approximately 4-kDa faster than in liver lysates (Figure 2.8A, Liver). Following sucrose gradient fractionation of brain protein, this predominant species was evident in both $Cx32^{Y/+}$ and $Cx32^{Y/-}$ lysates (Figure 2.8C, D), but could be distinguished from a less abundant, higher molecular weight species (Figure 2.8C, arrow) migrating at approximately the same position as liver-derived Cx32 (compare Figure 2.8A and C). This band was absent from $Cx32^{Y/-}$ fractions (Figure 2.8D). The fractions enriched for the higher molecular weight Cx32-specific band (fractions 4, 5, and 6) were also enriched for the mitochondrial marker coxIV, both lipid-raft–associated protein markers caveolin-1 and flotillin-1, and the plasma

Figure 2.8 Sucrose gradient fractionation reveals that the brain-specific cross-reactive protein is approximately 4-kDa smaller than Cx32 and exhibits a distinct subcellular localization. (A–D) Total tissue lysates (T) or the Triton X-100–insoluble pellet (P) and (E) fractions 1 to 10 obtained through sucrose fractionation were immunoblotted under denaturing/reducing conditions using AB1. To achieve maximal separation, proteins were separated on 15% Tris-HCl polyacrylamide gels. Each lane contains 5 μg of protein. (A) Sucrose gradient fractions of $Cx32^{Y/+}$ liver are compared to total tissue lysates of $Cx32^{Y/+}$ liver or brain. Note the ~4-kDa size difference between the species predominating in $Cx32^{Y/+}$ liver compared to brain. (B) Sucrose gradient fractions of $Cx32^{Y/-}$ liver are compared to total tissue lysates of $Cx32^{Y/+}$ liver or brain. No signal was detected in $Cx32^{Y/-}$ control lysates. (C) Sucrose gradient fractions of $Cx32^{Y/+}$ brain are compared to total brain lysates prepared from $Cx32^{Y/+}$ and $Cx32^{Y/-}$ mice (top panel). Exposure times were extended from that shown in A and B to enable detection of endogenous Cx32 in fractions 4 and 5 (arrow), migrating 4-kDa higher than the cross-reactive protein that was present at higher abundance and enriched in fractions 6 to 10. Lower panels characterize each fraction using organelle-specific markers: mitochondria (coxIV), lipid rafts (caveolin-1 and flotillin-1), plasma membrane (syntaxin-1), lysosomes (LAMP-1), and the trans-Golgi (golgin-97).

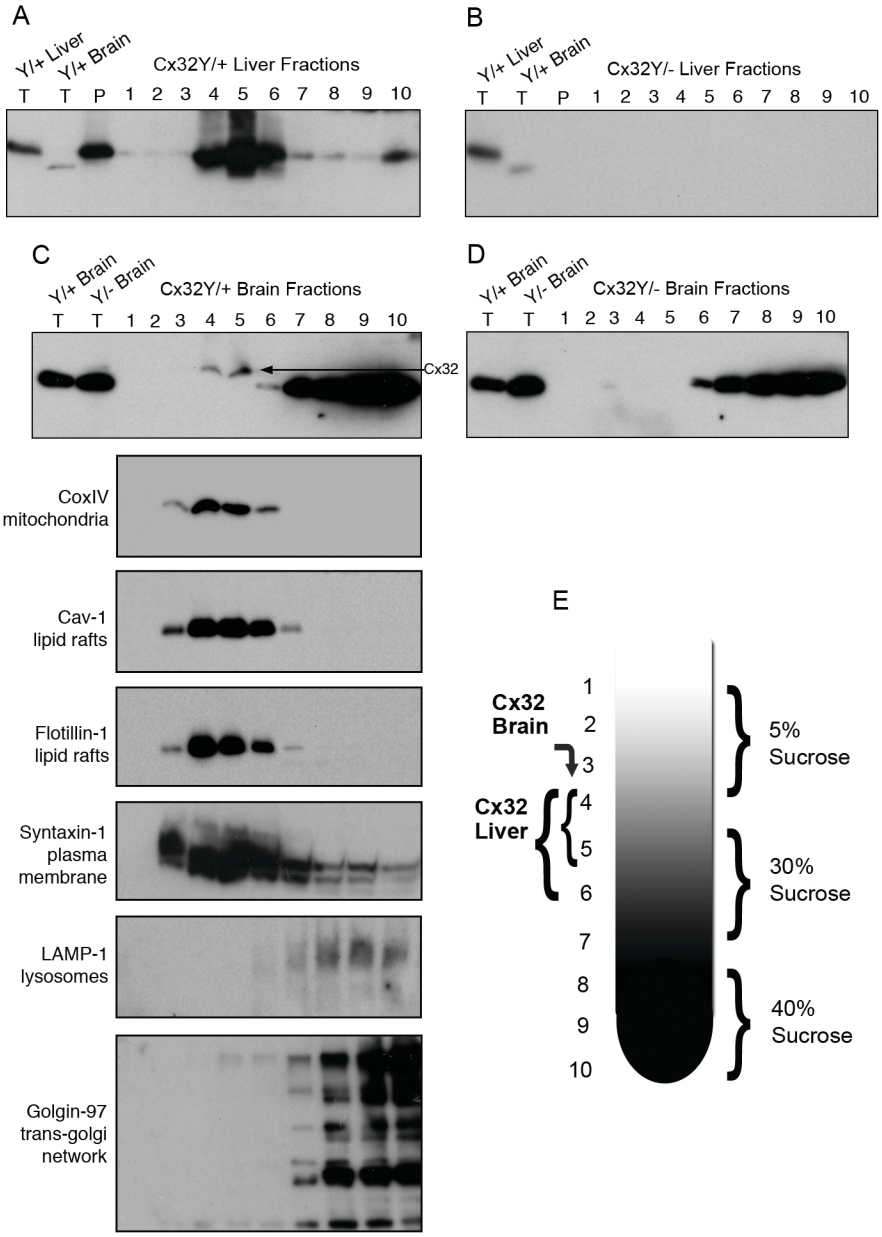
A
Y/+ Liver
Y/+ Brain
Cx32Y/+ Liver Fractions
T T P 1 2 3 4 5 6 7 8 9 10
B
Y/+ Liver
Y/+ Brain
Cx32Y/- Liver Fractions
T T P 1 2 3 4 5 6 7 8 9 10
C
Y/+ Brain
Y/- Brain
Cx32Y/+ Brain Fractions
T T 1 2 3 4 5 6 7 8 9 10
Cx32
D
Y/+ Brain
Y/- Brain
Cx32Y/- Brain Fractions
T T 1 2 3 4 5 6 7 8 9 10
CoxIV
mitochondria
Cav-1
lipid rafts
Flotillin-1
lipid rafts
Syntaxin-1
plasma
membrane
LAMP-1
lysosomes
Golgin-97
trans-golgi
network
E
Cx32
Brain
Cx32
Liver
1
2
3
4
5
6
7
8
9
10
5%
Sucrose
30%
Sucrose
40%
Sucrose

Figure 2.8

membrane marker syntaxin-1 (Figure 2.8C). This subcellular fractionation matched that observed in liver (Figure 2.8A). Conversely, the fractions enriched for the smaller cross-reactive protein (fractions 7 to 10) in both $Cx32^{Y/+}$ and $Cx32^{Y/-}$ lysates (Figure 2.8C, D) were enriched for LAMP-1 (lysosomes) and golgin-97 (trans-Golgi network) (Figure 2.8C). Together, these data suggested that brain, but not liver, expresses Cx32 at both plasma and perhaps mitochondrial membranes, as well as a cross-reactive protein enriched in the Golgi apparatus and lysosomes that is ~4-kDa smaller than Cx32.

2.6.5 Bioinformatic and western analyses suggest that the cross-reactive protein is not another connexin.

We were surprised that antibodies directed at both the intracellular loop and the C-terminal region of Cx32 exhibited the same cross-reactivity. To address this, we used a bioinformatics approach to identify candidate proteins based on the pattern of cross-reactivity detected in Figures 2.3 and 2.4, the antigenic sites predicted in Table 2.2, and the tissue-specific expression pattern.

Three potential antigenic sequences were detected within the intracellular loop of Cx32 (Figure 2.3A-E, Table 2.2). Two of these sequences were present in the peptide used to generate AB1. All three sequences were present in AB2 and AB3. Because AB1, AB2, and AB3 are monoclonal antibodies and generated identical banding patterns (Figure 2.3A-C), it is likely that they recognize the same epitope, either the EEVKRHKV or EGHGDPLH/GDPLHLEE antigenic sequences, located towards the C-terminus of the intracellular loop encompassed by the peptides used to generate AB1 (Table 2.2). Although the exact peptide sequence used to generate AB4 and AB5 was not disclosed by the manufacturer, both antibodies were distinguished from AB1-3 by a species variation in the

doublet detected in human samples (Figure 2.3D). Based on this difference, we hypothesized that they likely detect one of the two potential epitope variants (EGHGDPLH/GDPLHLEE) (Table 2.2). Only polyclonal AB5 demonstrated specificity and thus we hypothesized that it recognizes the only antigenic sequence that does not overlap with AB1 (i.e., QQHIEKKM) located towards the N-terminus of the intracellular loop (Table 2.2). This analysis predicted that the cross-reactive protein would contain contiguous amino acid sequences, exposed under reducing/denaturing conditions that share the EEVKRHKV and EGHGDPLH/GDPLHLEE but not the QQHIEKKM epitopes with Cx32.

In the C-terminal tail of Cx32, five potentially antigenic sequences were detected (Figure 2.4A-E, Table 2.2). Polyclonal AB6 (Figure 2.4A) was directed against a known sequence that encompassed the most distal C-terminal tail antigen (GLAEKSDR, Table 2.2). Polyclonal AB7 generated a pattern distinct from all of the other reagents and thus likely recognizes epitope(s) distinct from AB6 (Figure 2.4B). AB8 and AB9 detected a doublet in human brain samples and thus likely recognize the same species-specific antigenic sequences (Figure 2.4C, D). AB10 was Cx32-specific and, as a monoclonal antibody, is raised against a single epitope (Figure 2.4E). Based on this pattern, we predicted that the cross-reactive protein would contain, in addition to the epitopes recognized by the intracellular loop antibodies, contiguous sequences in primary sequence homologous to at least three and likely four of the Cx32 C-terminal tail epitopes but no significant homology with the fifth predicted antigenic sequences (recognized by Cx32-specific AB10).

We used these assumptions to establish search criteria for other connexins with sufficient contiguous antigenic peptide sequences, tissue specificity, and electrophoretic mobility for potential cross-reactivity. Two connexins (Cx26 and Cx29) met some but not all

parameters. Only Cx30 met all criteria. The intracellular loop EEVKRHKV epitopes exhibited a significant alignment score of 62% whereas alignment of the EGHGDPLH/GDPLHLEE antigenic sequences met the minimum number of adjacent amino acids required to raise an antigenic response (contiguous alignment score of 25). Further, as predicated, the QQHIEKKM epitope was not found in the Cx30 primary sequence (alignment score of 12%). Four of the five Cx32 C-terminal tail epitopes produced significant alignment scores of 25-62. The fifth epitope NPPSRKGS did not exhibit any significant alignment in contiguous sequence (≤12%). Despite this potential homology, stringent testing with null-mutant controls provided conclusive evidence that Cx32 antibodies do not cross-react with Cx30 (Figure 2.9). Using lysates prepared from $Cx29^{-/-}$, $Cx29^{-/-}/Cx32^{Y/-}$, or $Cx30^{-/-}$ brain tissue, the cross-reactive protein was still present in double- and single-null-mutant brain tissue and thus was not Cx29 or Cx30 (Figure 2.9A, B). Further, although Cx26 could be detected abundantly in WT mouse liver and, weakly in brain, Cx26 protein levels were substantively reduced in $Cx32^{Y/-}$ brain or liver tissue (Figure 2.9C) and thus Cx26 is unlikely to represent the cross-reactive protein. This reduction in Cx26 protein levels in Cx32 null-mutant animals is consistent with previous studies (34).

When placed in context with the subcellular localization evident in sucrose gradient fractionation (Figure 2.8), these data provided converging evidence to indicate that the cross-reactive protein is likely not another connexin but rather an immature (Golgi-localized) or partially degraded (lysosome-localized) subunit of a larger unidentified protein complex with homologous epitopes unmasked only after protein denaturation and the reduction of disulfide bonds.

Figure 2.9 Cx32 antibodies do not cross-react with Cx26, Cx29, or Cx30 under denaturing/reducing conditions. (A) Liver and brain samples were prepared from wild-type ($Cx32^{Y/+}$), $Cx32^{Y/-}$, and $Cx29^{-/-}$. $Cx32^{Y/-}/Cx29^{-/-}$, or $Cx30^{-/-}$ null-mutant mice, separated on 15% Tris-HCl polyacrylamide gels, and immunoblotted for Cx32 using monoclonal AB1. To distinguish between the cross-reactive protein(s) and endogenous Cx32 in brain samples, fraction 5 lysate from sucrose gradient separations (see Figure 2.7) of WT ($Cx32^{Y/+}$) was included as a positive control. All brain samples, except WT brain fraction 5, exhibited the lower molecular weight cross-reactive band. Arrowheads indicate Cx32; arrows indicate the cross-reactive (CR) protein. (B) Immunoblotting of Cx30 in lysates prepared from human brain, wild-type mouse brain and liver, and $Cx30^{-/-}$ brain confirmed the presence of Cx30 in CNS tissue (arrowhead), absent from liver. Specificity was established using null-mutant controls. (C) Cx26 protein, present in $Cx32^{Y/+}$ brain and liver (arrowhead), was below detection levels in $Cx32^{Y/-}$ tissue.

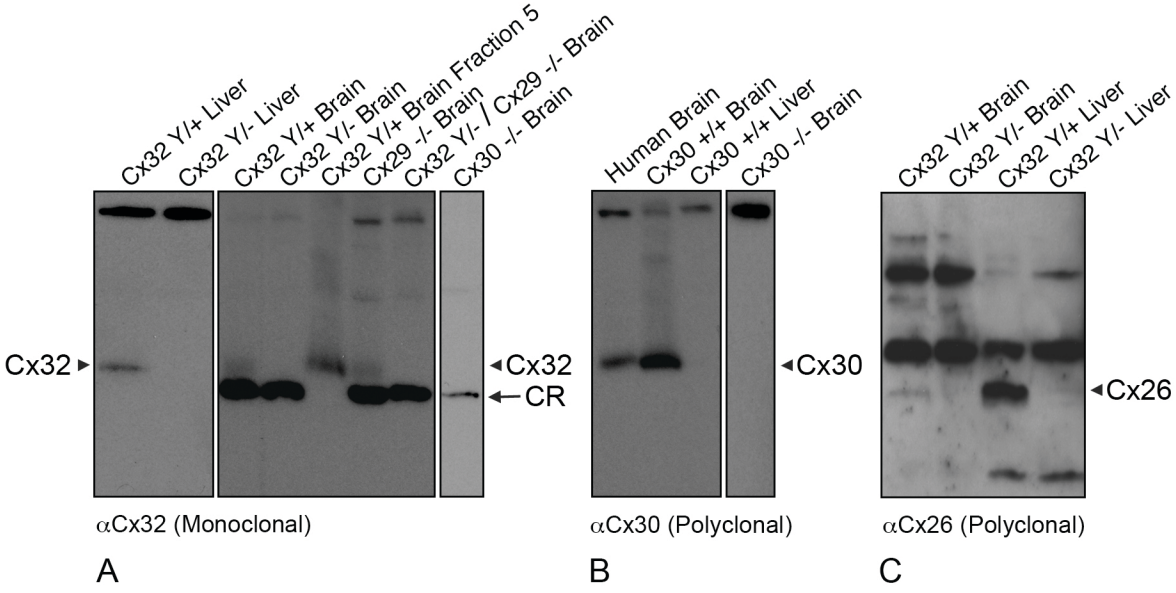
Cx32 Y/+ Liver
Cx32 Y/- Liver
Cx32 Y/+ Brain
Cx32 Y/- Brain
Cx32 Y/+ Brain Fraction 5
Cx29 -/- Brain
Cx32 Y/- / Cx29 -/- Brain
Cx30 -/- Brain
Cx32
Cx32
CR
αCx32 (Monoclonal)
A
Human Brain
Cx30 +/+ Brain
Cx30 +/+ Liver
Cx30 -/- Brain
Cx30
αCx30 (Polyclonal)
B
Cx32 Y/+ Brain
Cx32 Y/- Brain
Cx32 Y/+ Liver
Cx32 Y/- Liver
Cx26
αCx26 (Polyclonal)
C

Figure 2.9

2.7 Discussion

Here, we characterize a tissue-specific cross-reactivity with multiple commonly used Cx32 antibodies that impacts upon the interpretation of Western blots performed using CNS tissue. Although all 10 of the reagents tested reliably detect Cx32 in liver as expected, we found that 8 of these reagents cross-react with a CNS protein(s) that exhibits the same approximate electrophoretic mobility as Cx32. Comparing immunoblotting, immunofluorescence, and immunoprecipitation detection methods using $Cx32^{Y/+}$ and $Cx32^{Y/-}$ brain and liver tissue, we concluded that this artifactual cross-reactivity is only observed under reducing/denaturing conditions and does not complicate analyses that retain tertiary protein structure during initial immunodetection or immunopurification (i.e., in situ immunofluorescence or immunoprecipitation studies). These data indicate that cross-reactivity is likely the result of the unmasking of epitopes found in primary sequence not accessible in situ upon proper protein folding. Finally, two antibodies, polyclonal AB5 and monoclonal AB10 (Table 2.1), reliably detected Cx32 in Western analysis of brain tissue. These data are consistent with previous reports wherein AB5 and AB10 were shown to specifically recognize Cx32 in brain and liver (141), emphasizing the need for careful choice of antibody and methodology in the study of Cx32 in brain tissue.

To provide further insight into this tissue specificity, we identified three highly antigenic sites in the intracellular loop and five highly antigenic sites in the C-terminus of the Cx32 protein sequence. Based on these sites and the banding patterns produced by each of antibodies tested in Cx32 null-mutant tissue, we predicted that the primary sequence of the cross-reactive protein(s) would exhibit strict homology to six of these eight antigenic sites but would not contain the two unique epitopes that rendered AB5 and AB10 Cx32

specific. Moreover, the protein would be expressed in brain but not liver. Bioinformatic analyses encompassing all of these criteria identified only one protein, Cx30, with potential to cross-react under denaturing/reducing conditions. However, direct assessment revealed that the brain-specific cross-reactive protein was still present in brain lysates prepared from not only $Cx30^{-/-}$ but also $Cx29^{-/-}/Cx32^{Y/-}$ mice and in the absence of Cx26. Further, sucrose gradient fractionation analyses revealed that the antigenically related cross-reactive protein(s) exhibited an ~4-kDa size difference, localized to different subcellular compartments, and was expressed at higher levels than Cx32 in brain tissue. Cx32 was found in fractions enriched for plasma membrane, lipid rafts, and mitochondrial markers; the brain-specific cross-reactive protein was found in fractions enriched for golgi and lysosome markers. This subcellular localization indicates that the cross-reactive protein is likely not a member of the connexin family.

In summary, this study addresses a CNS-specific problem in Cx32 antibody cross-reactivity that has been reported anecdotally but not analyzed directly. We show that, although all of the reagents tested are specific for Cx32 in liver, protein denaturation/reduction unmasks epitopes present in primary sequence of a CNS-specific protein, likely not another connexin, that exhibits the same approximate electrophoretic mobility as Cx32 and is present in mouse brain prepared from multiple connexin null-mutants. We show that this technical obstacle can be easily overcome by choice of antibody, careful size analysis, or exclusive use of immunoprecipitation to quantify changes in Cx32 protein expression. These data are presented with the intent of reducing the amount of time laboratories currently expend in validating changes in Cx32 expression in CNS.

CHAPTER 3: PERFORMING VAGINAL LAVAGE, CRYSTAL VIOLET STAINING, AND VAGINAL CYTOLOGICAL EVALUATION FOR MOUSE ESTROUS CYCLE STAGING IDENTIFICATION

3.1 Objective of this study

The main objectives of this study were to a) minimize invasive procedures required to accurately assess and differentiate between the four stages of the estrous cycle by collection and analysis of predominant cell typology in vaginal smears and b) determine how these changes can be interpreted with respect to endocrine status. **This study was published in the Journal of Visualized Experiments** as McLean, A. C., Valenzuela, N., Fai, S. & Bennett, S. A. Performing vaginal lavage, crystal violet staining, and vaginal cytological evaluation for mouse estrous cycle staging identification. *Journal of visualized experiments : JoVE*, e4389 (2012).

3.2 Statement of author contributions

N. Valenzuela (Carleton University) performed all of technological audio/visual aspects and animations in this study under the supervision of Dr S. Fai. Manuscript, storyboard, script and scientific content of this study was prepared in full by A.C. McLean with critical insight and advice from all authors. The complete study was performed under the supervision of Dr S. Bennett who designed the experiments, analyzed the data, and wrote the manuscript with A.C. McLean.

3.3 Introduction

A rapid means of assessing reproductive status in rodents is useful not only in the study of reproductive dysfunction but is also required for production of new mouse models of disease and investigations into the hormonal regulation of tissue degeneration (or regeneration) following pathological challenge. Here we describe how to identify the stage of the reproductive cycle a female mouse is in on any given day by simple, non-invasive cytological assessment of the predominant cell type present in vaginal smears.

The murine reproductive (or estrous) cycle is divided into 4 stages: metestrus, diestrus, proestrus, and estrus (150). Defined fluctuations in the circulating levels of the ovarian steroids, 17-β-estradiol and progesterone, the gonadotropins, luteinizing and follicle stimulating hormones, and the luteotropic hormone prolactin, signal transition through these reproductive stages (151, 152). This is a methodological techniques paper and thus is presented in protocol format followed by results and discussion.

3.4 Experimental Procedures

Preparing Reagents

1. For sterile vaginal lavage, autoclave ddH_2O and store in a tightly sealed container at room temperature until needed.

2. For cytological assessment, add 0.1 g of crystal violet powder to 100 mL of ddH_2O. Mix well. Crystal violet stain (0.1%) can be stored in a tightly sealed container at room temperature until needed.

Collecting Vaginal Cells (Vaginal Lavage)

1. Place a latex bulb on the end of a sterile 200 µL tip and draw up approximately 100 µL of sterile ddH_2O using the gradations on the tip as a volume guideline.

2. Lift the mouse out of her cage and place her on the cage hopper (lid) with her hind/rear end towards you.

3. Firmly grasp the tail and elevate the rear end. The mouse will now have only her front paws grasping the hopper. At this point the mouse may urinate. If so, wait until urination stops. Should there be urine left at the entrance to the vaginal canal, you may want to rinse the opening with excess ddH_2O using a separate tip (i.e., not your sample collection tip).

4. Place the end of the ddH_2O-filled tip at the opening of the vaginal canal taking care to not penetrate the orifice as vaginal (and cervical) stimulation can induce pseudopregnancy in rats (153, 154). Recent reports suggest mice are less susceptible to this effect nonetheless care should be taken to minimize the degree of invasiveness in repeated analyses (155).

5. Gently depress the bulb to expel a quarter to half of the volume of water (~25-50 µL) at the opening of vaginal canal. The liquid will spontaneously aspirate into the canal without tip insertion. Slowly release the pressure exerted on the bulb. The fluid will withdraw back into the tip. Avoid releasing pressure too quickly to prevent aspiration of fluid into the bulb. A filtered tip may be useful for this purpose.

6. Repeat the previous step 4-5 times using the same tip, bulb, and fluid to obtain a sufficient number of cells in a single sample.

7. Place the fluid on glass slide, and allow the smear to completely dry at room temperature. Once dry, these estrous smears can be stained immediately or stored and stained at a later date.

Cytological Staining using Crystal Violet

1. Place the dry slide in a coplin jar (or other comparable staining vessel) containing the crystal violet stain for 1 min.

2. Remove to a second coplin jar containing ddH_2O. Wash the slide with ddH_2O for 1 min. Repeat.

3. Remove the excess ddH_2O from the edges of the slide with a light-duty tissue wiper, avoiding contact with the stained smear.

4. Pipette approximately 15 μL of glycerol on top of the smear and coverslip. Alternatively, other histological mounting reagents can be utilized to obtain a more permanent, non-diffusing stain.

Vaginal Cytology

1. Examine the smear under light microscopy to determine cell types present. Microscopic examination should be done immediately after staining as the crystal violet will diffuse from the cells over time when using glycerol for coverslipping. Photomicrographs should be taken at time of analysis to document cytology.

2. Start by examining the entire smear at a lower magnification. Select a representative area and move to a higher magnification. You will see cornified squamous epithelial cells, leukocytes, and/or nucleated epithelial cells (Figure 3.1A-C). The ratio of cells present will allow you to determine the estrous stage of your mouse at time of sample collection (Figure 3.1D-G) and her immediate hormonal status (Figure 3.2).

Figure 3.1 Cytological assessment of vaginal smears can be used to identify estrous stage. Three main cell types are detected in vaginal smear samples: (A) nucleated epithelial cells, (B) cornified squamous epithelial cells, and (C) leukocytes. The ratio of these cell types present in the smear can be used to identify mice in (D) proestrus, (E) estrus, (F) metestrus, or (G) diestrus as described in representative results. Black arrowheads in E, F, and G point to representative cornified squamous epithelial cells. Black arrows in C, F, and G point to representative leukocytes. White arrows in D and G highlight representative nucleated epithelial cells.

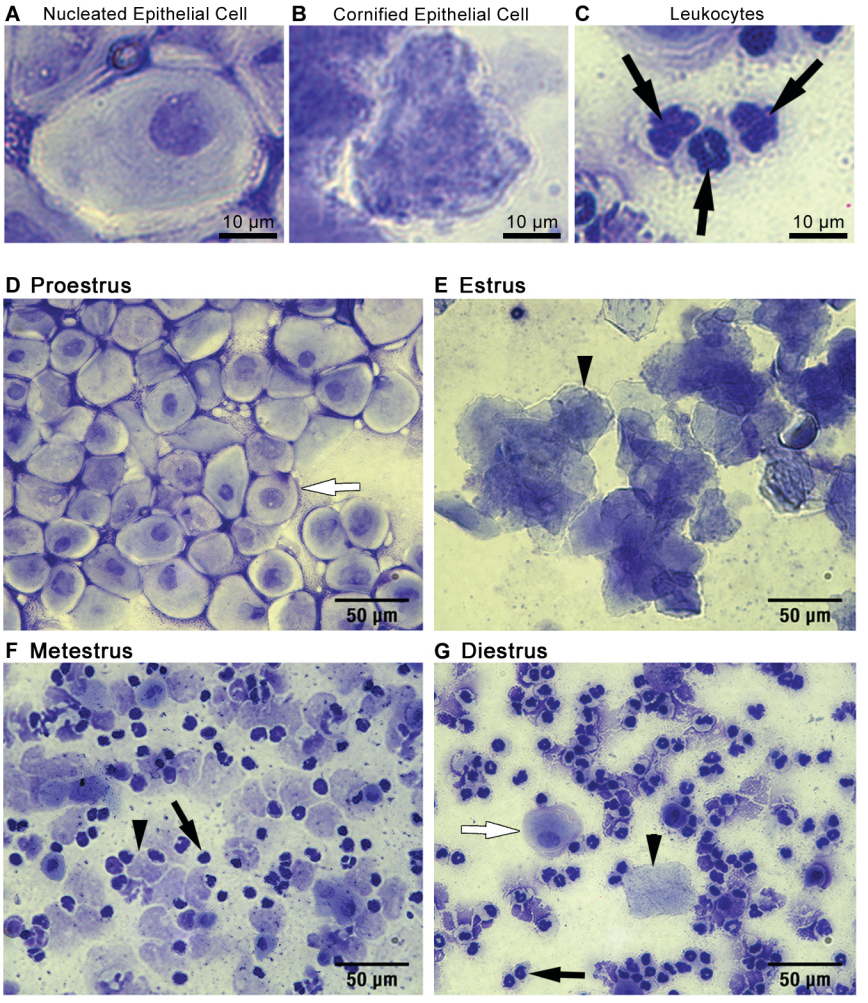
A Nucleated Epithelial Cell
B Cornified Epithelial Cell
C Leukocytes
10 µm
10 µm
10 µm
D Proestrus
E Estrus
50 µm
50 µm
F Metestrus
G Diestrus
50 µm
50 µm

Figure 3.1

Figure 3.2 Vaginal smear cytology reflects underlying endocrine events. Details are as provided in Discussion.

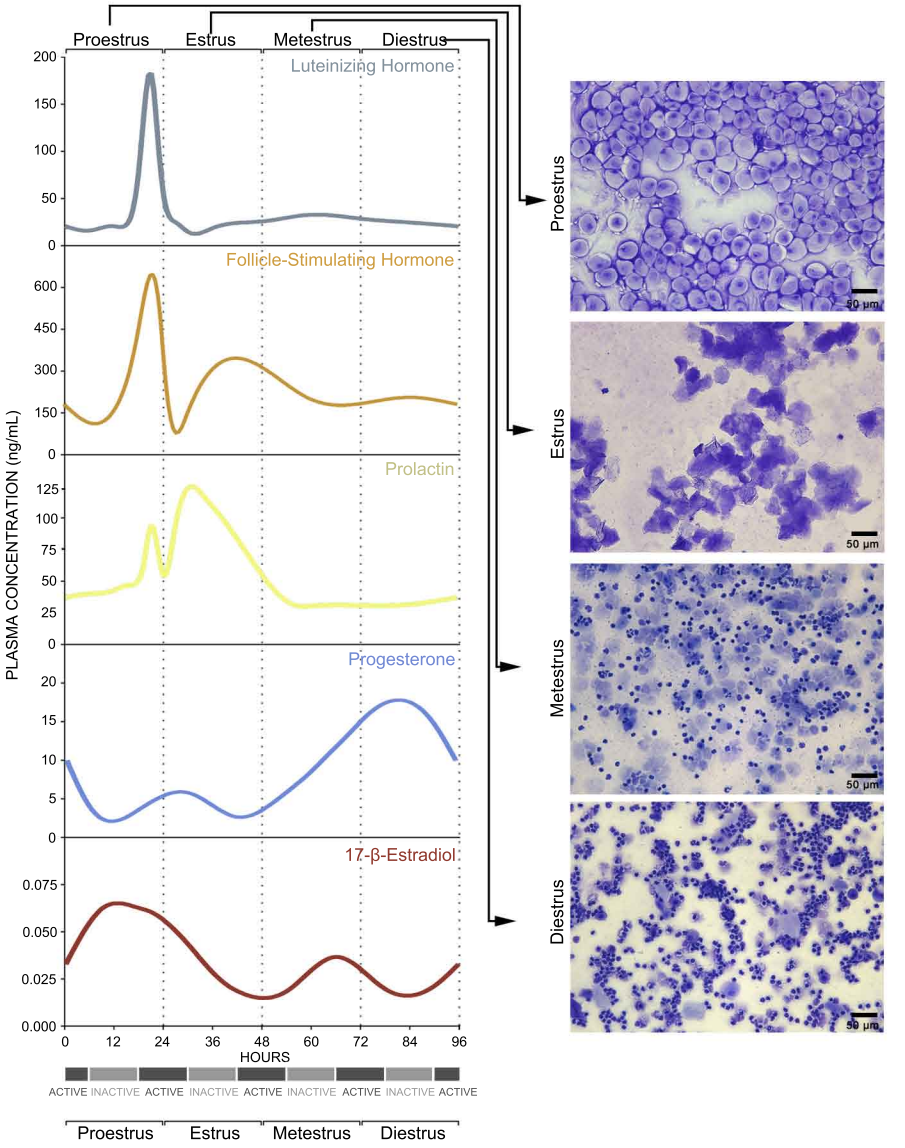
Proestrus
Estrus
Metestrus
Diestrus
Luteinizing Hormone
Follicle-Stimulating Hormone
Prolactin
Progesterone
17-β-Estradiol
PLASMA CONCENTRATION (ng/mL)
HOURS
ACTIVE INACTIVE ACTIVE INACTIVE ACTIVE INACTIVE ACTIVE INACTIVE ACTIVE
50 µm

Figure 3.2

3.5 Results

3.5.1 Cytological assessment of vaginal smears.

Three primary cell types can be detected in vaginal smear samples: (1) nucleated epithelial cells (Figure 3.1A), (2) cornified squamous epithelial cells (Figure 3.1B), and (3) leukocytes (Figure 3.1C). Nucleated epithelial cells have a lightly stained cytoplasm, darker stained plasma membrane, and an oval nucleus (Figure 3.1A). Cornified squamous epithelial cells are uniformly stained, more polygonal in shape than their nucleated epithelial predecessors, and lack a nucleus (Figure 3.1B). Polymorphonuclear leukocytes can be distinguished from epithelial cells by their irregular shape, darkly stained polymorphic nuclei, and small size (Figure 3.1C, black arrows). Should urine contamination be present in the smear, uric acid crystals are readily detected by their crystalline structures dissimilar to any expected cell types (Figure 3.3). Should this occur, and obscure detection of predominant cell type, the smear should be discarded and not used for staging purposes.

3.5.2 Cytological assessment can be used to identify estrous stage.

The relative ratio of cell types observed in smears can be used to identify the stage of the estrous cycle of your mouse on the day of sample collection (Figure 3.1D-G). During proestrus, cells are almost exclusively clusters of round, well-formed nucleated epithelial cells (Figure 3.1D, representative cell indicated by white arrow). During estrus, cells are predominantly cornified squamous epithelial cells, present in densely packed clusters (Figure 3.1E, representative cell indicated by arrowhead). During metestrus, small darkly stained leukocytes predominate (Figure 3.1F, representative cell indicated by black arrow). Cornified squamous epithelial cells may be observed, often in fragments, (Figure 3.1F,

Figure 3.3 Uric acid crystals may be present following crystal violet staining of urine-contaminated samples. (A) Crystals are transparent and can be of various sizes (arrows and boxed region magnified in (B)). No cells are present in this field. Should uric acid crystal contamination within fields used for cytological staining, it may be difficult to accurately identify cell types present and the smear should be discarded. Scale bars = 50 μm.

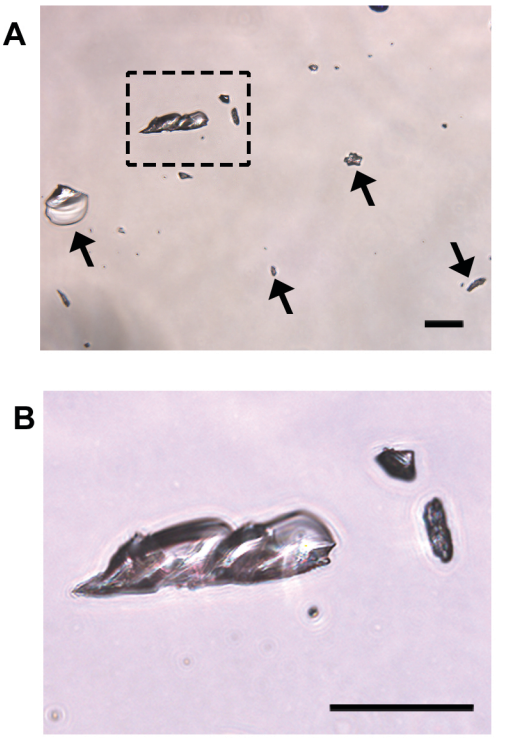

Figure 3.3

representative cell indicated by black arrowhead). During diestrus, rare cornified squamous epithelial cells may still be present (Figure 3.1G, representative cell indicated by black arrowhead), however leukocytes still predominate (Figure 3.1G, representative cell indicated by black arrow). Metestrus can be distinguished from diestrus by the appearance of nucleated epithelial cells in diestrus (Figure 3.1G, representative cell indicated by white arrow).

3.6 Discussion

Entry into metestrus coincides with the peak increase of a small surge in circulating follicle stimulating hormone levels initiated in estrus (152). In early metestrus, circulating levels of 17-β-estradiol, progesterone, prolactin, and luteinizing hormone are all relatively low (151, 152). Over the course of metestrus, there is a transient increase in plasma progesterone concentrations and a moderate rise in 17-β-estradiol levels (151). Entry into diestrus occurs when this first surge in circulating progesterone levels peak (151). Progesterone levels then drop to baseline (151). In proestrus, there is a sequential and dramatic rise in circulating levels of all five key hormones (151, 152). Concentrations of 17-β-estradiol peak first, followed by prolactin, progesterone, luteinizing hormone and follicle stimulating hormone (151, 152). Animals enter estrus following ovulation at which point there is a dramatic drop in circulating hormonal levels (151, 152). During estrus, there is a small second surge in 17-β-estradiol, a peak in prolactin, and a minor increase in circulating follicle stimulating hormone concentrations that initiate transition to metestrus (151, 152).

Changes in cell typology reflect these underlying endocrine events and the relative ratio of epithelial cells, cornified cells, and leukocytes detected in vaginal smears can be used to identify each of the estrous stages (150). The proestrus phase of the estrous cycle corresponds to the human follicular phase of the menstrual cycle (156) and is defined by a pre-ovulatory increase in circulating 17-β-estradiol levels (151), as well as a small surge in prolactin (152) (Figure 3.2, Proestrus, left panel). The increase in 17-β-estradiol indirectly stimulates gonadotropin-releasing hormone neurons in the hypothalamus and septum that, in turn, activate responsive cells in the anterior pituitary to release luteinizing hormone and follicle-stimulating hormone into the circulation (157, 158) (Figure 3.2, Proestrus, left panel). In vaginal smears taken from animals in proestrus, cells are almost exclusively oval nucleated epithelial cells (Figure 3.1D, Figure 3.2, Proestrus, right panel). The peak in follicle-stimulating hormone levels signals ovulation and entry into estrus (159, 160). During estrus, 17-β-estradiol levels decline and prolactin levels peak (151, 152) (Figure 3.2, Estrus, left panel). Vaginal smears are characterized by almost exclusive detection of irregular-shaped cornified squamous epithelial cells often in clumps (Figure 3.1E, Figure 3.2, Estrus, right panel). Entry into metestrus coincides with a continuous rise in progesterone hormone levels (151) and corresponds to the beginning of human luteal phase (161) (Figure 3.2, Metestrus, left panel). As progesterone levels start to rise and there is a small surge in 17-β-estradiol levels in response to corpus luteum activation (151, 162, 163) (Figure 3.2, Metestrus, left panel). The cell types present in vaginal smears during this stage are fragmented, cornified epithelial cells and smaller darker stained leukocytes (Figure 3.1F, Figure3. 2, Metestrus, right panel). Finally, entry into diestrus in mice occurs and circulating progesterone levels peak (151), corresponding to the human late luteal phase (161).

Regression of the corpus luteum leads to a subsequent sharp decline in progesterone levels (164, 165) (Figure 3.2, Diestrus, left panel). Leukocytes predominate in smears during diestrus. The frequency of cornified epithelial cells is reduced and nucleated epithelial cells begin to be detected just prior to transition to proestrus (Figure 3.1G, Figure 3.2, Diestrus, right panel). Although the staining method described here is the simplest procedure that can be performed in any laboratory, other methods can provide additional details. For example, using Papanicolaou staining, the maturity of nucleated epithelial cells can be distinguished with less mature cells stained turquoise and more mature cells pink- or orange-stained. These differences can be used to stage early or late proestrus (166).

In summary, this simple, routine protocol can be used to estimate daily hormonal fluctuations and establish estrous stage in experimental mice without altering reproductive status if the following precautions are taken. Sampling should be performed no more than once daily using the non-invasive protocol described here as compared to repeated penetration of the vaginal canal, aspiration, and agitation. This can cause vaginal irritation resulting in an inflammatory response (167) resulting in leukocytes and other cell types to be present in smears that may confound cytological assessment. Moreover, even in colony-housed females, it is normal to see extended diestrus and estrus stages in different mice as well induction of anestrous (168) and this identification is useful in the interpretation of hormonal impact in reproductive, gender, and disease studies. Variability in cycle length is also introduced with age and by housing differences within colonies (individual or group-housing) of females (150, 152, 169, 170). Females housed in female only colonies can cease cycling and enter a state of prolonged diestrus (168, 171, 172) although cycling can be re-instated by exposure to cages pretreated with male urine to elicit cycling (173, 174). Thus, to

establish individual cycle lengths for a given mouse, it is recommended that the non-invasive assessments described here be performed daily, with care, until two complete cycles are observed.

CHAPTER 4: HORMONAL REGULATION OF CONNEXIN EXPRESSION WITHIN THE CNS

4.1 Objective of this study

The overall objectives of this study were to a) identify connexins expressed in hippocampus and spinal cord of the intact adult female mouse and b) determine whether expression at the transcript level i) is differentially regulated between gender and/or ii) fluctuates over the course of the estrous cycle.

4.2 Statement of author contributions

The preoperative and postoperative animal procedures were assisted in part by University of Ottawa Animal Care Veterinary Services technical staff. All surgical and molecular procedures were carried out in full by AC McLean.

4.3 Introduction

Gliogenic and neurogenic niches exist within the CNS, capable of cellular regeneration (10, 175). Neuronal and glial precursors express specific subsets of connexin proteins (11, 176) forming gap junctions allowing for communication which have been shown to modulate proliferation, differentiation and survival (11, 24, 177). OLs have been shown to express Cx29, Cx32, and Cx47 (15-17), astrocytes express Cx30 and Cx43 (13,

14), while neurons express Cx36 and Cx45 (18, 178). Furthermore, proliferative cells express combinations of these various connexins in a regulated manner during specification that appear to dictate lineage outcome (11) (Figure 1.2). Modulation of connexin expression may be useful in the manipulation of endogenous systems for regeneration following CNS insult (49, 58).

Hormonal regulation may represent a key gender and temporal difference in connexin-mediated neuronal and glial progenitor response following injury. Connexins have been shown to have functional HREs within their promoter regions. For example, the Cx43 promoter, which contains EREs, can drive upregulation of the reporter gene luciferase *in vitro* following induction with estradiol in HeLa cells (82). *In vivo*, reproductive tissues have been the focus of much study, as the hormonal regulation of gap junctional communication is paramount in the electrical coupling and contractility of uterine lining during labour (93, 120, 121). Pregnant female rats treated with estrogen exhibit spontaneous ablation of the fetus, further supporting the hypothesis that Cx43 gap junctional communication within the uterus is estrogen-responsive (121). In myometrial tissue, the administration of estrogen significantly increased expression of Cx43 mRNA, whereas simultaneous treatment of estrogen and progesterone attenuates this increase (86). Connexin expression is hormone specific, as estrogen and progesterone have opposing actions, with Cx43 mRNA expression and function being regulated by the ratio of estrogen:progesterone in both pregnant and non-pregnant rats (86, 120). Little is known about the hormonal regulation of connexin expression within the CNS. Within the brain, modulation of Cx36 appears to be regionally and hormonally specific, with estrogen but not progesterone able to upregulate the expression of Cx36 mRNA within the SCN but not the CX (65). Evaluation of hormonal

regulation of the complete repertoire of connexins expressed within the neurogenic and gliogenic niches of the CNS is paramount to elucidate potential mechanisms of endogenous modulation of proliferation, differentiation and cell survival.

4.4 Experimental Procedures

Mice

The present study was carried out on male and female wild-type N12 C57BL/6 mice (4-5 months of age) (see below) or C57BL/6 females obtained from Charles River Laboratory. Cx32 null mutant mice ($Cx32^{Y/-}$ and $Cx32^{-/-}$) on a hybrid genetic background of 129SV/J1 and C57BL/6 strains were provided by Dr. K. Willecke (34). Mice were backbred in the Bennett laboratory for 12 generations (N12) to a pure C57BL/6 background and congenic wild-type and null-mutant colonies established. $Cx29^{-/-}$, $Cx36^{-/-}$, $Cx43^{F/F}$, $Cx45^{F/F}$, and $Cx47^{-/-}$ were generated by our laboratories as described in (15, 24, 179-181). Nestin-cre recombinase (nes-cre) transgenics (182) generated in the laboratory of Dr Ruth Slack were obtained from Drs. D. Picketts and R. Slack (University of Ottawa). The $Cx30^{-/-}$ mouse model (144) used in this study was obtained from Dr. K. Willecke (Universitat Bonn). All procedures were carried out in accordance with the Canadian Council on Animal Care and approved by the University of Ottawa Animal Care Veterinary Services ethics committee.

Estrous cycling determination

The estrous cycle of female C57BL/6 mice 3-4 months of age was examined following daily vaginal smears. In brief, vaginal cytology was examined with crystal violet staining of smears, examining the presence of leukocytes, polymorphonuclear cells, and/or

cornified epithelial cells, and mice were classified in proestrus, estrus, or metestrus/diestrus stages of the estrous cycle as described in Chapter 3. Animals were sacrificed (n=3 per stage) as described below following at least two typical estrous cycles. Full methodology is detailed in chapter 3 and published in the Journal of Visual Experimentation (127).

Surgical Ovariectomization

To eliminate circulating endogenous hormones, OVX surgeries were performed on female mice 3-4 months of age. Following a two-week recovery period, mice were staged to ensure no estrous cycling was present. Preoperative animal procedures included the following: intact female mice received one intra-peritoneal injection of buprenorphine (0.05 mg/kg) 1-3 hr prior to surgery. Mice were anesthetized with a constant flow of isoflurane/O_2. Anesthetized mice were prepared by hydrating with a 1.0 cc subcutaneous upper thoracic injection of saline solution and a small coat of Bacitracin/neomycin/polymyxin B ointment to cover each eye. Dorsal region of torso was shaved, washed with antiseptic soap (Eudral), rinsed with water, dried, and disinfected with chlorhexidine gluconate/isopropyl alcohol solution (Soluprep). Surgical animal procedures include the following: anesthetized mice were placed on their ventral surface. A sterilized stocking with a centre hole was used to create a sterile work window on the dorsal surface. With scalpel, a midline incision was made through skin along dorsal spine from mid thoracic to mid lumbar region. The fascia was grasped and separated from skin. The fascia was lifted away from dorso-lateral abdominal muscles and an incision 5 mm in length was created. The peri-ovarian fat pad surrounding the ovary was grasped and elevated out through the incision. The fallopian tube and uterine horn beneath the ovary was clamped. Above clamp, tissue was severed off using

scalpel, including ovary, fat pad, and any blood vessels present. Remainder of the horn was gently replaced within the abdominal cavity. The incision region was swabbed with saline to check for any substantial bleeding. One suture was secured within fascia, closing the incision, following which the removal of the contralateral ovary was performed. Two to four autoclips were used for dorsal skin closure. Post-operative animal procedures include the following: mice were placed in incubator for up to 24 hrs, and received buprenorphine [i.p. 0.05 mg/kg] (Day 1: 3x, Day 2: 2x, Day 3: 2x.). Mice were assessed for wellness twice daily for a week, then once weekly thereon. Autoclips were removed 10 days post-op.

Tissue collection

Mice were deeply anesthetized with intra-peritoneal Euthansol (65 mg/mL) and sacrificed. Animals were decapitated, hippocampus and spinal cord at the T11 region was dissected, flash frozen and stored at -80°C until RNA isolation. Experimental tissue was collected from cycling WT females (n=3 per stage), OVX WT females (n=3 spinal cord, n=6 hippocampus), and WT males (n=3). Control tissue was collected from null mutant male mice (n=1 per genotype; $Cx29^{-/-}$, $Cx30^{-/-}$, $Cx32^{Y/-}$, $Cx36^{-/-}$, nes-cre $Cx43^{F/F}$, nes-cre $Cx45^{F/F}$, and $Cx47^{-/-}$).

RNA isolation, preparation, and quality control

Total RNA was extracted using TRIzol (Invitrogen, Carlsbad, CA) as per manufacturer's protocol. In brief, tissue samples were homogenized in a borosilicate glass tube in 1 mL of TRIzol using a tissue tearor until mixture was homogenous, then incubated at room temperature for 5 min. TRIzol homogenate mixture was transferred to a 1.5 mL

epitube with glass pasteur pipette, 200 μL of chloroform was added, shaken vigourously by hand for 15 sec. Following a 5 min incubation at room temperature, epitube was centrifuged at 12,000 xg for 15 min at 4°C. Top phase was transferred to fresh 1.5 mL epitube, 500 μL of isopropyl alcohol was added and shaken by hand. Following a 10 min incubation at room temperature, epitube was centrifuged at 12,000 xg for 10 min at 4°C. Supernatant was discarded and raw RNA pellet was washed with 1 mL 75% ethanol-diethylpyrocarbonate (DEPC) and centrifuged at 7,500 xg for 5 min at 4°C twice. Supernatant was removed and raw RNA pellet was allowed to dry at room temperature before being resuspended in 22 μL of nuclease-free H_2O (NFH_2O). Following an incubation at 55-60°C for 10 min, raw RNA sample was stored at -80°C until further use.

RNA concentrations were determined using a Nanodrop 2000 spectrophotometer (Thermoscientific). Optical density at 260/280 was required to be between 1.8 and 2.0 for further use. Raw RNA samples were treated to eliminate any possible genomic contamination with DNase treatment (Sigma-Aldrich) as per manufacturer's protocol. In brief, 6.0 μg of raw RNA was added to 6.0 μL of DNase-1, 4 μL of 10X buffer, and NFH_2O to a final reaction volume of 40 μL in a 1.5 mL epitube and incubated for 30 min at 37°C. Following incubation, each sample was precipitated by adding 200 μL of phenol/chloroform and 160 μL of NFH_2O. Epitubes were shaken by hand and centrifuged at 16,100 xg for 1 min at 4°C. 180 μL of the upper aqueous phase was transferred to a fresh 1.5 mL epitube. 22 μL of 3 M sodium acetate and 900 μL of 100% ethanol was added, gently mixed, and incubated overnight at -80°C. Following overnight incubation, samples were centrifuged at 16,100 xg for 10 min at 4°C. Supernatant was discarded and DNase treated RNA pellet was washed twice with 500 μL 75% ethanol-DEPC and centrifugation at 16,100 xg for 1 min at

4°C. Supernatant was removed and pellet was allowed to dry at room temperature before being resuspended in 13.0 μL of NFH_2O. Samples were stored at -80°C until further use. Following DNase treatment, RNA concentrations were re-determined by spectrophotometry. Samples with an optical density at 260/280 between 1.8 and 2.0 were considered an acceptable quality.

For each sample of acceptable quality, cDNA was produced by reverse transcription using Superscript II Reverse Transcriptase (Invitrogen) as per manufacturer's protocol. In brief, for each sample, 4.0 μg of DNAse treated RNA was divided into two separate PCR tubes, each containing 2.0 μg (RT+ and RT-). To each RT+ tube was also added 1.0 μL pdN6 random primers (Promega) and brought to a final volume of 12.0 μL using NFH_2O. To each RT- tube was also added 1.0 μL pdN6 random primers and brought to a final volume of 13.0 μL using NFH_2O. No template control (NTC) sample received no RNA, solely 1.0 μL pdN6 random primers and brought to a final volume of 13.0 μL using NFH_2O. Samples were incubated in thermocycler (BioMetra) for 10 min at 70°C. Following a 2 min incubation at 4°C, all PCR reaction tubes (RT+, RT-, and NTC) received 4.0 μL 1^{st} strand buffer, 2.0 μL 0.1 M DTT and 1.0 μL 10 mM dNTPs. Samples were returned to thermocycler and incubated for 2 min at 37°C then brought to 25°C. All RT+ and NTC samples received 1.0 μL of Superscript reverse transcriptase, returned to thermocycler and incubated for 10 min at 25°C, 60 min at 42°C, 30 min at 50°C, then held at 4°C. cDNA samples (RT+, RT-, and NTC) were stored at -80°C until further use.

Given that many of our connexin primers amplify within a single exon, to ensure no genomic contamination following DNase treatment or genomic contamination master mixes, cDNA produced from reverse transcription reaction (RT+, RT-, and NTC) was used as

template for reverse transcription polymerase chain reaction (RT-PCR), amplifying glyceraldehyde 3-phosphate dehydrogenase (GAPDH) cDNA (within a single exon). Primers sequences used for the reaction were 5' GTG GCG TGA ATC GGC ACT CTA C 3' (mGAPDH forward primer) and 5' CTC CGC CAC GTT GAG GAT AAT G 3' (mGAPDH reverse primer). In a 1.5 mL epitube, a master mix was made up of the following; 10X Titanium buffer (2.5 μL per sample), 10 mM dNTPs (2.0 μL per sample), Titanium Taq (0.5 μL per sample), forward primer (10 pmol/μL, 0.5 μL per sample), reverse primer (10 pmol/μL, 0.5 μL per sample), and NFH_2O (18.0 μL per sample). In PCR reaction tubes, 24 μL of master mix was added to 1 μL of each cDNA template (RT+, RT-, and NTC). Using a thermocycler (BioMetra), reaction tubes were incubated for 5 min at 94°C, then cycled for 25 sec at 94°C, 50 sec at 59°C, and 1 min 45 sec at 72°C for 35 cycles, followed by at 7 min incubation at 72°C then held at 4°C until storage at -20°C. Each sample of RT-PCR product (RT+, RT-, and NTC) was ran on a 1.2% agarose gel. Amplicons (~300 bp) were visualized as bands using ethidium bromide staining. Any cDNA sample producing a band within from RT- template was assumed to have genomic contamination, in which case cDNA (both RT+ and RT-) was discarded and not used for further analysis. Any amplicon produced from NTC template would be indicative of potential contamination of reverse transcription reagents and all samples would be discarded, although this did not occur during the study. mRNA from null mutant mice was extracted and prepared as described above and used as negative controls for each respective connexin assay to ensure assay specificity.

Real-Time Quantitative reverse transcription PCR (qRT-PCR)

To determine connexin fold change expression at each estrous stage, we used the Strata MX3005P Real-Time PCR System for quantitative RNA analysis in conjunction with Applied Biosystems Taqman gene expression assays (standard reference genes and connexins). For all samples in this study (standard curve and experimental), qRT-PCR was performed as follows; in a 1.5 mL epitube, a master mix was made up of the following; Taqman (10.0 μL per sample), assay (1.0 μL per sample), and NFH_2O (4.0 μL per sample). 15.0 μL of master mix was added to each reaction tube (optical qRT-PCR strip tubes, Diamed) For each reaction, 5.0 μL of cDNA determined to be free of genomic contamination by RT-PCR (diluted in NFH_2O to appropriate concentration as described below) was used as template (RT+, RT-), as well as 5.0 μL of NFH_2O functioning as qRT-PCR NTC ensuring TaqMan reagents were not contaminated. Each sample was ran in triplicate. Using the Strata MX3005P Real-Time PCR System, reactions were incubated at 50°C for 2 min, 95°C for 10 min, then cycled 40 times at 95°C for 15 sec and 60°C for 1 min. Cycle threshold (CT) was evaluated at the end of each 60°C incubation by fluorescence detection, scanning with FAM/SYBR filter.

For each assay, the range of optimal cDNA concentrations to detect linear amplification was determined prior to quantitation of experimental samples using a dilution series of male WT cDNA examining a range of dilution factors of 1:12.5 to 1:800, representing 40 ng to 0.625 ng of starting RNA template. Samples were ran in triplicate. Using values from the dilution series, each known value of Log[RNA] was graphed against its respective average CT value (of triplicate) as determined by the Strata MX3005P Real-Time PCR System to produce a standard curve using Prism software (GraphPad Software

Inc.). Although a maximum of seven points could be used to generate standard curve, optimal linear range was determined by evaluating all possible R^2 values generated from at least four consecutive points. Experimental cDNA in subsequent assays were diluted to concentrations determined to fall within the linear range of the dilution series.

Standard reference gene RNA analysis

To identify transcripts that do not change over the course of the estrous cycle (standard reference genes) that could be used to normalize connexin expression for template concentration variation, we assessed the following genes: GAPDH, peptidylprolyl isomerase B (Ppib), 18S ribosomal RNA (Rn18s), and hypoxanthine-guanine phosphoribosyltransferase (Hprt). The range of optimal cDNA concentrations was determined for hippocampus using a dilution series of male cDNA as previously described using Applied Biosystems Taqman gene expression assays (GAPDH: Hs02758991_g1, Ppib: Mm00478295_m1, Rn18s: Mm03928990_g1, Hprt: Mm00446968_m1). Experimental cDNA from estrous cycle samples in subsequent assays were diluted to concentrations determined to fall within linear range of the dilution series, and a standard curve was ran on every experimental plate. Average CT values from experimental samples ran in triplicate were substituted into the straight-line equation produced by the experimental plate standard curve for the interpolation of experimental sample Log[RNA] values. The stability of standard reference genes was analyzed over the course of the estrous cycle by grouping experimental sample values as proestrus, estrus or met/diestrus and analyzed with a one-way ANOVA, followed by *post hoc* Tukey's (when applicable) using Prism software (GraphPad

Software Inc.). Ppib stability across the estrous cycle using spinal cord cDNA was performed as described above.

Connexin RNA analysis

Connexin mRNA expression was assessed by qRT-PCR using Applied Biosystems Taqman gene expression assays (Tables 4.1 and 4.2). The range of optimal cDNA concentrations was determined for hippocampus and spinal cord using a dilution series of male cDNA for each respective tissue and connexin as previously described. Due to the homologous nature of connexins, null mutant controls ($Cx29^{-/-}$, $Cx30^{-/-}$, $Cx32^{Y/-}$, $Cx36^{-/-}$, nes-cre $Cx43^{F/F}$, nes-cre $Cx45^{F/F}$, and $Cx47^{-/-}$) were used simultaneously to ensure specificity of each connexin assay.

Transient changes were analyzed over the course of the estrous cycle using Applied Biosystems Taqman gene expression assays. Assay specificity and optimal dilution factor concentrations are described in Tables 4.1 and 4.2. Ppib was used as a standard reference gene at 1:50. A standard curve of male cDNA examining a range of dilution factors of 1:12.5 to 1:800 (40 ng to 0.625 ng RNA) was used on every plate as described above. Average CT values of each experimental sample ran in triplicate was determined and substituted into the straight-line equation produced by the experimental plate standard curve for the interpolation of experimental sample Log[RNA] value, then corrected for respective Ppib loading control ($Log[RNA]_{Cx}$ / $Log[RNA]_{Ppib}$). Values corrected for loading were then standardized to mean of control group (corrected experimental $Log[RNA]_{Cx}$ / corrected control mean $Log[RNA]_{Cx}$). For estrous cycle studies, the control group was OVX females. For gender studies, control group was males. Changes in connexin mRNA expression was analyzed over

the course of the estrous cycle by grouping the corrected, standardized experimental sample values as proestrus, estrus or met/diestrus and analyzed with a one-way ANOVA, followed by *post hoc* Tukey's (when applicable) using Prism software (GraphPad Software Inc.).

Connexin	**Applied Biosciences Assay**	**Tissue**	**Dilution factor, linear range**	**Δ CT (dilution) (WT vs. KO)**
Cx29	Mm01204089_m1	Hippocampus	1:12.5 – 1:100	9.38 (1:50)
			(R^2 = 0.99)	(28.05 vs. 37.43)
Cx30	AIT95R9	Hippocampus	1:12.5 – 1:100	12.58 (1:50)
			(R^2 = 0.98)	(26.78 vs. 39.36)
Cx32	Hs00702141_s1	Hippocampus	1:12.5 – 1:200	2.99 (1:50)
			(R^2 = 0.99)	(29.97 vs. 32.96)
Cx36	Hs04259539_s1	Hippocampus	1:12.5 – 1:100	11.44 (1:50)
			(R^2 = 0.97)	(28.47 vs. 39.91)
Cx43	Mm00439105_m1	Hippocampus	1:12.5 – 1:100	6.22 (1:50)
			(R^2 = 0.99)	(23.64 vs. 29.85)
Cx45	Hs04259537_s1	Hippocampus	1:12.5 – 1:100	5.68 (1:50)
			(R^2 = 0.98)	(29.86 vs. 35.54)
Cx47	Mm04209851_m1	Hippocampus	1:12.5 – 1:200	(1:25)
			(R^2 = 0.97)	(32.77 vs. No CT)

Table 4.1 Hippocampus Connexin Expression Assays

Connexin	Applied Biosciences Assay	Tissue	Dilution factor, linear range	Δ CT (dilution) (WT vs. KO)
Cx29	Mm01204089_m1	Spinal Cord	1:12.5 – 1:100 (R^2 = 0.97)	10.15 (1:50) (27.31 vs. 37.46)
Cx30	AIT95R9	Spinal Cord	1:12.5 – 1:100 (R^2 = 0.97)	13.11 (1:50) (26.14 vs. 39.25)
Cx32	Hs00702141_s1	Spinal Cord	1:25 – 1:800 (R^2 = 0.99)	9.63 (1:50) (28.48 vs. 38.11)
Cx36	Hs04259539_s1	Spinal Cord	1:25 – 1:800 (R^2 = 0.98)	9.34 (1:50) (28.71 vs. 38.05)
Cx43	Hs04259536_g1	Spinal Cord	1:12.5 – 1:100 (R^2 = 0.97)	6.34 (1:25) (23.66 vs. 30.00)
Cx45	Hs04259537_s1	Spinal Cord	1:12.5 – 1:100 (R^2 = 0.97)	4.73 (1:50) (30.18 vs. 34.91)
Cx47	Mm04209851_m1	Spinal Cord	1:12.5 – 1:100 (R^2 = 0.97)	6.17 (1:50) (32.05 vs. 38.22)

Table 4.2 Spinal Cord Connexin Expression Assays

4.5 Results

4.5.1 Ppib expression does not fluctuate over the course of the estrous cycle.

Analysis of four potential "housekeeping" or reference genes found that three of four putatively stable transcripts were, in fact, under hormonal control in the hippocampus (Figure 4.1). Linear range of GAPDH cDNA amplification was determined to be within a cDNA dilution factor of 1:50 to 1:400, corresponding to RNA template ranging from 10 ng to 1.25 ng (R^2 = 0.99), with expression under hormonal regulation over the course of the

Figure 4.1 Ppib mRNA expression levels in the hippocampus are not hormonally sensitive and can be used as a reference standard to control for cDNA concentration. Dilution series of hippocampal cDNA (1:12.5 to 1:800, corresponding to 40 - 0.625 ng RNA) were used to determine linear range of amplification for each reference gene (A). Linear range of GAPDH amplification fell within a cDNA dilution factor of 1:50 to 1:400 (R^2 = 0.99) corresponding to 10 – 1.25 ng RNA, Rn18s between cDNA dilution factor of 1:25 and 1:400 (R^2 = 0.92) corresponding to 20 – 1.25 ng RNA, Hprt between cDNA dilution factor of 1:25 to 1:400 (R^2 = 0.98), corresponding to 20 – 1.25 ng RNA, and Ppib between cDNA dilution factor of 12.5 to 1:100 (R^2 = 0.93) corresponding to 20 – 5.0 RNA. Using concentrations of cDNA within linear range for each respective reference gene assay, it was determined that GAPDH expression levels (B) significantly fluctuated between proestrus and met/diestrus. Rn18s (C) significantly decreased following OVX in the proestrus stage of the estrous cycle and increased between the proestrus and met/diestrus stages. Hprt (D) significantly decreased during proestrus when compared to met/diestrus. Ppib expression (E) displayed no significant changes between OVX females or across the female mouse estrous cycle. Statistics were one way ANOVA, * *post hoc* Tukey's $p<0.05$, ** *post hoc* Tukey's $p<0.01$.

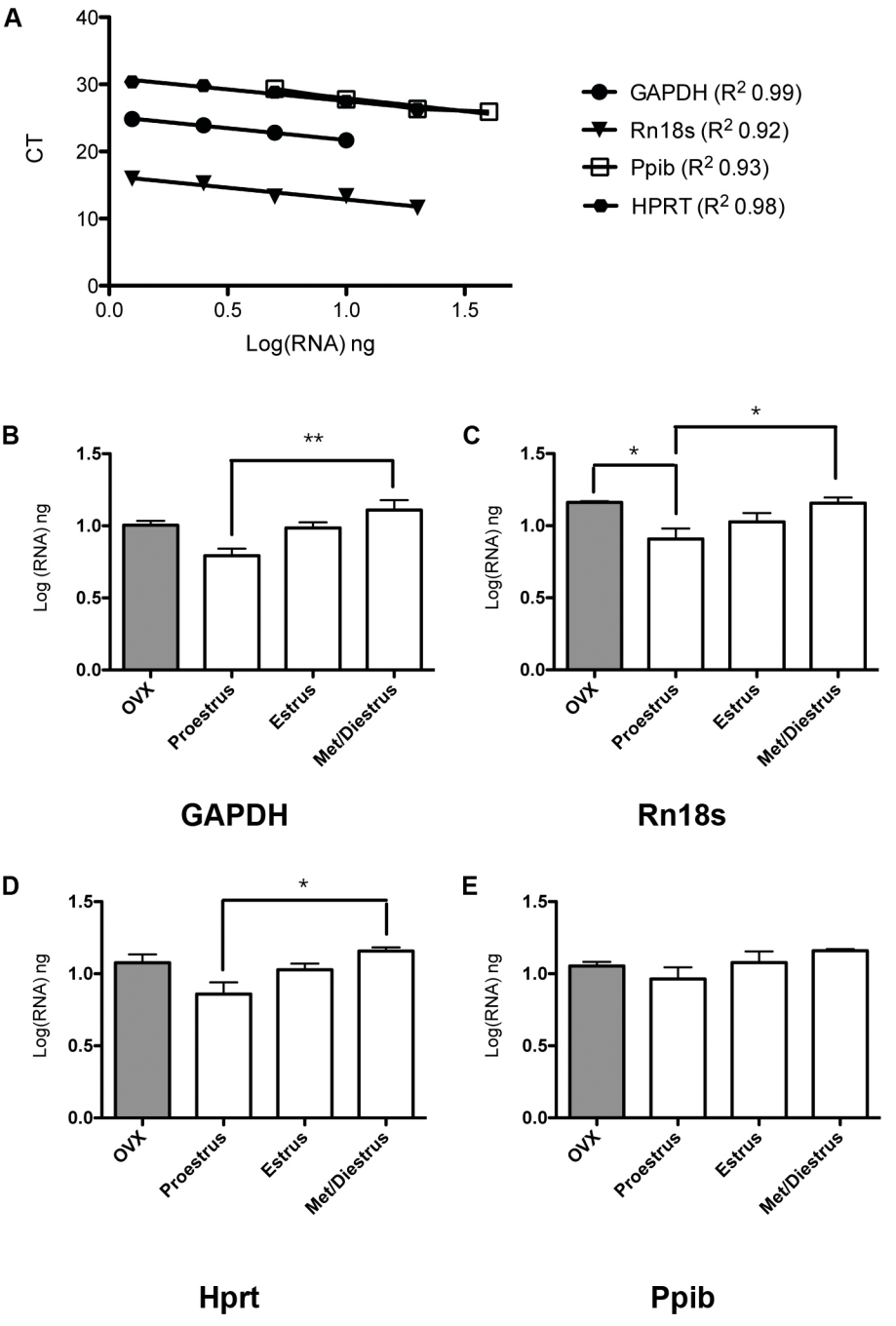
A
CT
Log(RNA) ng
GAPDH (R2 0.99)
Rn18s (R2 0.92)
Ppib (R2 0.93)
HPRT (R2 0.98)
B
Log (RNA) ng
OVX
Proestrus
Estrus
Met/Diestrus
GAPDH
C
Log(RNA) ng
Rn18s
D
Hprt
E
Ppib

Figure 4.1

female mouse estrous cycle, significantly different between proestrus and met/diestrus (Figure 4.1A, B). Detection of Rn18s expression was optimal using a cDNA dilution factor between 1:25 and 1:400, corresponding to RNA template ranging from 20 ng to 1.25 ng (R^2 = 0.92) and showed a significant difference in mRNA expression between OVX females and the proestrus stage of the estrous cycle (Figure 4.1A, C). Furthermore, Rn18s increased between the proestrus and met/diestrus stage within the hippocampus (Figure 4.1C). Hprt mRNA expression was detected between optimal cDNA dilution factors of 1:25 to 1:400, corresponding to RNA template ranging from 20 ng to 1.25 ng (R^2 = 0.98), and fluctuated during the estrous cycle, with levels significantly decreased during proestrus when compared to met/diestrus (Figure 4.1A, D). Ppib was determined to be a suitable standard reference gene, with optimal detection of mRNA expression using a cDNA dilution factor following RT of 12.5 to 1:100, corresponding to RNA template ranging from 40 ng to 5.0 ng (R^2 = 0.93) and no significant changes following OVX or during the female mouse estrous cycle (Figure 4.1A, E). In all experiments presented, no amplification was observed in identical reactions performed using RT product "amplified" in the absence of RT (RT- control) confirming lack of genomic contamination in assays amplifying transcript within the same exon. Furthermore, Ppib was determined to be a suitable control gene for spinal cord expression assays as it did not fluctuate over the course of estrous (Figure 4.2B) and was within linear range using cDNA between a dilution factor of 1:12.5 to 1:800, corresponding to RNA template ranging from 40 ng to 0.625 ng (R^2 = 0.99, Figure 4.2A).

Figure 4.2 Ppib mRNA expression levels in the spinal cord are not hormonally sensitive and can be used as a reference standard to control for cDNA concentration. Dilution series of thoracic (T11) spinal cord cDNA (1:12.5 to 1:800, corresponding to 40 - 0.625 ng RNA) was used to determine linear range of amplification for reference gene Ppib (A). Linear range of Ppib amplification fell within a cDNA dilution factor of 1:12.5 to 1:800 (R^2 = 0.99) corresponding to 40 – 0.625 ng RNA. Using a concentration of cDNA within linear range for the Ppib reference gene assay (1:50), it was determined that Ppib expression displayed no significant changes between OVX females or across the female mouse estrous cycle (B). Statistics were one way ANOVA.

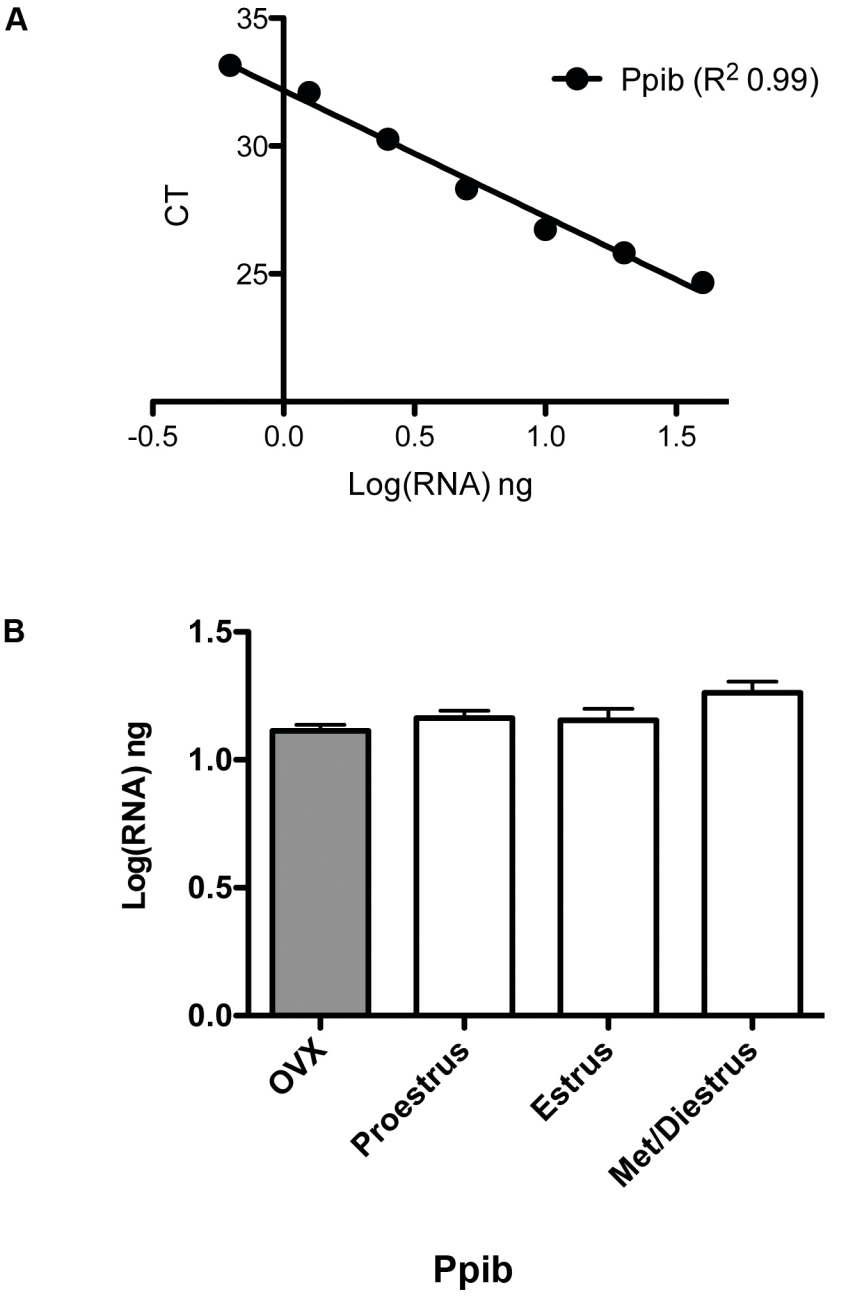
A
35
30
25
CT
Ppib (R2 0.99)
-0.5
0.0
0.5
1.0
1.5
Log(RNA) ng
B
1.5
1.0
0.5
0.0
Log(RNA) ng
OVX
Proestrus
Estrus
Met/Diestrus
Ppib

Figure 4.2

4.5.2 Optimization of hippocampal connexin expression assays.

Expression assays used for analysis of seven CNS connexins (Cx29, Cx30, Cx32, Cx36, Cx43, Cx45 and Cx47) were determined to be specific using null mutant controls at optimal dilutions of hippocampal cDNA (as summarized in Table 4.1). Hippocampal Cx29 expression was amplified in a linear manner using the Cx29 expression assay (Mm01204089_m1) at a cDNA dilution factor of 1:12.5 to 1:100, corresponding to RNA template ranging from 40 ng to 5.0 ng ($R^2 = 0.99$). At a cDNA dilution of 1:50, expression was determined to be specific to Cx29 (WT CT 28.05 vs. KO CT 37.43). Cx30 expression assay (AIT95R9) produced linear detection of cDNA between the dilution factors of 1:12.5 to 1:100, corresponding to RNA template ranging from 40 ng to 5.0 ng ($R^2 = 0.93$), and specificity for Cx30 at 1:50 (WT CT 26.78 vs. KO CT 39.36). Using an expression assay for Cx32 (Hs00702141_s1), optimal cDNA detection was found between 1:12.5 to 1:200, corresponding to RNA template ranging from 40 ng to 2.5 ng ($R^2 = 0.99$), with 1:50 proving to convey desired specificity for Cx32 (WT CT 29.97 vs. KO CT 32.96). The Cx36 expression assay (Hs04259539_s1) showed optimal detection using cDNA between dilution factors of 12.5 to 1:100, corresponding to RNA template ranging from 40 ng to 5.0 ng ($R^2 = 0.97$), with 1:50 specific to connexin of interest (WT CT 28.47 vs. KO CT 39.91). Cx43 expression assay (Mm00439105_m1) yielded an optimal detection range between 1:12.5 to 1:100, corresponding to RNA template ranging from 40 ng to 5.0 ng ($R^2 = 0.9857$), with specificity at 1:50 (WT CT 23.64 vs. KO CT 29.85). Detection of Cx45 expression with assay (Hs04259537_s1) at dilution factors between 1:12.5 to 1:100 was optimal, corresponding to RNA template ranging from 40 ng to 5.0 ng ($R^2 = 0.98$) with a 1:50 dilution factor being specific for Cx45 (WT CT 29.86 vs. KO CT 35.54). Using the Cx47

assay (Mm04209851_m1) to detect expression, optimal cDNA dilution factor of 1:12.5 to 1:200 was used, corresponding to RNA template ranging from 40 ng to 2.5 ng ($R^2 = 0.97$), and a 1:25 dilution proved Cx47 specificity of assay (WT CT 32.77 vs. KO undetectable).

4.5.3 No gender differences exist within overall hippocampal connexin expression, but Cx43 and Cx47 fluctuates over the course of the female mouse estrous cycle.

Using optimized and specific assays to quantify connexins within the hippocampus (Table 4.1), there was no significant difference in overall expression between males and OVX females or males and intact cycling females in all seven connexins (Cx29, Cx30, Cx32, Cx36, Cx43, Cx45 and Cx47,) following normalization to Ppib loading control (Figure 4.3A-G). Data are expressed standardized to males. Further evaluation of potential fluctuations in hippocampal connexin expression in females across the estrous cycle determined that five of the seven connexins, did not significantly change (Cx29, Cx30, Cx32, Cx36, and Cx45, Figure 4.4A-D, F) whereas two connexins were under hormonal control (Cx43 and Cx47, Figure 4.4E, G). Both Cx43 and Cx47 quantification displayed a similar trend, with expression levels in the hippocampus being significantly lower during proestrus than expression levels in met/diestrus (Figure 4.4E, G). In all experiments presented, no amplification was observed in identical reactions performed using RT product "amplified" in the absence of RT (RT- control) confirming lack of genomic contamination in assays amplifying transcript within the same exon. No amplification was detected in NTC samples, validating no contamination in ABI reagents used.

Figure 4.3 No differences are found between genders in relative mRNA expression of seven connexin within the mouse hippocampus. Cx29 (A), Cx30 (B), Cx32 (C), Cx36 (D), Cx43 (E), Cx45 (F) and Cx47 (G) expression levels are not different between males (n=3) and OVX females (n=6), males and intact females (n=9), or OVX females and intact females. Relative expression was standardized to males (n=3), Ppib was used as reference gene at cDNA dilution factor 1:50. Statistics were one way ANOVA.

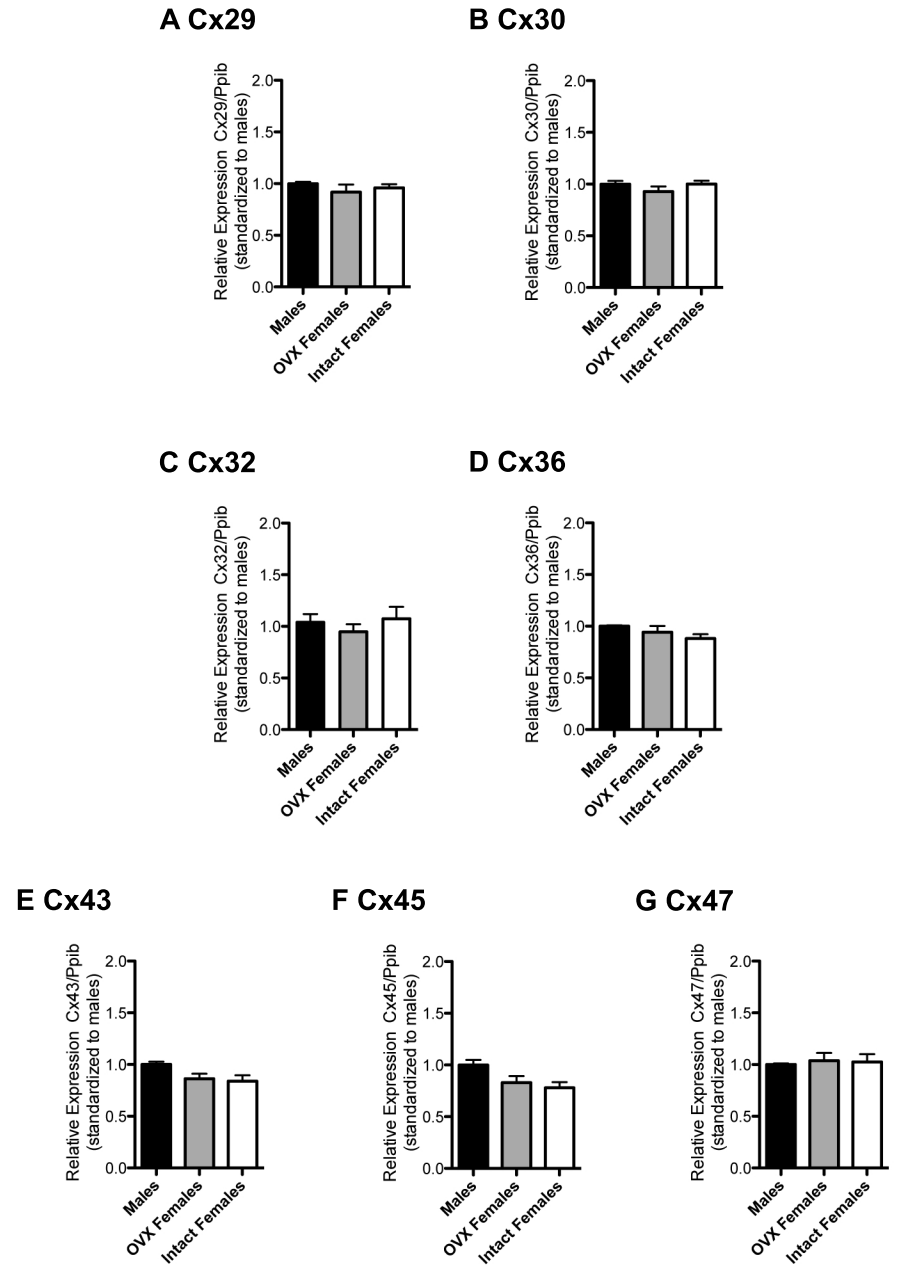
A Cx29
B Cx30
C Cx32
D Cx36
E Cx43
F Cx45
G Cx47
Relative Expression Cx29/Ppib (standardized to males)
Relative Expression Cx30/Ppib (standardized to males)
Relative Expression Cx32/Ppib (standardized to males)
Relative Expression Cx36/Ppib (standardized to males)
Relative Expression Cx43/Ppib (standardized to males)
Relative Expression Cx45/Ppib (standardized to males)
Relative Expression Cx47/Ppib (standardized to males)
2.0
1.5
1.0
0.5
0.0
Males
OVX Females
Intact Females

Figure 4.3

Figure 4.4 Relative mRNA expression levels of two of seven connexins fluctuate within the hippocampus over the female mouse estrous cycle. Cx29 (A), Cx30 (B), Cx32 (C), Cx36 (D) and Cx45 (F) do not significantly change between proestrus (n=3), estrus (n=3) and met/diestrus (n=3) stages of the estrous cycle. Expression levels of Cx43 (E) and Cx47 (G) were determined to be significantly lower during proestrus when compared to met/diestrus. Relative expression was standardized to OVX females (n=6), Ppib was used as reference gene at cDNA dilution factor 1:50. Statistics were one way ANOVA, * *post hoc* Tukey's $p<0.05$.

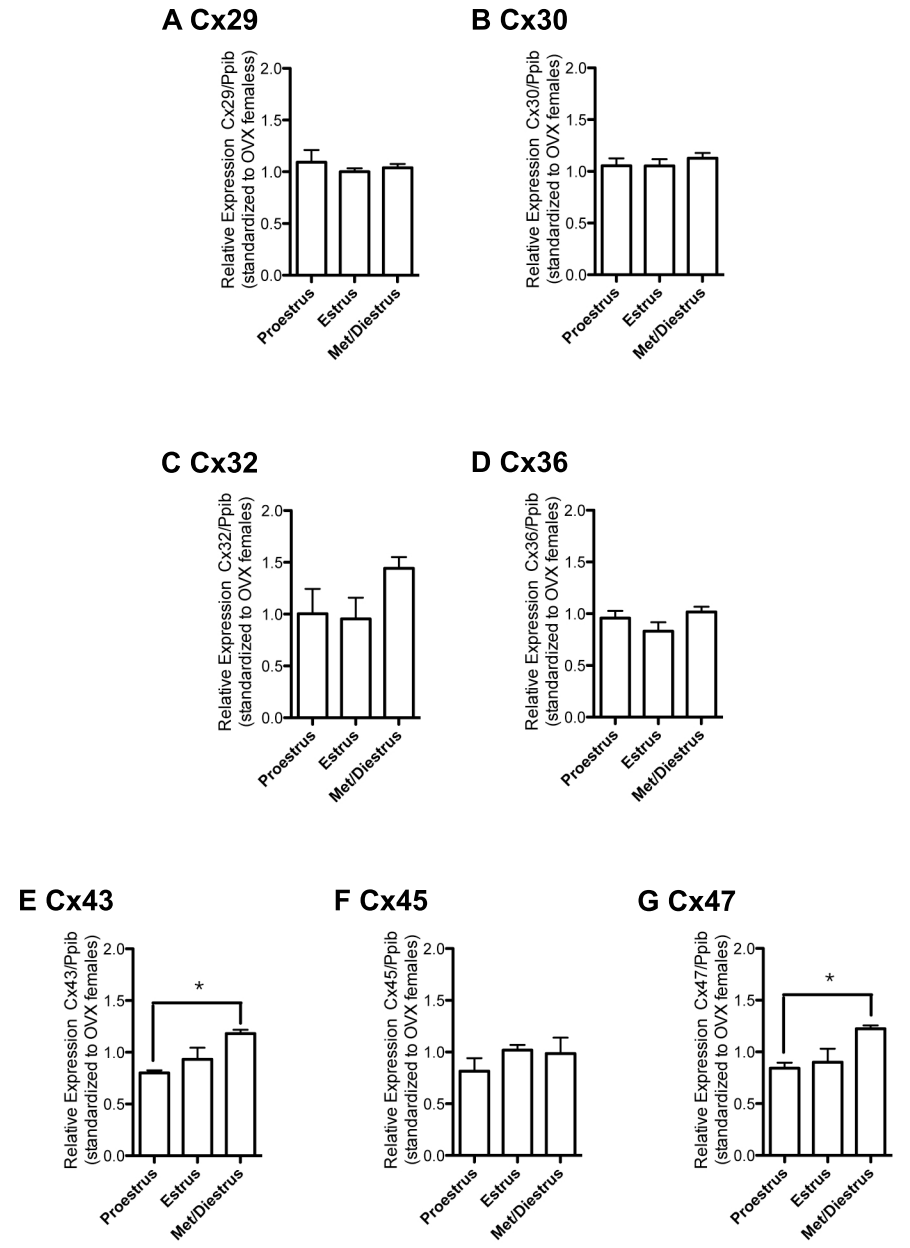
A Cx29
Relative Expression Cx29/Ppib (standardized to OVX femaless)
2.0
1.5
1.0
0.5
0.0
Proestrus
Estrus
Met/Diestrus
B Cx30
Relative Expression Cx30/Ppib (standardized to OVX females)
C Cx32
Relative Expression Cx32/Ppib (standardized to OVX females)
D Cx36
Relative Expression Cx36/Ppib (standardized to OVX females)
E Cx43
Relative Expression Cx43/Ppib (standardized to OVX females)
*
F Cx45
Relative Expression Cx45/Ppib (standardized to OVX females)
G Cx47
Relative Expression Cx47/Ppib (standardized to OVX females)
*

Figure 4.4

4.5.4 Optimization of spinal cord connexin expression assays

Expression assays were optimized using spinal cord cDNA to determine linear range of detection and null mutant cDNA was used to ensure specificity (as summarized in Table 4.2). Spinal cord Cx29 expression was amplified in a linear manner using Cx29 expression assay (Mm0120489_m1) within a cDNA dilution factor range of 1:12.5 to 1:100, corresponding to RNA template ranging from 40 ng to 5.0 ng ($R^2 = 0.97$). Using a dilution of 1:50, assay was determined to be specific for Cx29 (WT CT 27.31 vs. KO CT 37.16). Cx30 expression was detected using Cx30 expression assay (AIT95R9) within the cDNA dilution factor ranges of 1:12.5 to 1:100, corresponding to RNA template ranging from 40 ng to 5.0 ng ($R^2 = 0.97$), with a 1:50 dilution specific for Cx30 (WT CT 26.14 vs. KO CT 39.25). Optimal expression of Cx32 within the spinal cord was detected using Cx32 assay (Hs00702141_s1) between dilutions of cDNA from 1:25 to 1:800, corresponding to RNA template ranging from 20 ng to 0.625 ng ($R^2 = 0.99$), and specific for Cx32 at a 1:50 dilution (WT CT 28.48 vs. KO CT 38.11). Cx36 expression assay (Hs04259539_s1) detected expression of Cx36 within linear range between cDNA dilution factors of 1:25 to 1:800, corresponding to RNA template ranging from 20 ng to 0.625 ng ($R^2 = 0.98$) and specific for Cx36 at 1:50 (WT CT 28.71 vs. KO CT 38.05). Initial Cx43 expression assay used in hippocampal analysis (Mm00439105_m1) was found to not be specific for Cx43 expression within the spinal cord (WT CT 30.24 vs. KO CT 31.32). Subsequent Cx43 expression assay examined (Hs04259536_g1) detected Cx43 expression within spinal cord within a linear range of cDNA diluted 1:12.5 to 1:100, corresponding to RNA template ranging from 40 ng to 5.0 ng ($R^2 = 0.97$), and specific for Cx43 at 1:25 (WT CT 23.66 vs. KO CT 30.00). Cx45 expression was detected using an assay designed for Cx45 (Hs04259537_s1) and was within

linear range of detection using cDNA dilution factors between 1:12.5 to 1:100, corresponding to RNA template ranging from 40 ng to 5.0 ng (R^2 = 0.97), and specific at 1:50 for Cx45 (WT CT 30.18 vs. KO CT 34.91). The Cx47 expression assay (Hs04259538_s1) was not able to specifically detect Cx47 within the spinal cord (WT CT 26.61 vs. KO CT 28.39). A second Cx47 expression assay (Mm04209851_m1) was optimized and found to detect Cx47 spinal cord expression within a linear range between cDNA dilution factors of 1:12.5 to 1:100, corresponding to RNA template ranging from 40 ng to 5.0 ng (R^2 = 0.97), with expression being specific to Cx47 (WT CT 32.05 vs. KO CT 38.22).

4.5.5 Cx43 gender differences exist, although connexin expression does not fluctuate over the course of the estrous cycle within the female mouse spinal cord.

Using optimized assays for spinal cord connexin quantification (Table 4.2), no difference between genders was present in six of seven connexins examined (Cx29, Cx30, Cx32, Cx36, Cx45 and Cx47, Figure 4.5A-D, F, G). Cx43 expression levels were significantly lower in males when compared to OVX females, as well as males compared to intact cycling females (Figure 4.5E). Over the course of the estrous cycle, all seven connexins (Cx29, Cx30, Cx32, Cx36, Cx43, Cx45, and Cx47, Figure 4.6A-G) did not significantly change within the female mouse spinal cord. In all experiments presented, no amplification was observed in identical reactions performed using RT product "amplified" in the absence of RT (RT- control) confirming lack of genomic contamination in assays amplifying transcript within the same exon. No amplification was detected in NTC samples, validating no contamination in ABI reagents used.

Figure 4.5 Relative mRNA expression levels of one of seven connexins significantly differ between genders fluctuate within the mouse spinal cord. Cx29 (A), Cx30 (B), Cx32 (C), Cx36 (D), Cx45 (F) and Cx47 (G) levels are not different between males (n=3) and OVX females (n=3), males and intact females (n=9), or OVX females and intact females. Relative expression levels of Cx43 (E) was determined to be significantly lower in males when compared to both OVX females and intact females. Relative expression was standardized to males (n=3), Ppib was used as reference gene at cDNA dilution factor 1:50. Statistics were one way ANOVA, * *post hoc* Tukey's $p<0.05$.

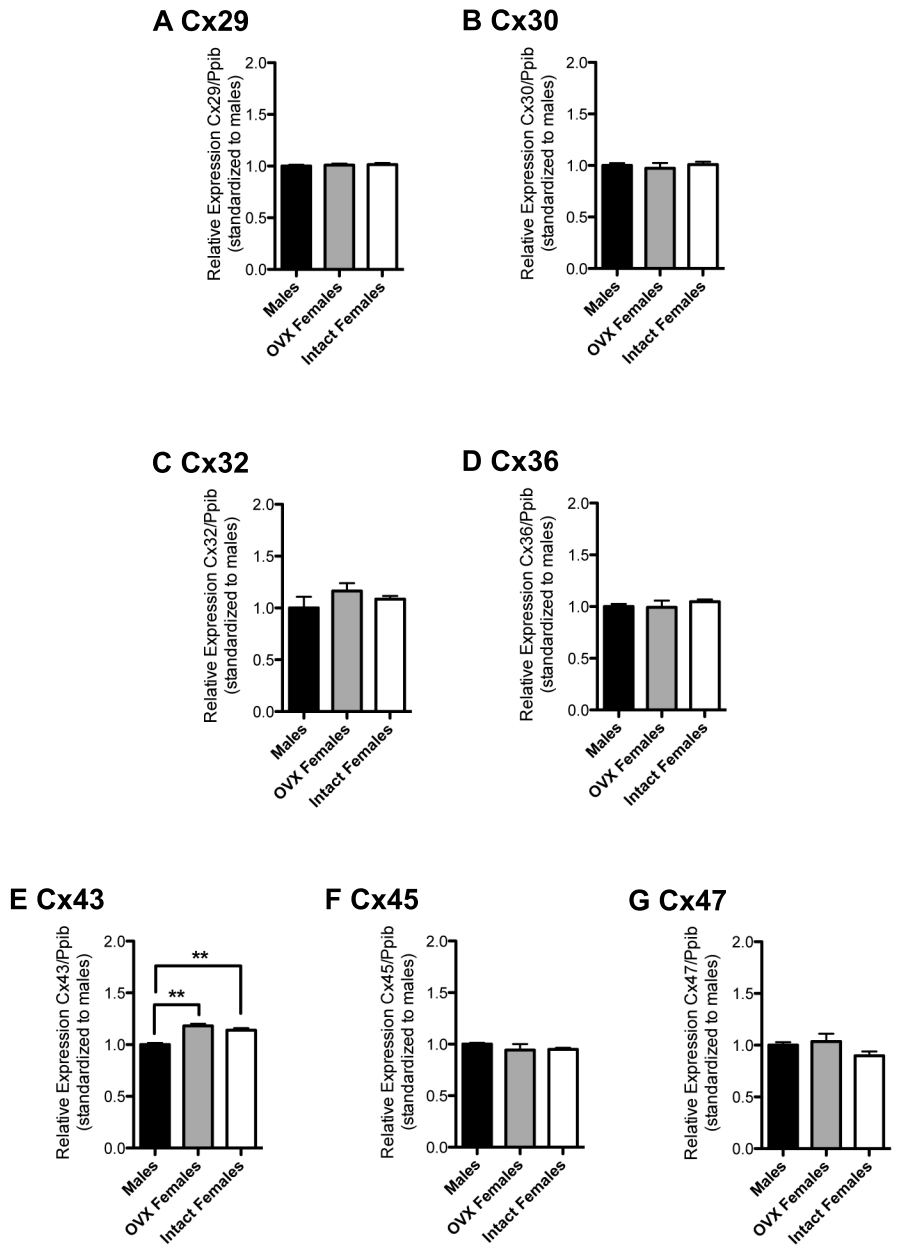
A Cx29
Relative Expression Cx29/Ppib (standardized to males)
2.0
1.5
1.0
0.5
0.0
Males
OVX Females
Intact Females
B Cx30
Relative Expression Cx30/Ppib (standardized to males)
C Cx32
Relative Expression Cx32/Ppib (standardized to males)
D Cx36
Relative Expression Cx36/Ppib (standardized to males)
E Cx43
Relative Expression Cx43/Ppib (standardized to males)
**
**
F Cx45
Relative Expression Cx45/Ppib (standardized to males)
G Cx47
Relative Expression Cx47/Ppib (standardized to males)

Figure 4.5

Figure 4.6 No differences are found in relative mRNA expression of seven connexin over the female mouse estrous cycle within the spinal cord. Cx29 (A), Cx30 (B), Cx32 (C), Cx36 (D), Cx43 (E), Cx45 (F) and Cx47 (G) expression levels do not significantly change between proestrus (n=3), estrus (n=3) and met/diestrus (n=3) stages of the estrous cycle. Relative expression was standardized to OVX females (n=3), Ppib was used as reference gene at cDNA dilution factor 1:50. Statistics were one way ANOVA.

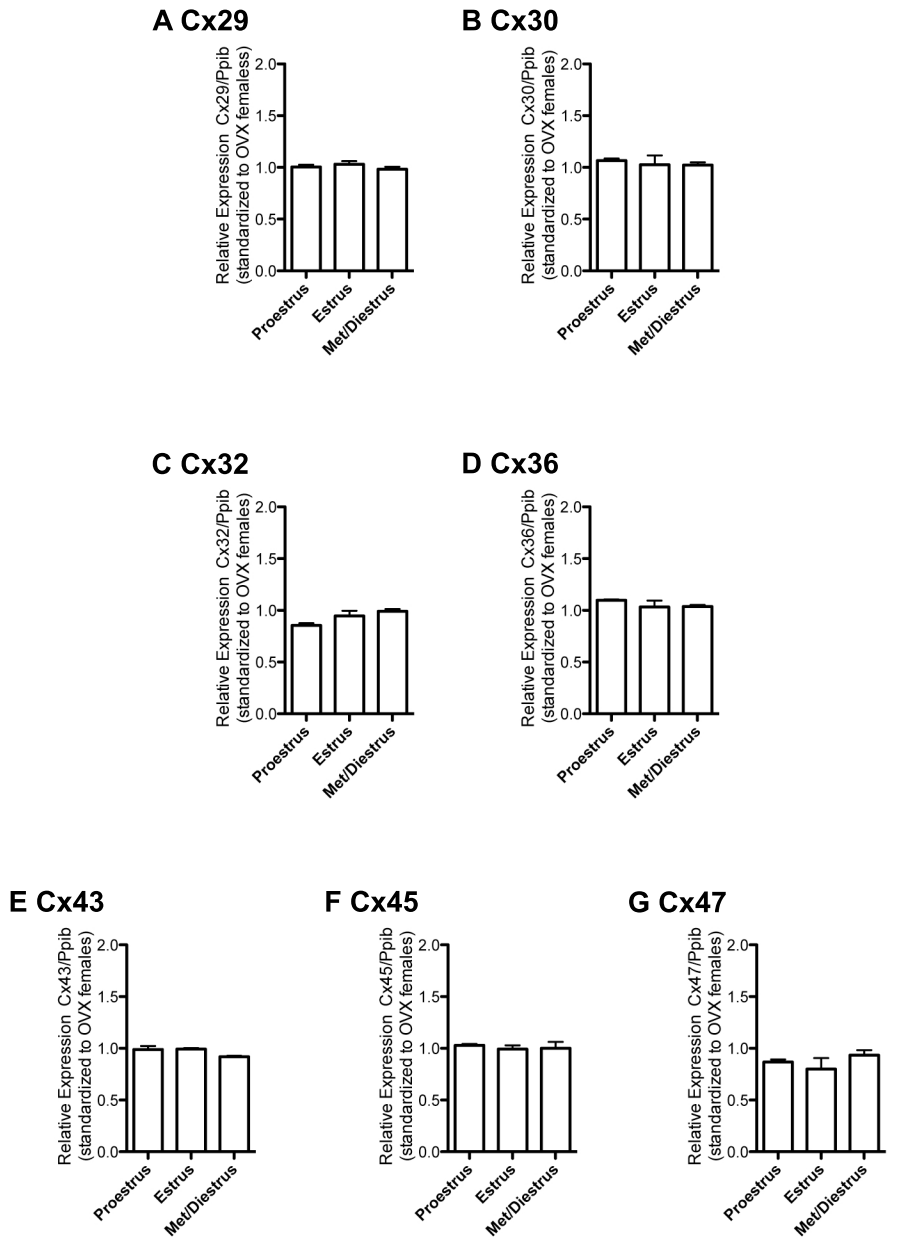
A Cx29
Relative Expression Cx29/Ppib (standardized to OVX femaless)
2.0
1.5
1.0
0.5
0.0
Proestrus
Estrus
Met/Diestrus
B Cx30
Relative Expression Cx30/Ppib (standardized to OVX females)
C Cx32
Relative Expression Cx32/Ppib (standardized to OVX females)
D Cx36
Relative Expression Cx36/Ppib (standardized to OVX females)
E Cx43
Relative Expression Cx43/Ppib (standardized to OVX females)
F Cx45
Relative Expression Cx45/Ppib (standardized to OVX females)
G Cx47
Relative Expression Cx47/Ppib (standardized to OVX females)

Figure 4.6

4.6 Discussion

Any study using quantitative analysis of mRNA expression levels requires the proper reference genes for standardization to ensure equal template amplification (i.e., loading control) (183). Consistent with previous reports that GAPDH mRNA expression is estradiol sensitive in human thyroid cells *in vitro* (183), we found that GAPDH expression fluctuated over the course of estrous, with mRNA levels significantly lower in proestrus (Figure 4.1B) when 17-β-estradiol levels peak (127). Furthermore, this finding was seen with Rn18s and Hprt, two other potential reference genes examined. Surprisingly, we found that expression of the majority of HKGs was suppressed during proestrus in hippocampus when estradiol levels are higher (Figure 4.1B). These data contrast with the traditional view that ER activation induces gene transactivation (82). Given our findings, one may speculate that the presence of 17-β-estradiol ligand binding causes ER activation, and by subsequent binding of EREs within promoter regions of these reference genes, represses the transcription resulting in lower mRNA expression by recruiting co-repressors. Certainly in peripheral tissues, 17-β-estradiol has been shown to increase GAPDH transcription (184). My data differ from this finding and likely suggest tissue-specific regulation. GAPDH has seven classical and nine half palindromic ERE sites (184), which are sufficient in altering GADPH expression in uterine tissue of the C57BL/6 female mouse as early as 6 h following estradiol treatment (184). Further, the significant decrease between OVX and proestrus in the expression of Rn18s but not Hprt and GAPDH (compare Figure 4.1C and B, D) may be caused by potential differences in ERE sites, as well as AP-1 response elements between the promoter regions of the reference genes, with 17-β-estradiol levels during proestrus having a more pronounced effect on the repression of Rn18s expression.

I show here that Ppib mRNA levels do not change over the estrous cycle. These data are consistent with previous northern blot analysis of rat pituitary cells cultured *in vitro* following estradiol treatment (185). Thus, Ppib mRNA expression levels are stable within the hippocampus (Figure 4.1E) or spinal cord (Figure 4.2B), and therefore it was selected as the optimal reference gene.

The seven connexin assays employed in qRT-PCR of hippocampal mRNA expression were specifically validated when mRNA from null mutant controls were utilized simultaneously (Table 4.1). Within the hippocampus, Cx43 and Cx47 significantly fluctuated during the female mouse estrous cycle (Figure 4.4E, G). During the peak of 17-β-estradiol during proestrus (127), Cx43 and Cx47 expression was significantly lower than previous stage of met/diestrus when progesterone levels are known to be elevated (127). From these findings one may speculate a) elevated progesterone during met/diestrus may cause transcriptional activation of Cx43 and Cx47 gene expression, or b) elevated 17-β-estradiol during proestrus may cause transcriptional repression of Cx43 and Cx47 gene expression in the hippocampus. However, as no significant differences of Cx43 and Cx47 mRNA expression were detected between estrus (low progesterone) and met/diestrus (peak progesterone), one can conclude that the elevated progesterone levels during diestrus did not cause transcriptional activation of connexin gene expression and therefore would not account for the significant expression differences present between met/diestrus and proestrus (Figure 4.1B-D). This would suggest that, as seen with GAPDH, Rn18s, and Hprt (Figure 4.1B-D), during proestrus, 17-β-estradiol may be acting as a ligand for its receptor and causing downstream events, by the direct binding of EREs located within promoter regions and, surprisingly, causing transcriptional repression following the recruitment of co-repressors

(Figure 4.7B). Alternatively, ligand activated ERs may indirectly suppress transcription by binding transcription supressors or co-repressor complexes (Figure 4.7C). It has previously been shown that co-regulatory proteins including histone deacetylases, which form complexes and can bind to promoter regions, such as the AP-1 responsive gene element site, act as co-repressors producing a dominant negative effect on connexin transcription (186) (Figure 4.7C). Furthermore, the finding that alterations in connexin expression was limited to two of the seven connexins examined suggests the differences in number and functionality of EREs and responsive gene elements within the various connexin promoter regions dictates the connexin specific effects of hormonal regulation.

Although Cx43 and Cx47 do appear to be under hormonal regulation over the estrous cycle in intact females within the hippocampus, no significant gender differences of Cx43 and Cx47 expression were present in this region (compare Figure 4.4E, G to Figure 4.3E, G). To address effects of estrous in intact females, I ensured intact female group consisted of three experimental samples from each stage (proestrus n=3, estrus n=3, and met/diestrus n=3). Thus, the average expression level across the female estrous cycle did not significantly differ from males.

Intriguingly, Cx43 and Cx47 did not fluctuate over the female mouse estrous cycle within the spinal cord (compare Figure 4.4E, G vs. Figure 4.6E, G). Three plausible explanations may account for this regionally-specific finding a) alternative promoter usage, b) epigenetic modification and/or c) hormone receptor expression. The most likely explanation is differential promoter usage defined by differential HRE response. Nine murine Cx43 mRNA species are generated as a result differential promoter usage and alternative splicing likely with different hormonal sensitivity (102). There are also two Cx47

Figure 4.7 Transcriptional activation and repression. Estrogen (red pentagon, E) can act as a ligand causing ERs (dark red oval, ER) to dimerize bind to (A, B) EREs (pink box, ERE) leading to transcriptional (A) activation or (B) repression by recruitment of a co-repression complex (blue circles, Co-R complex). Activated ERs can also dimerize and bind to transcription factors (green oval, TF) which may recruit co-repression complexes and bind to (C) gene responsive elements (green box, GRE) within the promoter region of genes resulting in transcriptional repression. Co-repressors may induce epigenetic modifications such as (D) histone modification (blue pentagon) or (E) DNA methylation which may block promoter responsive elements and result in transcriptional repression. Furthermore, epigenetic modifications (D, E) may be present within promoter regions in a cell specific manner.

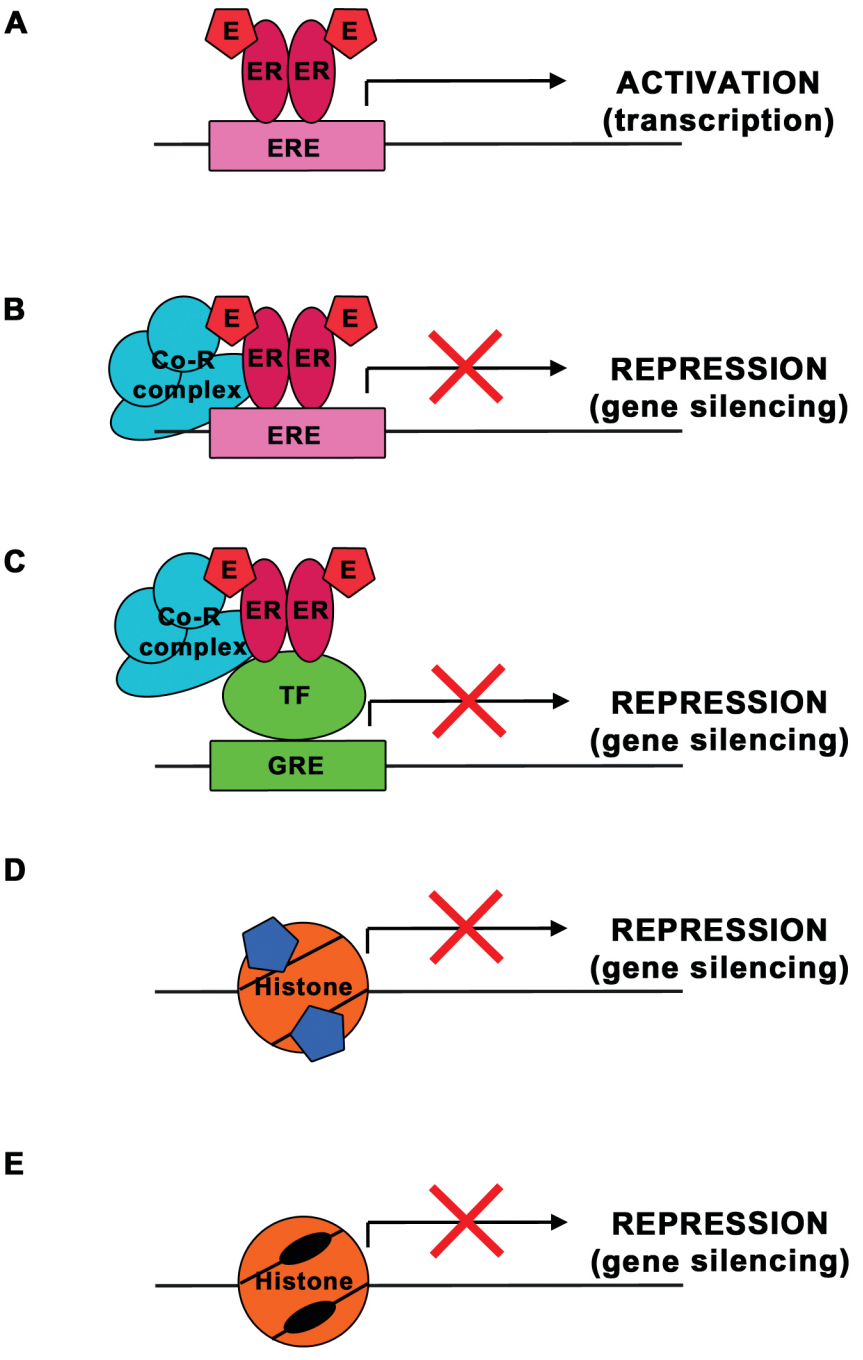
A
E
E
ER
ER
ERE
ACTIVATION
(transcription)
B
E
E
Co-R
complex
ER
ER
ERE
REPRESSION
(gene silencing)
C
E
E
Co-R
complex
ER
ER
TF
GRE
REPRESSION
(gene silencing)
D
Histone
REPRESSION
(gene silencing)
E
Histone
REPRESSION
(gene silencing)

Figure 4.7

transcripts that code for the same protein but different in their 5' UTR length generated by alterative promoters (115). It remains to be determined whether these promoters are differentially used in hippocampus and spinal cord.

It is also possible that epigenetic factors, such as histone modification (Figure 4.7D) and DNA methylation (Figure 4.7E) status within the promoter regions of Cx43 and Cx47 may differ between the hippocampus and spinal cord. Gene expression of connexins can be activated or silenced by the effects of histone modification through the acetylation or methylation of histone proteins (187, 188). This process has been linked to the involvement of protein complexes with histone acetyltransferase activity and transcription factors such as AP-1 and Sp1, with the acetylation state of histones being modifiable near responsive gene elements within connexin promoter regions (189). More specifically, the induction of Cx43 in human prostate cancer cells treated with a deacetylation inhibitor Trichostatin A (TSA) has been associated with the hyperacetylation of histone H4 adjacent to AP-1 and Sp1 responsive gene elements (189). Furthermore, this epigenetic modification can be cell specific, with TSA increasing Cx36 expression in pancreatic cells (αTC1-9, βTC3) but not in neuronal (SN56) or pituitary (AtT20) cell lines examined (188). These cell type specific differences in Cx36 were specifically linked to epigenetic markers on histone H3, with methylation of lysine residue 9 corresponding to gene silencing whereas methylation of lysine residue 4 marked for active transcription (188). A second possible epigenetic mechanism is the DNA methylation (Figure 4.7E) of connexin promoter regions, which can also lead to inactivation of gene expression in a connexin dependent and cell type specific manner (190). Studies have suggested that hypermethylation of the Cx43 promoter may interfere with AP-1 binding, leading to the repression of Cx43 expression *in vivo* (191). A

more recent mechanism of much study is the function of microRNAs (miRNAs), which can modulate the expression of many connexins at the transcriptional and posttranscriptional level by directly binding to 3' untranslated regions of mRNA leading to a) the transcript being targeted for degradation or b) translational repression (190). Within the CNS, the expression of unique miRNAs are highly cell specific as shown by microarray analysis of neurons, astrocytes, OLs, and microglia from primary cultures of rat cortex (192). Whether $Cx43^{+}$ astrocytes or $Cx47^{+}$ OLs have distinct miRNAs expressed between regions (i.e. hippocampus and spinal cord) currently remains unknown. Furthermore, the expression of miRNAs over the course of the mouse estrous cycle has not yet been examined.

Another plausible explanation that may account for any gene activation/repression effects of 17-β-estradiol on Cx43 and Cx47 expression may be the differential receptor expression between regions of the CNS, as the overall density and labeling of ERβ is higher in the rat hippocampus than spinal cord (124). Furthermore, hormone receptors have been shown to fluctuate across the rodent estrous cycle with expression levels detectable at different amounts between various CNS regions (125, 193, 194). Within the intact female mouse hippocampus, PR expression peaked during proestrus (125) when estrogen levels are elevated (127, 151), ERβ expression was elevated throughout estrus/diestrus, and ERα peaked during diestrus (125) when progesterone levels are elevated (127, 151). Although 17-β-estradiol levels peak during proestrus in the mouse hippocampus (Figure 4.8A), the reduction in ERα and ERβ expression during this stage (Figure 4.8B) may lead to a reduction in ligand-binding (Figure 4.8C) and subsequently reduce any potential downstream transactivation effects on the transcription of Cx43 and Cx47 with basal levels present during proestrus (Figure 4.8C-D, compare arrows across stages). Should this be the case, no

Figure 4.8 Fluctuations in transcription of Cx43 and Cx47 may be related to ligand-bound estrogen receptor levels over the course of estrous. During the mouse estrous cycle, circulating estrogen level peak during proestrus (A, adapted from Figure 3.2). Within the mouse hippocampus, Mitterling et. al. 2010 has shown that the expression of estrogen receptors (B, dark pink oval, ER) fluctuate over the course of the estrous cycle, with ERβ elevated between estrus and diestrus, whereas ERα is elevated during diestrus, both having high affinity for the binding of estrogen (Kuiper et. al. 1997). With elevated bound estrogen receptor levels during met/diestrus, and lowest during proestrus (C), this may lead to a significant increase in transcriptional activation during met/diestrus when compared to proestrus (compare red arrows between stages, D).

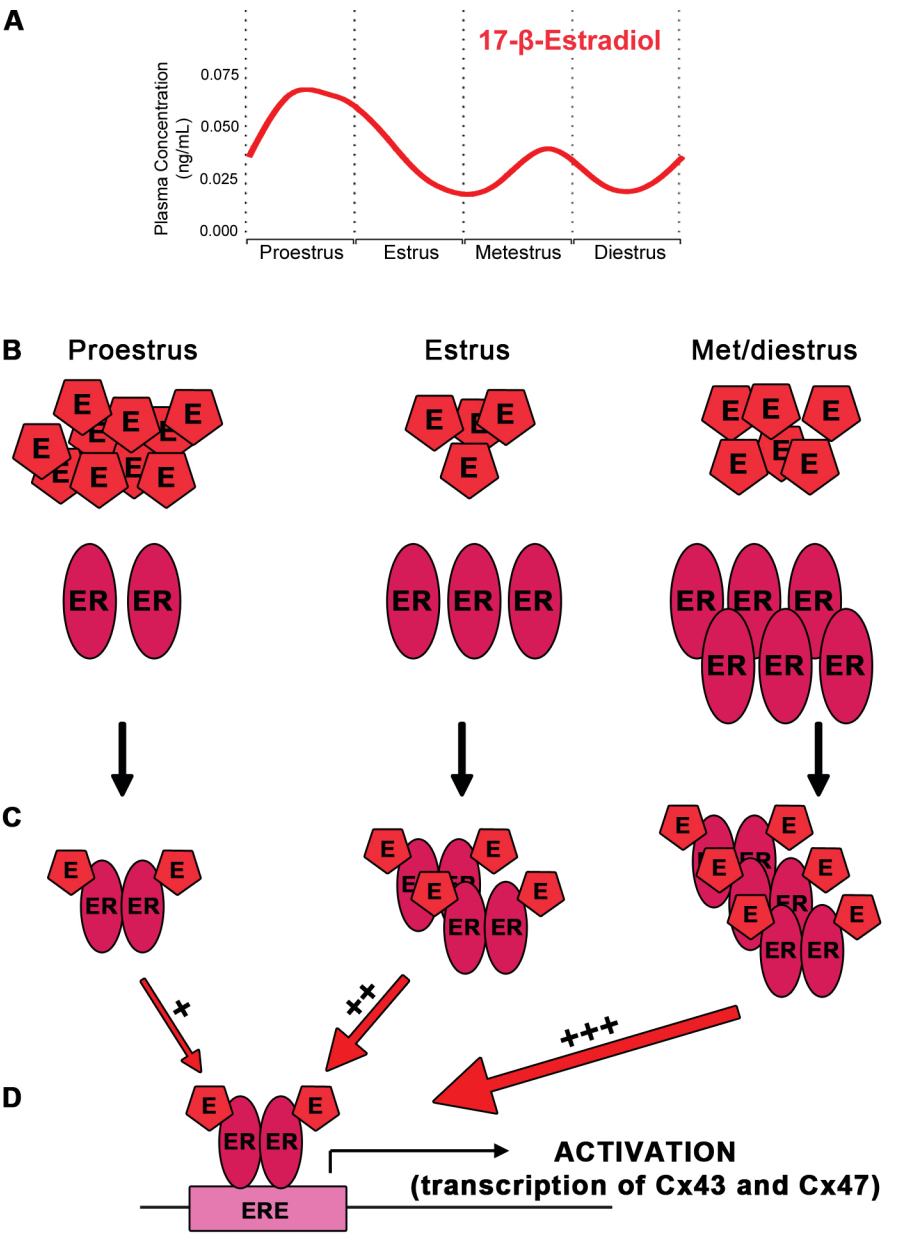
A
17-β-Estradiol
Plasma Concentration (ng/mL)
0.075
0.050
0.025
0.000
Proestrus
Estrus
Metestrus
Diestrus
B
Proestrus
Estrus
Met/diestrus
E
ER
C
+
++
+++
D
ERE
ACTIVATION
(transcription of Cx43 and Cx47)

Figure 4.8

changes are seen in Cx43 and Cx47 expression in the thoracic spinal cord, which may lead one to postulate that hormone receptor expression may be different or not fluctuate within spinal cord during the mouse estrous cycle. Although cyclic fluctuations in spinal cord hormone receptor expression patterns in the mouse have yet to be elucidated, studies have shown expression does fluctuate in rat (193, 194).

Within the intact cycling rat, hormone receptors fluctuate over the course of the estrous cycle in lumbar regions (193, 194). Fluctuating ER concentrations corresponded to changes in serum estradiol concentrations, which both peaked during the afternoon of proestrus (194), whereas PR expression peaked during late proestrus (193). PR expression appeared to be estrogen-inducible as seen by a significant increase in PR expression in castrated male rats treated with estradiol (193). These findings in rat spinal cord must be interpreted with caution with respect to our study. The spinal cord regions of interest in these studies included the lumbar (193) and lumbosacral (194) regions. No studies evaluating hormone receptor expression within the thoracic region (our region of focus) have been undertaken as of current. Furthermore, changes in receptor expression in rat may differ in mouse. In the rat estrous cycle, 17-β-estradiol peaks during mid-proestrus, which followed by a peak of progesterone in late proestrus (195), which strengthens the argument for biological relevance of upregulation of PR expression being estrogen inducible in rats (193). But one must note that the hormonal fluctuations within the rat and mouse estrous cycle differ significantly, with rats displaying a peak in 17-β-estradiol followed by peak in progesterone during proestrus approximately 6 hr apart (195) and mice displaying a peak in progesterone during diestrus followed by peak 17-β-estradiol during proestrus approximately

24 hr apart (127, 151) and given such differences among rodents, it is plausible to hypothesize that receptor expression may differ significantly as well.

When examining connexin expression between genders within the spinal cord, Cx43 was significantly decreased in males when compared to both OVX females and intact females (Figure 4.5E). As OVX females have lower levels of the fluctuating hormones seen in the intact cycling females, the fluctuating hormones cannot be attributed to this finding. Cx43 protein levels and subsequent gap junctional coupling has been shown to be suppressed *in vitro* following the treatment of human granulosa cells with high levels of androgen treatment through androgen receptor activation (196). Our findings suggest that androgens and/or receptor expression present in males may repress the Cx43 expression levels within the spinal cord, and as hippocampal Cx43 levels are not significantly different between genders, androgen receptor expression may vary between hippocampus and spinal cord.

Gap junctional communication between glial cells is imperative for cell survival (24) and connexins play an important role in preventing cell death in an ion buffering capacity during excitotoxicity. With mRNA expression of Cx43 and Cx47 regulated in an estrogen dependent manner in the hippocampus and Cx43 responsive to androgens in spinal cord, manipulation of hormonal responsiveness through modulation of receptor expression, direct hormone levels and/or receptor agonists/antagonists to enhance buffering capacity in a connexin specific and regionally specific manner may be potential therapeutic targets for the reduction of cell death during CNS insult.

CHAPTER 5: DISCUSSION

In summary, I have shown that, due to the homology of connexin genes, validation of expression using null-mutant controls is of utmost importance to ensure accurate assessment of expression. In this thesis, this was particularly highlighted in Chapter 2 for Cx32 where a tissue-specific epitope was unmasked following protein denaturation not detected when protein tertiary conformation was maintained. This study was published in the journal of Cell Communication and Adhesion (197). As the initial overarching objective was to identify connexins in hippocampus and spinal cord that were under hormonal control, I further optimized a standard technique to determine the murine reproductive estrous stages as dictated by cyclic hormonal fluctuations by adapting the protocol to minimize invasive procedures using crystal violet histology and cell typology. This study was published in the Journal of Visualized Experiments (127). Finally, I assessed mRNA expression of Cx29, Cx30, Cx32, Cx36, Cx43, Cx45 and Cx47 in both hippocampus and spinal cord and determined that the expression of Cx43 and Cx47 fluctuates over the course of the estrous cycle in hippocampus but not spinal cord. These data indicate that connexin mRNA expression within the CNS is under hormonal control, albeit to a moderate extent, in a regionally specific, hormonally specific, and connexin specific manner.

Findings in Chapter 2 are consistent with previous reports of connexin antibody cross-reactivity. We determined that eight antibodies developed for Cx32 detection produced an anti-Cx32 reactive band with western blot analysis when probing brain but not liver protein homogenate of $Cx32^{Y/-}$ mice (Figure 2.3 and 2.4). The cross-reactive banding was eliminated by retaining tertiary conformation of protein lysates using immunofluorescence

(Figure 2.5) and/or immunoprecipitation (Figure 2.7). These findings lead to our hypothesis that the primary sequence of the cross-reactive protein contained epitopes which were masked with proper structure folding, but due to the reducing/denaturing conditions of our western blotting, these epitopes were now accessible for antibody detection. Using sucrose gradient fractionation, we were able to localize the cross-reactive band to a subcellular compartment differing from Cx32, with bands displaying a 4-kDa size difference (Figure 2.8). Through analysis of antigenic sites of Cx32 and banding patterns of cross-reactive bands, we used a bioinformatics approach to identify possible cross-reactive candidate proteins, which suggested Cx30 as a plausible target. Using Cx32 antibodies, the cross-reactive band was not eliminated when probing $Cx30^{-/-}$ brain protein homogenate (Figure 2.9A). Furthermore, Cx26 and Cx29 were eliminated as possible cross-reactive targets (Figure 2.9C, A). Given these findings, we concluded that the cross-reactive band was likely not a connexin family member and the employment of null mutant controls are crucial when evaluating connexin expression.

The overarching goal of this thesis was to address role of Cx32 in SCI hypothesizing that hormonal control would alter NPC and OL fate over the course of the estrous cycle. Within the CNS, cell survival following excitotoxicity requires proper gap junctional communication between astrocytes and OLs (24), specifically Cx32 and Cx47 of mature OLs(30) and Cx30 and Cx43 of astrocytes (36). The presence of these connexins and capacity of astrocytes to act as a ‘sink’ to remove excess ions following excitotoxicity is crucial in the prevention of vacuolation and subsequent neuronal death (36).

This hypothesis fit in the larger context of a sizable body of literature suggesting the myelination is under hormonal control (198-200). However, I found little evidence for

hormonal regulation of connexin expression at the mRNA level with the exception of cyclic changes in Cx43 and Cx45 in hippocampus but not spinal cord over the course of the estrous cycle. These data were initially surprising. Shinohara et. al. (65) have shown that Cx36 mRNA expression was significantly elevated in the SCN following estradiol treatment in female OVX rats (65). This increase did not occur when treated with progesterone alone (65). Interestingly, treatment with estradiol followed by progesterone suppressed the increase in Cx36 mRNA, with levels remaining comparable to vehicle. When evaluating the treatments in the CX of female OVX rats (estradiol alone, progesterone alone, or estradiol and progesterone), Cx36 mRNA levels were not altered when compared to vehicle control further demonstrating the regional specificity of hormonal regulation on connexin expression (65). Regional specificity of connexin expression regulation is not as surprising, as described in great detail by Shughrue et. al. (124), hormone receptor expression within regions of the rodent brain is highly variable (124). As well, ERα, ERβ and PR have been shown to fluctuate over the course of the estrous cycle within the hippocampus (125).

My findings are, however consistent with previous reports that Cx43 is hormonally regulated and report, for the first time, a potential hormonal regulation for Cx47. At the protein level, within the POA of rats, an area rich with gonadotropin releasing hormone (GnRH) cell bodies, Cx43 protein expression is regulated in a sexually dimorphic manner (66). Following gonadectomy to eliminate endogenous fluctuating hormones, female rats treated with estradiol benzoate and progesterone produced a significant increase in Cx43 protein expression when evaluated by western blot analysis in the POA, whereas the identical treatment in male rats produced a significant decrease in Cx43 protein expression (66). The hormonal treatment was found to be regionally specific in the female

gonadectomized rats, as western blot analysis determined that within the hypothalamus, a region rich with GnRH nerve terminals, Cx43 protein levels significantly decreased (66). Furthermore, female mice heterozygous for Cx43 ($Cx43^{+/-}$) had disrupted sexual behaviour, with the occurrence of lordosis decreasing, and abnormal estrous cycling present, typically remaining longer in estrus or diestrus, or fluctuating between estrus and diestrus (66). The estrous cycle of female $Cx43^{+/-}$ mice was significantly affected as these mice overall entered the proestrus stage significantly less often than WT female mice, suggesting that Cx43 expression may be functioning in the regulation of reproduction not only at the reproductive tissue level (i.e. myometrium), but within the brain as well (66). It may be, in this thesis, that cyclic fluctuations in steady state Cx43 and Cx47 mRNA levels can be attributed to the fluctuating levels of a) 17-β-estradiol (127) and/or b) ERs (125). There are two primary estrogen receptor subtypes, ERα and ERβ, which are homologous in their DNA and ligand-binding domains (97% and 60% respectively) (201) and have a high affinity for binding 17-β-estradiol (73). Differences lie in localization and function (73, 123, 124, 202), although hippocampus expresses both ERα and ERβ (97). Although plasma hormonal fluctuations would be systemic within the rodent, changes in ERs within the spinal cord may be occurring in a manner dissimilar to hippocampus (124), a plausible explanation for the differential findings between hippocampus and spinal cord connexin expression. Interestingly, ERβ density is greater in the rat hippocampus than spinal cord overall (124) and should this occur in mouse, this may account for the hippocampal sensitivity during proestrus when 17-β-estradiol peak.

Moreover, I have shown that significant differences were present in Cx43 mRNA expression, between genders within the spinal cord (Chapter 4). Cx43 was found to be

significantly decreased in males when compared to OVX and intact cycling females, suggesting that Cx43 mRNA expression may be affected directly by androgens and/or androgen receptor expression. This finding is consistent with previous studies conducted by Wu et. al. (196) demonstrating Cx43 is in fact suppressed by androgen treatment *in vitro* via androgen receptor activation, a phenomenon which may be occurring in our spinal cord studies.

Although not assessed here, both the post-translational modifications of connexin proteins and their intracellular trafficking have been shown to be under hormonal regulation (67, 203). As described in chapter 1, six connexin proteins oligomerize to form a single trans-membrane pore or channel, termed a connexon (19). Hendrix et. al. (67) found within myometrial tissue of ovariectomized rats treated with progesterone, trafficking of Cx43 from golgi was significantly suppressed and did not form connexons within the plasma membrane as visualized with immunofluorescence, although synthesis of individual Cx43 connexin protein subunits themselves did not appear to be altered (67). Whether stability, localization and/or degradation may be altered over the course of the estrous cycle within the CNS has yet to be evaluated, and may be occurring while no effects are present on mRNA expression levels. With the exception of Cx26, connexins typically have a short half-life of ~1.5-5 h (204). Mitra et. al. (203) have shown that stability is under hormonal regulation in androgen-responsive human prostate cancer cells *in vitro* (203). Cx32 expression is modulated in a post-translational manner by the treatment of androgens, which prevents protein degradation and promotes the assembly of gap junctions within the plasma membrane (203).

Initially, I hypothesized that changes in connexin expression over the course of the estrous cycle would render females more susceptible to demyelinating diseases than males

and represent a therapeutic target for MS. Within the CNS, gap junctional communication between astrocytes and OLs are crucial for cell survival (24). The buffering capacity of astrocytes is imperative to excitotoxic production of potassium, acting as a 'sink' to remove excess ions and preventing neuronal death (36). The transfer of excess potassium ions requires gap junctional communication, specifically Cx32 and Cx47 of mature OLs (30) and Cx30 and Cx43 of astrocytes (36). When combinations of these gap junctional proteins are absent, an increase in vacuolation is present and cell death occurs (24, 36). The potential for modulation of Cx43 expression within the spinal cord, and Cx43 and/or Cx47 expression within the hippocampus by genetic manipulation of hormonal responsiveness through modulation of receptor expression to enhance buffering capacity may be potential therapeutic targets for the reduction of cell death during demyelinating diseases of the CNS such as SCI and MS. Data presented in this thesis do not support a role for cyclic fluctuations in connexin expression in disease progression as I show that mRNA expression levels are not altered in spinal cord by fluctuating hormones during the murine estrous cycle.

REFERENCES

1. **Simon AM, Goodenough DA.** 1998. Diverse functions of vertebrate gap junctions. Trends in cell biology **8:**477-483.
2. **Stout C, Goodenough DA, Paul DL.** 2004. Connexins: functions without junctions. Current opinion in cell biology **16:**507-512.
3. **Sohl G, Willecke K.** 2004. Gap junctions and the connexin protein family. Cardiovascular research **62:**228-232.
4. **Rouach N, Avignone E, Meme W, Koulakoff A, Venance L, Blomstrand F, Giaume C.** 2002. Gap junctions and connexin expression in the normal and pathological central nervous system. Biology of the cell **94:**457-475.
5. **Vandecasteele M, Glowinski J, Venance L.** 2006. Connexin mRNA expression in single dopaminergic neurons of substantia nigra pars compacta. Neuroscience research **56:**419-426.
6. **Kreuzberg MM, Deuchars J, Weiss E, Schober A, Sonntag S, Wellershaus K, Draguhn A, Willecke K.** 2008. Expression of connexin30.2 in interneurons of the central nervous system in the mouse. Molecular and cellular neuroscience **37:**119-134.
7. **Dere E, Zheng-Fischhofer Q, Viggiano D, Gironi Carnevale UA, Ruocco LA, Zlomuzica A, Schnichels M, Willecke K, Huston JP, Sadile AG.** 2008. Connexin31.1 deficiency in the mouse impairs object memory and modulates open-field exploration, acetylcholine esterase levels in the striatum, and cAMP response element-binding protein levels in the striatum and piriform cortex. Neuroscience **153:**396-405.
8. **Condorelli DF, Trovato-Salinaro A, Mudo G, Mirone MB, Belluardo N.** 2003. Cellular expression of connexins in the rat brain: neuronal localization, effects of kainate-induced seizures and expression in apoptotic neuronal cells. The European journal of neuroscience **18:**1807-1827.
9. **Hombach S, Janssen-Bienhold U, Sohl G, Schubert T, Bussow H, Ott T, Weiler R, Willecke K.** 2004. Functional expression of connexin57 in horizontal cells of the mouse retina. The European journal of neuroscience **19:**2633-2640.
10. **Kempermann G, Jessberger S, Steiner B, Kronenberg G.** 2004. Milestones of neuronal development in the adult hippocampus. Trends in neurosciences **27:**447-452.
11. **Imbeault S, Gauvin LG, Toeg HD, Pettit A, Sorbara CD, Migahed L, DesRoches R, Menzies AS, Nishii K, Paul DL, Simon AM, Bennett SA.** 2009. The extracellular matrix controls gap junction protein expression and function in postnatal hippocampal neural progenitor cells. BMC neuroscience **10:**13.
12. **Nagy JI, Li X, Rempel J, Stelmack G, Patel D, Staines WA, Yasumura T, Rash JE.** 2001. Connexin26 in adult rodent central nervous system: demonstration at astrocytic gap junctions and colocalization with connexin30 and connexin43. The Journal of comparative neurology **441:**302-323.
13. **Kunzelmann P, Schroder W, Traub O, Steinhauser C, Dermietzel R, Willecke K.** 1999. Late onset and increasing expression of the gap junction protein connexin30 in adult murine brain and long-term cultured astrocytes. Glia **25:**111-119.

14. **Yamamoto T, Ochalski A, Hertzberg EL, Nagy JI.** 1990. On the organization of astrocytic gap junctions in rat brain as suggested by LM and EM immunohistochemistry of connexin43 expression. The Journal of comparative neurology **302:**853-883.
15. **Altevogt BM, Kleopa KA, Postma FR, Scherer SS, Paul DL.** 2002. Connexin29 is uniquely distributed within myelinating glial cells of the central and peripheral nervous systems. The Journal of neuroscience **22:**6458-6470.
16. **Scherer SS, Deschenes SM, Xu YT, Grinspan JB, Fischbeck KH, Paul DL.** 1995. Connexin32 is a myelin-related protein in the PNS and CNS. The Journal of neuroscience **15:**8281-8294.
17. **Odermatt B, Wellershaus K, Wallraff A, Seifert G, Degen J, Euwens C, Fuss B, Bussow H, Schilling K, Steinhauser C, Willecke K.** 2003. Connexin 47 (Cx47)-deficient mice with enhanced green fluorescent protein reporter gene reveal predominant oligodendrocytic expression of Cx47 and display vacuolized myelin in the CNS. The Journal of neuroscience **23:**4549-4559.
18. **Belluardo N, Mudo G, Trovato-Salinaro A, Le Gurun S, Charollais A, Serre-Beinier V, Amato G, Haefliger JA, Meda P, Condorelli DF.** 2000. Expression of connexin36 in the adult and developing rat brain. Brain research **865:**121-138.
19. **Altevogt BM, Paul DL.** 2004. Four classes of intercellular channels between glial cells in the CNS. The Journal of neuroscience **24:**4313-4323.
20. **Kamermans M, Fahrenfort I, Schultz K, Janssen-Bienhold U, Sjoerdsma T, Weiler R.** 2001. Hemichannel-mediated inhibition in the outer retina. Science **292:**1178-1180.
21. **Dale N.** 2008. Dynamic ATP signalling and neural development. The Journal of physiology **586:**2429-2436.
22. **Hung J, Colicos MA.** 2008. Astrocytic Ca(2+) waves guide CNS growth cones to remote regions of neuronal activity. PLoS ONE **3:**e3692.
23. **Elias LA, Wang DD, Kriegstein AR.** 2007. Gap junction adhesion is necessary for radial migration in the neocortex. Nature **448:**901-907.
24. **Menichella DM, Goodenough DA, Sirkowski E, Scherer SS, Paul DL.** 2003. Connexins are critical for normal myelination in the CNS. The Journal of neuroscience **23:**5963-5973.
25. **Menichella DM, Majdan M, Awatramani R, Goodenough DA, Sirkowski E, Scherer SS, Paul DL.** 2006. Genetic and physiological evidence that oligodendrocyte gap junctions contribute to spatial buffering of potassium released during neuronal activity. The Journal of neuroscience **26:**10984-10991.
26. **Orthmann-Murphy JL, Freidin M, Fischer E, Scherer SS, Abrams CK.** 2007. Two distinct heterotypic channels mediate gap junction coupling between astrocyte and oligodendrocyte connexins. The Journal of neuroscience **27:**13949-13957.
27. **Wasseff SK, Scherer SS.** 2011. Cx32 and Cx47 mediate oligodendrocyte:astrocyte and oligodendrocyte:oligodendrocyte gap junction coupling. Neurobiology of disease **42:**506-513.
28. **Maglione M, Tress O, Haas B, Karram K, Trotter J, Willecke K, Kettenmann H.** 2010. Oligodendrocytes in mouse corpus callosum are coupled via gap junction channels formed by connexin47 and connexin32. Glia **58:**1104-1117.

29. **Bone LJ, Deschenes SM, Balice-Gordon RJ, Fischbeck KH, Scherer SS.** 1997. Connexin32 and X-linked Charcot-Marie-Tooth disease. Neurobiology of disease **4:**221-230.
30. **Kamasawa N, Sik A, Morita M, Yasumura T, Davidson KG, Nagy JI, Rash JE.** 2005. Connexin-47 and connexin-32 in gap junctions of oligodendrocyte somata, myelin sheaths, paranodal loops and Schmidt-Lanterman incisures: implications for ionic homeostasis and potassium siphoning. Neuroscience **136:**65-86.
31. **Gencic S, Abuelo D, Ambler M, Hudson LD.** 1989. Pelizaeus-Merzbacher disease: an X-linked neurologic disorder of myelin metabolism with a novel mutation in the gene encoding proteolipid protein. American journal of human genetics **45:**435-442.
32. **Tress O, Maglione M, Zlomuzica A, May D, Dicke N, Degen J, Dere E, Kettenmann H, Hartmann D, Willecke K.** 2011. Pathologic and phenotypic alterations in a mouse expressing a connexin47 missense mutation that causes Pelizaeus-Merzbacher-like disease in humans. PLoS genetics **7:**e1002146.
33. **Bergoffen J, Scherer SS, Wang S, Scott MO, Bone LJ, Paul DL, Chen K, Lensch MW, Chance PF, Fischbeck KH.** 1993. Connexin mutations in X-linked Charcot-Marie-Tooth disease. Science **262:**2039-2042.
34. **Nelles E, Butzler C, Jung D, Temme A, Gabriel HD, Dahl U, Traub O, Stumpel F, Jungermann K, Zielasek J, Toyka KV, Dermietzel R, Willecke K.** 1996. Defective propagation of signals generated by sympathetic nerve stimulation in the liver of connexin32-deficient mice. Proceedings of the National Academy of Sciences of the United States of America **93:**9565-9570.
35. **Sargiannidou I, Vavlitou N, Aristodemou S, Hadjisavvas A, Kyriacou K, Scherer SS, Kleopa KA.** 2009. Connexin32 mutations cause loss of function in Schwann cells and oligodendrocytes leading to PNS and CNS myelination defects. The Journal of neuroscience **29:**4736-4749.
36. **Lutz SE, Zhao Y, Gulinello M, Lee SC, Raine CS, Brosnan CF.** 2009. Deletion of astrocyte connexins 43 and 30 leads to a dysmyelinating phenotype and hippocampal CA1 vacuolation. The Journal of neuroscience **29:**7743-7752.
37. **Magnotti LM, Goodenough DA, Paul DL.** 2011. Deletion of oligodendrocyte Cx32 and astrocyte Cx43 causes white matter vacuolation, astrocyte loss and early mortality. Glia **59:**1064-1074.
38. **Neusch C, Rozengurt N, Jacobs RE, Lester HA, Kofuji P.** 2001. Kir4.1 potassium channel subunit is crucial for oligodendrocyte development and in vivo myelination. The Journal of neuroscience **21:**5429-5438.
39. **Sohl G, Eiberger J, Jung YT, Kozak CA, Willecke K.** 2001. The mouse gap junction gene connexin29 is highly expressed in sciatic nerve and regulated during brain development. Biological chemistry **382:**973-978.
40. **Perez Velazquez JL, Frantseva MV, Naus CC.** 2003. Gap junctions and neuronal injury: protectants or executioners? The Neuroscientist **9:**5-9.
41. **Lin JH, Weigel H, Cotrina ML, Liu S, Bueno E, Hansen AJ, Hansen TW, Goldman S, Nedergaard M.** 1998. Gap-junction-mediated propagation and amplification of cell injury. Nature neuroscience **1:**494-500.
42. **Sanson M, Marcaud V, Robin E, Valery C, Sturtz F, Zalc B.** 2002. Connexin 43-mediated bystander effect in two rat glioma cell models. Cancer gene therapy **9:**149-155.

43. **Neijssen J, Herberts C, Drijfhout JW, Reits E, Janssen L, Neefjes J.** 2005. Cross-presentation by intercellular peptide transfer through gap junctions. Nature **434:**83-88.
44. **Ye ZC, Wyeth MS, Baltan-Tekkok S, Ransom BR.** 2003. Functional hemichannels in astrocytes: a novel mechanism of glutamate release. The Journal of neuroscience **23:**3588-3596.
45. **Takeuchi H, Jin S, Wang J, Zhang G, Kawanokuchi J, Kuno R, Sonobe Y, Mizuno T, Suzumura A.** 2006. Tumor necrosis factor-alpha induces neurotoxicity via glutamate release from hemichannels of activated microglia in an autocrine manner. The Journal of biological chemistry **281:**21362-21368.
46. **Frantseva MV, Kokarovtseva L, Perez Velazquez JL.** 2002. Ischemia-induced brain damage depends on specific gap-junctional coupling. Journal of cerebral blood flow and metabolism **22:**453-462.
47. **Perez Velazquez JL, Kokarovtseva L, Sarbaziha R, Jeyapalan Z, Leshchenko Y.** 2006. Role of gap junctional coupling in astrocytic networks in the determination of global ischaemia-induced oxidative stress and hippocampal damage. The European journal of neuroscience **23:**1-10.
48. **Siushansian R, Bechberger JF, Cechetto DF, Hachinski VC, Naus CC.** 2001. Connexin43 null mutation increases infarct size after stroke. The Journal of comparative neurology **440:**387-394.
49. **Nakase T, Fushiki S, Naus CC.** 2003. Astrocytic gap junctions composed of connexin 43 reduce apoptotic neuronal damage in cerebral ischemia. Stroke **34:**1987-1993.
50. **Nakase T, Naus CC.** 2004. Gap junctions and neurological disorders of the central nervous system. Biochimica et biophysica acta **1662:**149-158.
51. **Condorelli DF, Mudo G, Trovato-Salinaro A, Mirone MB, Amato G, Belluardo N.** 2002. Connexin-30 mRNA is up-regulated in astrocytes and expressed in apoptotic neuronal cells of rat brain following kainate-induced seizures. Molecular and cellular neuroscience **21:**94-113.
52. **Lin JH, Yang J, Liu S, Takano T, Wang X, Gao Q, Willecke K, Nedergaard M.** 2003. Connexin mediates gap junction-independent resistance to cellular injury. The Journal of neuroscience **23:**430-441.
53. **Herve JC, Sarrouilhe D.** 2005. Connexin-made channels as pharmacological targets. Current pharmaceutical design **11:**1941-1958.
54. **Takano T, Kang J, Jaiswal JK, Simon SM, Lin JH, Yu Y, Li Y, Yang J, Dienel G, Zielke HR, Nedergaard M.** 2005. Receptor-mediated glutamate release from volume sensitive channels in astrocytes. Proceedings of the National Academy of Sciences of the United States of America **102:**16466-16471.
55. **Suadicani SO, Brosnan CF, Scemes E.** 2006. P2X7 receptors mediate ATP release and amplification of astrocytic intercellular Ca2+ signaling. The Journal of neuroscience **26:**1378-1385.
56. **Huang C, Han X, Li X, Lam E, Peng W, Lou N, Torres A, Yang M, Garre JM, Tian GF, Bennett MV, Nedergaard M, Takano T.** 2012. Critical role of connexin 43 in secondary expansion of traumatic spinal cord injury. The Journal of neuroscience **32:**3333-3338.

57. **O'Carroll SJ, Alkadhi M, Nicholson LF, Green CR.** 2008. Connexin 43 mimetic peptides reduce swelling, astrogliosis, and neuronal cell death after spinal cord injury. Cell communication & adhesion **15:**27-42.
58. **Markoullis K, Sargiannidou I, Gardner C, Hadjisavvas A, Reynolds R, Kleopa KA.** 2012. Disruption of oligodendrocyte gap junctions in experimental autoimmune encephalomyelitis. Glia **60:**1053-1066.
59. **Brand-Schieber E, Werner P, Iacobas DA, Iacobas S, Beelitz M, Lowery SL, Spray DC, Scemes E.** 2005. Connexin43, the major gap junction protein of astrocytes, is down-regulated in inflamed white matter in an animal model of multiple sclerosis. Journal of neuroscience research **80:**798-808.
60. **Roscoe WA, Messersmith E, Meyer-Franke A, Wipke B, Karlik SJ.** 2007. Connexin 43 gap junction proteins are up-regulated in remyelinating spinal cord. Journal of neuroscience research **85:**945-953.
61. **Lutz SE, Raine CS, Brosnan CF.** 2012. Loss of astrocyte connexins 43 and 30 does not significantly alter susceptibility or severity of acute experimental autoimmune encephalomyelitis in mice. Journal of neuroimmunology **245:**8-14.
62. **Magnano I, Aiello I, Piras MR.** 2006. Cognitive impairment and neurophysiological correlates in MS. Journal of the neurological sciences **245:**117-122.
63. **Ziehn MO, Avedisian AA, Tiwari-Woodruff S, Voskuhl RR.** 2010. Hippocampal CA1 atrophy and synaptic loss during experimental autoimmune encephalomyelitis, EAE. Laboratory investigation; a journal of technical methods and pathology **90:**774-786.
64. **Melanson-Drapeau L, Beyko S, Dave S, Hebb AL, Franks DJ, Sellitto C, Paul DL, Bennett SA.** 2003. Oligodendrocyte progenitor enrichment in the connexin32 null-mutant mouse. The Journal of neuroscience **23:**1759-1768.
65. **Shinohara K, Funabashi T, Nakamura TJ, Kimura F.** 2001. Effects of estrogen and progesterone on the expression of connexin-36 mRNA in the suprachiasmatic nucleus of female rats. Neuroscience letters **309:**37-40.
66. **Gulinello M, Etgen AM.** 2005. Sexually dimorphic hormonal regulation of the gap junction protein, CX43, in rats and altered female reproductive function in CX43+/- mice. Brain research **1045:**107-115.
67. **Hendrix EM, Myatt L, Sellers S, Russell PT, Larsen WJ.** 1995. Steroid hormone regulation of rat myometrial gap junction formation: effects on cx43 levels and trafficking. Biology of reproduction **52:**547-560.
68. **Granot I, Dekel N.** 1994. Phosphorylation and expression of connexin-43 ovarian gap junction protein are regulated by luteinizing hormone. The Journal of biological chemistry **269:**30502-30509.
69. **Lisse TS, Hewison M, Adams JS.** 2011. Hormone response element binding proteins: novel regulators of vitamin D and estrogen signaling. Steroids **76:**331-339.
70. **Pfaff DW, McEwen BS.** 1983. Actions of estrogens and progestins on nerve cells. Science **219:**808-814.
71. **McEwen BS.** 1976. Interactions between hormones and nerve tissue. Scientific American **235:**48-58.

72. **Kuiper GG, Enmark E, Pelto-Huikko M, Nilsson S, Gustafsson JA.** 1996. Cloning of a novel receptor expressed in rat prostate and ovary. Proceedings of the National Academy of Sciences of the United States of America **93:**5925-5930.
73. **Kuiper GG, Carlsson B, Grandien K, Enmark E, Haggblad J, Nilsson S, Gustafsson JA.** 1997. Comparison of the ligand binding specificity and transcript tissue distribution of estrogen receptors alpha and beta. Endocrinology **138:**863-870.
74. **Jensen EV.** 1962. On the mechanism of estrogen action. Perspectives in biology and medicine **6:**47-59.
75. **Mani SK, Reyna AM, Chen JZ, Mulac-Jericevic B, Conneely OM.** 2006. Differential response of progesterone receptor isoforms in hormone-dependent and -independent facilitation of female sexual receptivity. Molecular endocrinology **20:**1322-1332.
76. **Mani S.** 2008. Progestin receptor subtypes in the brain: the known and the unknown. Endocrinology **149:**2750-2756.
77. **Chakraborty S, Cole S, Rader N, King C, Rajnarayanan R, Biswas PK.** 2012. In silico design of peptidic inhibitors targeting estrogen receptor alpha dimer interface. Molecular diversity **16:**441-451.
78. **Chakraborty S, Willett H, Biswas PK.** 2012. Insight into estrogen receptor beta-beta and alpha-beta homo- and heterodimerization: A combined molecular dynamics and sequence analysis study. Biophysical chemistry **170:**42-50.
79. **Allan GF, Tsai SY, Tsai MJ, O'Malley BW.** 1992. Ligand-dependent conformational changes in the progesterone receptor are necessary for events that follow DNA binding. Proceedings of the National Academy of Sciences of the United States of America **89:**11750-11754.
80. **Danielian PS, White R, Lees JA, Parker MG.** 1992. Identification of a conserved region required for hormone dependent transcriptional activation by steroid hormone receptors. The EMBO journal **11:**1025-1033.
81. **Oltra E, Pfeifer I, Werner R.** 2003. Ini, a small nuclear protein that enhances the response of the connexin43 gene to estrogen. Endocrinology **144:**3148-3158.
82. **Yu W, Dahl G, Werner R.** 1994. The connexin43 gene is responsive to oestrogen. Proceedings. Biological sciences / The Royal Society **255:**125-132.
83. **Hurtado A, Holmes KA, Ross-Innes CS, Schmidt D, Carroll JS.** 2011. FOXA1 is a key determinant of estrogen receptor function and endocrine response. Nature genetics **43:**27-33.
84. **Miranda-Carboni GA, Guemes M, Bailey S, Anaya E, Corselli M, Peault B, Krum SA.** 2011. GATA4 regulates estrogen receptor-alpha-mediated osteoblast transcription. Molecular endocrinology **25:**1126-1136.
85. **Kong SL, Li G, Loh SL, Sung WK, Liu ET.** 2011. Cellular reprogramming by the conjoint action of ERalpha, FOXA1, and GATA3 to a ligand-inducible growth state. Molecular systems biology **7:**526.
86. **Petrocelli T, Lye SJ.** 1993. Regulation of transcripts encoding the myometrial gap junction protein, connexin-43, by estrogen and progesterone. Endocrinology **133:**284-290.
87. **Frye CA, DeBold JF.** 1992. Muscimol facilitates sexual receptivity in hamsters when infused into the ventral tegmentum. Pharmacology, biochemistry, and behavior **42:**879-887.

88. **Wade CB, Robinson S, Shapiro RA, Dorsa DM.** 2001. Estrogen receptor (ER)alpha and ERbeta exhibit unique pharmacologic properties when coupled to activation of the mitogen-activated protein kinase pathway. Endocrinology **142:**2336-2342.
89. **Walf AA, Frye CA.** 2008. Rapid and estrogen receptor beta mediated actions in the hippocampus mediate some functional effects of estrogen. Steroids **73:**997-1007.
90. **Murphy DD, Segal M.** 1997. Morphological plasticity of dendritic spines in central neurons is mediated by activation of cAMP response element binding protein. Proceedings of the National Academy of Sciences of the United States of America **94:**1482-1487.
91. **Zhou Y, Watters JJ, Dorsa DM.** 1996. Estrogen rapidly induces the phosphorylation of the cAMP response element binding protein in rat brain. Endocrinology **137:**2163-2166.
92. **Borowczyk E, Johnson ML, Bilski JJ, Bilska MA, Redmer DA, Reynolds LP, Grazul-Bilska AT.** 2007. Role of gap junctions in regulation of progesterone secretion by ovine luteal cells in vitro. Reproduction **133:**641-651.
93. **Karasinski J, Galas J, Semik D, Fiertak A, Bilinska B, Kilarski WM.** 2010. Changes of connexin43 expression in non-pregnant porcine myometrium correlate with progesterone concentration during oestrous cycle. Reproduction in domestic animals **45:**959-966.
94. **Geimonen E, Boylston E, Royek A, Andersen J.** 1998. Elevated connexin-43 expression in term human myometrium correlates with elevated c-Jun expression and is independent of myometrial estrogen receptors. The Journal of clinical endocrinology and metabolism **83:**1177-1185.
95. **Sohl G, Hombach S, Degen J, Odermatt B.** 2013. The oligodendroglial precursor cell line Oli-neu represents a cell culture system to examine functional expression of the mouse gap junction gene connexin29 (Cx29). Frontiers in pharmacology **4:**83.
96. **Sohl G, Willecke K.** 2003. An update on connexin genes and their nomenclature in mouse and man. Cell communication & adhesion **10:**173-180.
97. **Sullivan R, Ruangvoravat C, Joo D, Morgan J, Wang BL, Wang XK, Lo CW.** 1993. Structure, sequence and expression of the mouse Cx43 gene encoding connexin 43. Gene **130:**191-199.
98. **Oyamada M, Takebe K, Oyamada Y.** 2013. Regulation of connexin expression by transcription factors and epigenetic mechanisms. Biochimica et biophysica acta **1828:**118-133.
99. **Field JM, Tate LA, Chipman JK, Minchin SD.** 2003. Identification of functional regulatory regions of the connexin32 gene promoter. Biochimica et biophysica acta **1628:**22-29.
100. **Geimonen E, Jiang W, Ali M, Fishman GI, Garfield RE, Andersen J.** 1996. Activation of protein kinase C in human uterine smooth muscle induces connexin-43 gene transcription through an AP-1 site in the promoter sequence. The Journal of biological chemistry **271:**23667-23674.
101. **Hennemann H, Kozjek G, Dahl E, Nicholson B, Willecke K.** 1992. Molecular cloning of mouse connexins26 and -32: similar genomic organization but distinct promoter sequences of two gap junction genes. European journal of cell biology **58:**81-89.

102. **Pfeifer I, Anderson C, Werner R, Oltra E.** 2004. Redefining the structure of the mouse connexin43 gene: selective promoter usage and alternative splicing mechanisms yield transcripts with different translational efficiencies. Nucleic acids research **32:**4550-4562.
103. **Sohl G, Theis M, Hallas G, Brambach S, Dahl E, Kidder G, Willecke K.** 2001. A new alternatively spliced transcript of the mouse connexin32 gene is expressed in embryonic stem cells, oocytes, and liver. Experimental cell research **266:**177-186.
104. **Essenfelder GM, Larderet G, Waksman G, Lamartine J.** 2005. Gene structure and promoter analysis of the human GJB6 gene encoding connexin 30. Gene **350:**33-40.
105. **Miller T, Dahl G, Werner R.** 1988. Structure of a gap junction gene: rat connexin-32. Bioscience reports **8:**455-464.
106. **Bondurand N, Girard M, Pingault V, Lemort N, Dubourg O, Goossens M.** 2001. Human Connexin 32, a gap junction protein altered in the X-linked form of Charcot-Marie-Tooth disease, is directly regulated by the transcription factor SOX10. Human molecular genetics **10:**2783-2795.
107. **Houlden H, Girard M, Cockerell C, Ingram D, Wood NW, Goossens M, Walker RW, Reilly MM.** 2004. Connexin 32 promoter P2 mutations: a mechanism of peripheral nerve dysfunction. Annals of neurology **56:**730-734.
108. **Topilko P, Schneider-Maunoury S, Levi G, Baron-Van Evercooren A, Chennoufi AB, Seitanidou T, Babinet C, Charnay P.** 1994. Krox-20 controls myelination in the peripheral nervous system. Nature **371:**796-799.
109. **Warner LE, Mancias P, Butler IJ, McDonald CM, Keppen L, Koob KG, Lupski JR.** 1998. Mutations in the early growth response 2 (EGR2) gene are associated with hereditary myelinopathies. Nature genetics **18:**382-384.
110. **Magnaghi V, Ballabio M, Roglio I, Melcangi RC.** 2007. Progesterone derivatives increase expression of Krox-20 and Sox-10 in rat Schwann cells. Journal of molecular neuroscience **31:**149-157.
111. **Bremer M, Frob F, Kichko T, Reeh P, Tamm ER, Suter U, Wegner M.** 2011. Sox10 is required for Schwann-cell homeostasis and myelin maintenance in the adult peripheral nerve. Glia **59:**1022-1032.
112. **Sohl G, Degen J, Teubner B, Willecke K.** 1998. The murine gap junction gene connexin36 is highly expressed in mouse retina and regulated during brain development. FEBS letters **428:**27-31.
113. **Carystinos GD, Kandouz M, Alaoui-Jamali MA, Batist G.** 2003. Unexpected induction of the human connexin 43 promoter by the ras signaling pathway is mediated by a novel putative promoter sequence. Molecular pharmacology **63:**821-831.
114. **Baldridge D, Lecanda F, Shin CS, Stains J, Civitelli R.** 2001. Sequence and structure of the mouse connexin45 gene. Bioscience reports **21:**683-689.
115. **Anderson CL, Zundel MA, Werner R.** 2005. Variable promoter usage and alternative splicing in five mouse connexin genes. Genomics **85:**238-244.
116. **Jacob A, Beyer EC.** 2001. Mouse connexin 45: genomic cloning and exon usage. DNA and cell biology **20:**11-19.
117. **Teubner B, Odermatt B, Guldenagel M, Sohl G, Degen J, Bukauskas F, Kronengold J, Verselis VK, Jung YT, Kozak CA, Schilling K, Willecke K.** 2001.

Functional expression of the new gap junction gene connexin47 transcribed in mouse brain and spinal cord neurons. The Journal of neuroscience **21:**1117-1126.

118. **Schlierf B, Werner T, Glaser G, Wegner M.** 2006. Expression of connexin47 in oligodendrocytes is regulated by the Sox10 transcription factor. Journal of molecular biology **361:**11-21.
119. **Meyer E, Kurian MA, Morgan NV, McNeill A, Pasha S, Tee L, Younis R, Norman A, van der Knaap MS, Wassmer E, Trembath RC, Brueton L, Maher ER.** 2011. Promoter mutation is a common variant in GJC2-associated Pelizaeus-Merzbacher-like disease. Molecular genetics and metabolism **104:**637-643.
120. **Lye SJ, Nicholson BJ, Mascarenhas M, MacKenzie L, Petrocelli T.** 1993. Increased expression of connexin-43 in the rat myometrium during labor is associated with an increase in the plasma estrogen:progesterone ratio. Endocrinology **132:**2380-2386.
121. **MacKenzie LW, Cole WC, Garfield RE.** 1985. Structural and functional studies of myometrial gap junctions. Acta physiologica Hungarica **65:**461-472.
122. **Karasinski J, Galas J, Semik D, Fiertak A, Bilinska B, Kilarski WM.** 2010. Changes of connexin43 expression in non-pregnant porcine myometrium correlate with progesterone concentration during oestrous cycle. Reproduction in domestic animals **45:**959-966.
123. **Shughrue PJ, Scrimo PJ, Merchenthaler I.** 1998. Evidence for the colocalization of estrogen receptor-beta mRNA and estrogen receptor-alpha immunoreactivity in neurons of the rat forebrain. Endocrinology **139:**5267-5270.
124. **Shughrue PJ, Lane MV, Merchenthaler I.** 1997. Comparative distribution of estrogen receptor-alpha and -beta mRNA in the rat central nervous system. The Journal of comparative neurology **388:**507-525.
125. **Mitterling KL, Spencer JL, Dziedzic N, Shenoy S, McCarthy K, Waters EM, McEwen BS, Milner TA.** 2010. Cellular and subcellular localization of estrogen and progestin receptor immunoreactivities in the mouse hippocampus. The Journal of comparative neurology **518:**2729-2743.
126. **Pfaff D, Keiner M.** 1973. Atlas of estradiol-concentrating cells in the central nervous system of the female rat. The Journal of comparative neurology **151:**121-158.
127. **McLean AC, Valenzuela N, Fai S, Bennett SA.** 2012. Performing vaginal lavage, crystal violet staining, and vaginal cytological evaluation for mouse estrous cycle staging identification. Journal of visualized experiments**:**e4389.
128. **Filippov MA, Hormuzdi SG, Fuchs EC, Monyer H.** 2003. A reporter allele for investigating connexin 26 gene expression in the mouse brain. The European journal of neuroscience **18:**3183-3192.
129. **Nagy JI, Li X, Rempel J, Stelmack G, Patel D, Staines WA, Yasumura T, Rash JE.** 2001. Connexin26 in adult rodent central nervous system: demonstration at astrocytic gap junctions and colocalization with connexin30 and connexin43. The Journal of comparative neurology **441:**302-323.
130. **Sohl G, Maxeiner S, Willecke K.** 2005. Expression and functions of neuronal gap junctions. Nature reviews. Neuroscience **6:**191-200.
131. **Goodenough DA, Paul DL.** 2003. Beyond the gap: functions of unpaired connexon channels. Nature reviews. Molecular cell biology **4:**285-294.

132. **Bruzzone R, White TW, Paul DL.** 1996. Connections with connexins: the molecular basis of direct intercellular signaling. European journal of biochemistry / FEBS **238:**1-27.
133. **Paul DL.** 1986. Molecular cloning of cDNA for rat liver gap junction protein. The Journal of cell biology **103:**123-134.
134. **Goodenough DA, Paul DL, Jesaitis L.** 1988. Topological distribution of two connexin32 antigenic sites in intact and split rodent hepatocyte gap junctions. The Journal of cell biology **107:**1817-1824.
135. **Hertzberg EL.** 1985. Antibody probes in the study of gap junctional communication. Annual review of physiology **47:**305-318.
136. **Traub O, Janssen-Timmen U, Druge PM, Dermietzel R, Willecke K.** 1982. Immunological properties of gap junction protein from mouse liver. Journal of cellular biochemistry **19:**27-44.
137. **Altevogt BM, Kleopa KA, Postma FR, Scherer SS, Paul DL.** 2002. Connexin29 is uniquely distributed within myelinating glial cells of the central and peripheral nervous systems. The Journal of neuroscience **22:**6458-6470.
138. **Dermietzel R, Farooq M, Kessler JA, Althaus H, Hertzberg EL, Spray DC.** 1997. Oligodendrocytes express gap junction proteins connexin32 and connexin45. Glia **20:**101-114.
139. **Li J, Hertzberg EL, Nagy JI.** 1997. Connexin32 in oligodendrocytes and association with myelinated fibers in mouse and rat brain. The Journal of comparative neurology **379:**571-591.
140. **Nagy JI, Ionescu AV, Lynn BD, Rash JE.** 2003. Connexin29 and connexin32 at oligodendrocyte and astrocyte gap junctions and in myelin of the mouse central nervous system. The Journal of comparative neurology **464:**356-370.
141. **Nagy JI, Ionescu AV, Lynn BD, Rash JE.** 2003. Coupling of astrocyte connexins Cx26, Cx30, Cx43 to oligodendrocyte Cx29, Cx32, Cx47: Implications from normal and connexin32 knockout mice. Glia **44:**205-218.
142. **Traub O, Willecke K.** 1982. Cross reaction of antibodies against liver gap junction protein (26K) with lens fiber junction protein (MIP) suggests structural homology between these tissue specific gene products. Biochemical and biophysical research communications **109:**895-901.
143. **Nagy JI, Dudek FE, Rash JE.** 2004. Update on connexins and gap junctions in neurons and glia in the mammalian nervous system. Brain research. Brain research reviews **47:**191-215.
144. **Teubner B, Michel V, Pesch J, Lautermann J, Cohen-Salmon M, Sohl G, Jahnke K, Winterhager E, Herberhold C, Hardelin JP, Petit C, Willecke K.** 2003. Connexin30 (Gjb6)-deficiency causes severe hearing impairment and lack of endocochlear potential. Human molecular genetics **12:**13-21.
145. **Luque-Garcia JL, Zhou G, Spellman DS, Sun TT, Neubert TA.** 2008. Analysis of electroblotted proteins by mass spectrometry: protein identification after Western blotting. Molecular & cellular proteomics **7:**308-314.
146. **Lambert JP, Mitchell L, Rudner A, Baetz K, Figeys D.** 2009. A novel proteomics approach for the discovery of chromatin-associated protein networks. Molecular & cellular proteomics **8:**870-882.

147. **Hopp TP, Woods KR.** 1981. Prediction of protein antigenic determinants from amino acid sequences. Proceedings of the National Academy of Sciences of the United States of America **78:**3824-3828.
148. **Kolaskar AS, Tongaonkar PC.** 1990. A semi-empirical method for prediction of antigenic determinants on protein antigens. FEBS letters **276:**172-174.
149. **Kyte J, Doolittle RF.** 1982. A simple method for displaying the hydropathic character of a protein. Journal of molecular biology **157:**105-132.
150. **Felicio LS, Nelson JF, Finch CE.** 1984. Longitudinal studies of estrous cyclicity in aging C57BL/6J mice: II. Cessation of cyclicity and the duration of persistent vaginal cornification. Biology of reproduction **31:**446-453.
151. **Walmer DK, Wrona MA, Hughes CL, Nelson KG.** 1992. Lactoferrin expression in the mouse reproductive tract during the natural estrous cycle: correlation with circulating estradiol and progesterone. Endocrinology **131:**1458-1466.
152. **Parkening TA, Collins TJ, Smith ER.** 1982. Plasma and pituitary concentrations of LH, FSH, and prolactin in aging C57BL/6 mice at various times of the estrous cycle. Neurobiology of aging **3:**31-35.
153. **Adler NT, Resko JA, Goy RW.** 1970. The effect of copulatory behavior on hormonal change in the female rat prior to implantation. Physiology & behavior **5:**1003-1007.
154. **Adler NT, Zoloth SR.** 1970. Copulatory behavior can inhibit pregnancy in female rats. Science **168:**1480-1482.
155. **Yang JJ, Larsen CM, Grattan DR, Erskine MS.** 2009. Mating-induced neuroendocrine responses during pseudopregnancy in the female mouse. Journal of neuroendocrinology **21:**30-39.
156. **Hawkins SM, Matzuk MM.** 2008. The menstrual cycle: basic biology. Annals of the New York Academy of Sciences **1135:**10-18.
157. **Rajendren G, Gibson MJ.** 2001. A confocal microscopic study of synaptic inputs to gonadotropin-releasing hormone cells in mouse brain: regional differences and enhancement by estrogen. Neuroendocrinology **73:**84-90.
158. **Sarkar DK, Chiappa SA, Fink G, Sherwood NM.** 1976. Gonadotropin-releasing hormone surge in pro-oestrous rats. Nature **264:**461-463.
159. **Kumar TR, Wang Y, Lu N, Matzuk MM.** 1997. Follicle stimulating hormone is required for ovarian follicle maturation but not male fertility. Nature genetics **15:**201-204.
160. **Montgomery V, Loutradis D, Tulchinsky D, Kiessling A.** 1988. FSH-induced ovulation in intact and hypophysectomized mice. Journal of reproduction and fertility **84:**1-6.
161. **Mihm M, Gangooly S, Muttukrishna S.** 2011. The normal menstrual cycle in women. Animal reproduction science **124:**229-236.
162. **Appelgren LE.** 1969. Histochemical demonstration of drug interference with progesterone synthesis. Journal of reproduction and fertility **19:**185-186.
163. **Sander VA, Facorro GB, Piehl L, Rubin de Celis E, Motta AB.** 2009. Effect of DHEA and metformin on corpus luteum in mice. Reproduction **138:**571-579.
164. **Rudolph M, Docke WD, Muller A, Menning A, Rose L, Zollner TM, Gashaw I.** 2012. Induction of overt menstruation in intact mice. PloS ONE **7:**e32922.

165. **Stocco C, Telleria C, Gibori G.** 2007. The molecular control of corpus luteum formation, function, and regression. Endocrine reviews **28:**117-149.
166. **Hong H, Yen HY, Brockmeyer A, Liu Y, Chodankar R, Pike MC, Stanczyk FZ, Maxson R, Dubeau L.** 2010. Changes in the mouse estrus cycle in response to BRCA1 inactivation suggest a potential link between risk factors for familial and sporadic ovarian cancer. Cancer research **70:**221-228.
167. **Yano J, Lilly E, Barousse M, Fidel PL, Jr.** 2010. Epithelial cell-derived S100 calcium-binding proteins as key mediators in the hallmark acute neutrophil response during Candida vaginitis. Infection and immunity **78:**5126-5137.
168. **Whitten WK.** 1959. Occurrence of anoestrus in mice caged in groups. The Journal of endocrinology **18:**102-107.
169. **Lamond DR.** 1959. Effect of stimulation derived from other animals of the same species on oestrous cycles in mice. The Journal of endocrinology **18:**343-349.
170. **Nelson JF, Felicio LS, Randall PK, Sims C, Finch CE.** 1982. A longitudinal study of estrous cyclicity in aging C57BL/6J mice: I. Cycle frequency, length and vaginal cytology. Biology of reproduction **27:**327-339.
171. **Van Der Lee S, Boot LM.** 1955. Spontaneous pseudopregnancy in mice. Acta physiologica et pharmacologica Neerlandica **4:**442-444.
172. **Van Der Lee S, Boot LM.** 1956. Spontaneous pseudopregnancy in mice. II. Acta physiologica et pharmacologica Neerlandica **5:**213-215.
173. **Armaiz-Pena GN, Mangala LS, Spannuth WA, Lin YG, Jennings NB, Nick AM, Langley RR, Schmandt R, Lutgendorf SK, Cole SW, Sood AK.** 2009. Estrous cycle modulates ovarian carcinoma growth. Clinical cancer research **15:**2971-2978.
174. **Jemiolo B, Harvey S, Novotny M.** 1986. Promotion of the Whitten effect in female mice by synthetic analogs of male urinary constituents. Proceedings of the National Academy of Sciences of the United States of America **83:**4576-4579.
175. **Weiss S, Dunne C, Hewson J, Wohl C, Wheatley M, Peterson AC, Reynolds BA.** 1996. Multipotent CNS stem cells are present in the adult mammalian spinal cord and ventricular neuroaxis. The Journal of neuroscience **16:**7599-7609.
176. **Russo RE, Reali C, Radmilovich M, Fernandez A, Trujillo-Cenoz O.** 2008. Connexin 43 delimits functional domains of neurogenic precursors in the spinal cord. The Journal of neuroscience **28:**3298-3309.
177. **Garcia G, Libisch G, Trujillo-Cenoz O, Robello C, Russo RE.** 2012. Modulation of gene expression during early stages of reconnection of the turtle spinal cord. Journal of neurochemistry **121:**996-1006.
178. **Rozental R, Srinivas M, Gokhan S, Urban M, Dermietzel R, Kessler JA, Spray DC, Mehler MF.** 2000. Temporal expression of neuronal connexins during hippocampal ontogeny. Brain research. Brain research reviews **32:**57-71.
179. **Deans MR, Gibson JR, Sellitto C, Connors BW, Paul DL.** 2001. Synchronous activity of inhibitory networks in neocortex requires electrical synapses containing connexin36. Neuron **31:**477-485.
180. **Nishii K, Kumai M, Egashira K, Miwa T, Hashizume K, Miyano Y, Shibata Y.** 2003. Mice lacking connexin45 conditionally in cardiac myocytes display embryonic lethality similar to that of germline knockout mice without endocardial cushion defect. Cell communication & adhesion **10:**365-369.

181. **Liao Y, Day KH, Damon DN, Duling BR.** 2001. Endothelial cell-specific knockout of connexin 43 causes hypotension and bradycardia in mice. Proceedings of the National Academy of Sciences of the United States of America **98:**9989-9994.
182. **Berube NG, Mangelsdorf M, Jagla M, Vanderluit J, Garrick D, Gibbons RJ, Higgs DR, Slack RS, Picketts DJ.** 2005. The chromatin-remodeling protein ATRX is critical for neuronal survival during corticogenesis. The Journal of clinical investigation **115:**258-267.
183. **Santin AP, Souza AF, Brum LS, Furlanetto TW.** 2013. Validation of Reference Genes for Normalizing Gene Expression in Real-Time Quantitative Reverse Transcription PCR in Human Thyroid Cells in Primary Culture Treated with Progesterone and Estradiol. Molecular biotechnology **54:**278-282.
184. **Schroder AL, Pelch KE, Nagel SC.** 2009. Estrogen modulates expression of putative housekeeping genes in the mouse uterus. Endocrine **35:**211-219.
185. **Lee MS, Zhu YL, Sun Z, Rhee H, Jeromin A, Roder J, Dannies PS.** 2000. Accumulation of synaptosomal-associated protein of 25 kDa (SNAP-25) and other proteins associated with the secretory pathway in GH4C1 cells upon treatment with estradiol, insulin, and epidermal growth factor. Endocrinology **141:**3485-3492.
186. **Xie N, Liu L, Li Y, Yu C, Lam S, Shynlova O, Gleave M, Challis JR, Lye S, Dong X.** 2012. Expression and function of myometrial PSF suggest a role in progesterone withdrawal and the initiation of labor. Molecular endocrinology **26:**1370-1379.
187. **Ogawa T, Hayashi T, Tokunou M, Nakachi K, Trosko JE, Chang CC, Yorioka N.** 2005. Suberoylanilide hydroxamic acid enhances gap junctional intercellular communication via acetylation of histone containing connexin 43 gene locus. Cancer research **65:**9771-9778.
188. **Hohl M, Thiel G.** 2005. Cell type-specific regulation of RE-1 silencing transcription factor (REST) target genes. The European journal of neuroscience **22:**2216-2230.
189. **Hernandez M, Shao Q, Yang XJ, Luh SP, Kandouz M, Batist G, Laird DW, Alaoui-Jamali MA.** 2006. A histone deacetylation-dependent mechanism for transcriptional repression of the gap junction gene cx43 in prostate cancer cells. The Prostate **66:**1151-1161.
190. **Vinken M, De Rop E, Decrock E, De Vuyst E, Leybaert L, Vanhaecke T, Rogiers V.** 2009. Epigenetic regulation of gap junctional intercellular communication: more than a way to keep cells quiet? Biochimica et biophysica acta **1795:**53-61.
191. **Chen JT, Cheng YW, Chou MC, Sen-Lin T, Lai WW, Ho WL, Lee H.** 2003. The correlation between aberrant connexin 43 mRNA expression induced by promoter methylation and nodal micrometastasis in non-small cell lung cancer. Clinical cancer research **9:**4200-4204.
192. **Jovicic A, Roshan R, Moisoi N, Pradervand S, Moser R, Pillai B, Luthi-Carter R.** 2013. Comprehensive Expression Analyses of Neural Cell-Type-Specific miRNAs Identify New Determinants of the Specification and Maintenance of Neuronal Phenotypes. The Journal of neuroscience **33:**5127-5137.
193. **Monks DA, Arciszewska G, Watson NV.** 2001. Estrogen-inducible progesterone receptors in the rat lumbar spinal cord: regulation by ovarian steroids and fluctuation across the estrous cycle. Hormones and behavior **40:**490-496.

194. **Williams SJ, Chung K, Om AS, Papka RE.** 1997. Cytosolic estrogen receptor concentrations in the lumbosacral spinal cord fluctuate during the estrous cycle. Life sciences **61:**2551-2559.
195. **Butcher RL, Collins WE, Fugo NW.** 1974. Plasma concentration of LH, FSH, prolactin, progesterone and estradiol-17beta throughout the 4-day estrous cycle of the rat. Endocrinology **94:**1704-1708.
196. **Wu CH, Yang JG, Yang JJ, Lin YM, Tsai HD, Lin CY, Kuo PL.** 2010. Androgen excess down-regulates connexin43 in a human granulosa cell line. Fertility and sterility **94:**2938-2941.
197. **Fowler SL, McLean AC, Bennett SA.** 2009. Tissue-specific cross-reactivity of connexin32 antibodies: problems and solutions unique to the central nervous system. Cell communication & adhesion **16:**117-130.
198. **Acs P, Kipp M, Norkute A, Johann S, Clarner T, Braun A, Berente Z, Komoly S, Beyer C.** 2009. 17beta-estradiol and progesterone prevent cuprizone provoked demyelination of corpus callosum in male mice. Glia **57:**807-814.
199. **Taylor LC, Puranam K, Gilmore W, Ting JP, Matsushima GK.** 2010. 17beta-estradiol protects male mice from cuprizone-induced demyelination and oligodendrocyte loss. Neurobiology of disease **39:**127-137.
200. **Hu X, Qin X.** 2013. Lentivirus-mediated estrogen receptor alpha overexpression in the central nervous system ameliorates experimental autoimmune encephalomyelitis in mice. International journal of molecular medicine **31:**1209-1221.
201. **Tremblay GB, Tremblay A, Copeland NG, Gilbert DJ, Jenkins NA, Labrie F, Giguere V.** 1997. Cloning, chromosomal localization, and functional analysis of the murine estrogen receptor beta. Molecular endocrinology **11:**353-365.
202. **Paech K, Webb P, Kuiper GG, Nilsson S, Gustafsson J, Kushner PJ, Scanlan TS.** 1997. Differential ligand activation of estrogen receptors ERalpha and ERbeta at AP1 sites. Science **277:**1508-1510.
203. **Mitra S, Annamalai L, Chakraborty S, Johnson K, Song XH, Batra SK, Mehta PP.** 2006. Androgen-regulated formation and degradation of gap junctions in androgen-responsive human prostate cancer cells. Molecular biology of the cell **17:**5400-5416.
204. **Musil LS, Le AC, VanSlyke JK, Roberts LM.** 2000. Regulation of connexin degradation as a mechanism to increase gap junction assembly and function. The Journal of biological chemistry **275:**25207-25215.

Ashleigh McLean

Education

M.Sc. candidate, Neuroscience, Medicine, University of Ottawa, Ottawa, ON 2007-2013
Supervisor: Dr. Steffany Bennett (Neural Regeneration Laboratory)
Thesis: Examining the regulation of connexin expression over the course of the estrous cycle in hippocampus and spinal cord

B.Sc. (Hon. Genetics), The University of Western Ontario, London, ON 2005

OAC High School Diploma, St. Mary's College, Sault Ste. Marie, ON 2001

Work Experience

Teaching Assistant, Anatomy and Physiology (ANP1105)
University of Ottawa, Ottawa, ON 2009-2012
Course coordinator: Dr. Joanna Komoroski

Teaching Assistant, Introduction to Biochemistry (BCH2333)
University of Ottawa, Ottawa, ON 2008-2013
Course coordinator: Dr. Vasek Mezl

Supervisor of undergraduate summer, co-op and honours research students,
Neural Regeneration Laboratory, University of Ottawa, Ottawa, ON 2005-2013

Laboratory Manager, Neural Regeneration Laboratory,
University of Ottawa, Ottawa, ON 2005-2007

Travel Awards

Multiple Sclerosis Society of Canada	2010
Canadian Association for Neuroscience	2009
CIHR Institute of Gender and Health	2009
International Gap Junction Conference	2009
CIHR Training Program in Neurodegenerative Lipidomics	2009

Student Awards

Canadian Institutes Health Research Doctoral Award	2010-2013
Multiple Sclerosis Society of Canada Studentship Award	2010
Ontario Graduate Scholarship	2010
University of Ottawa Excellence Scholarship	2009-2013
Scottish Rite Charitable Foundation Scholarship	2009-2010
Government of Ontario Graduate Scholarship in Science and Technology	2009

Relevant Skills

Molecular Biology: RNA & DNA isolation, primer construction and cloning, agarose gel electrophoresis, PCR, RT-PCR, real-time quantitative RT-PCR

Protein Biochemistry: protein isolation, immunoblotting, immunoprecipation, ELISA, enzyme assays, immunohistochemistry

Lipid Biochemistry: Bligh & Dyer lipid extraction, 2D TLC, HPTLC, ESI-LC/MS/MS

Culture work: Bacterial, yeast, tissue (HeLa, NT2/hNT, PC12, cerebellar granule neurons, Oli-*neu*)

Microscopy: Light, immunofluorescence, confocal

Animal work: mouse handling, breeding, colony maintenance, genetic profiling (PCR), tissue dissection and microdissection (whole brain, hippocampus, various cortices, cerebellum, striatum, spinal cord, dorsal root ganglia, sciatic nerve), surgeries (ovariectomization, laminectomies, spinal cord injury), experimental autoimmune encephalomyelitis (EAE) induction, behavioural analysis (Morris Water Maze, Basso Mouse Scale following spinal cord injury, clinical scoring following EAE)

Computer: Word processing, EXCEL, PPT, Prism, Adobe Photoshop, Image J, Pubmed, BLAST.

Leadership: Exceptional communication, organizational, public speaking and mentoring skills.

Publications

McLean, AC, Valenzuela N, Fai S, and Bennett, SAL (2012). Performing Vaginal Lavage, Crystal Violet Staining, and Vaginal Cytological Evaluation for Mouse Estrous Cycle Staging Identification. The Journal of Visualized Experiments 67, e4389, DOI: 10.3791/4389.

Fowler, SL*, **McLean, AC*** and Bennett, SAL (2009). Tissue-specific cross-reactivity of connexin32 antibodies: problems and solutions unique to the central nervous system. Cell Communication & Adhesion 16, 117-130.
***both authors contributed equally**

Graham K, Syrett A, Trickey B, Valenzuela, N, **McLean A**, Bartlett R, Akins M, Fai S, Bennett SAL (2013) Three Dimensional Volumetric Reconstruction of the C57BL/6 Mouse Brain. [Weblog entry.] CIHR Training Program in Neurodegenerative Lipidomics, Resource Animations, University of Ottawa, 4 Feb 2013.

Abstracts/Conference Proceedings

McLean AC, Haykal S, Bennett SAL (2012) Connexin32 expression is under hormonal control in the adult female central nervous system. Neuroscience 2012 (New Orleans, USA, poster presentation by A.C. McLean).

Taylor GP, Cooke DM, **McLean AC**, Cieniak C, Foster BC, Arnason JT, Bennett, SAL (2012) Identification of housekeeping gene calibrators for real-time quantitative reverse transcription PCR (qRT-PCR) analysis of gene expression during neurogenesis and gliogenesis. Neuroscience 2012 (New Orleans, USA, poster presentation by G. Taylor).

McLean AC, Berard J, David S, Bennett SAL (2011) Connexin32 protein expression is dysregulated during EAE progression. Ottawa Institute Systems Biology Annual Symposium 2011 (Montebello QC, poster presentation by AC McLean).

McLean AC, Berard J, Kamboj S, Kroner-Milsch A, David S, Bennett SAL (2010) Connexin32 protein expression is dysregulated during EAE progression. EndMS Conference 2010 (Whistler BC, poster presentation by AC McLean)

Juzwik CA, **McLean AC**, Cieniak C, Ahmed F, Blanchard AP, Harbilas D, Brault A, Haddad P, Figeys D, Bennett SAL (2010) Validating the impact of Cree med icine on the glycerophosphocholine lipidome in peripheral diabetic neuropathy. Neurolipidomics 2010 (Ottawa ON, oral presentation by CA Juzwik and C Cieniak)

McLean AC, David S, Bennett SAL (2010) Examining the role of Cx32 in the regulation of myelin specific lipid levels following spinal cord injury. Neurolipidomics 2010 (Ottawa ON, poster presentation by AC McLean)

McLean AC, Fowler SL, Redensek A, Lopez-Vales R, David S, Bennett SAL Glial connexin expression (2010) is dysregulated following spinal cord injury. Brain Health Research Day 2010 (Ottawa ON, poster presentation by AC McLean).

McLean AC, Fowler S, Bennett SAL (2009) Connexin32 expression is under hormonal control in the adult female mouse spinal cord. International Gap Junction Conference 2009 (Sedona AZ, poster presentation by AC McLean)

McLean AC, Fowler SL, Redensek A, Lopez-Vales R, David S, Bennett SAL (2009) Glial connexin expression is dysregulated following spinal cord injury. Canadian Association for Neuroscience Annual Meeting 2009 (Vancouver BC, poster presentation by AC McLean)

McLean AC, Redensek A, Lopez-Vales R, David S, Bennett SAL (2009) Glial Connexin expression is dysregulated following spinal cord injury. Ottawa Institute of Systems Biology Annual Symposium 2009 (Ottawa ON, poster presentation by AC McLean)

McLean AC, Fowler SL, Bennett SAL (2008) Connexin32 expression is under hormonal control in the adult female mouse spinal cord. Neuroscience 2008 (Washington D.C., poster presentation by AC McLean)

McLean AC, Fowler SL, Haykal S, Hebb ALO, Bennett SAL (2008) Connexin32 expression is under hormonal control in the adult female central nervous system. Canadian Association for Neuroscience 2008 (Montreal QC, poster presentation by AC McLean)

McLean AC, Fowler SL, Haykal S, Hebb ALO, Bennett SAL (2007) Gender specific expression of connexin 32 in the murine hippocampus. Neuroscience 2007 (San Diego CA, poster presentation by AC McLean)

Seminar Presentations

Promoting remyelination following spinal cord injury by altering connexin expression. *Department of Biochemistry, Microbiology and Immunology Work In Progress, University of Ottawa, 2009.*

Determining the role of connexin expression in the regulation of demyelination following spinal cord injury. *Department of Cellular and Molecular Medicine, Neuroscience Seminar Day, University of Ottawa, 2008.*

Scientific Memberships

Society for Neuroscience	2007-2013
Canadian Association for Neuroscience	2007-2013
Ottawa Institute of Systems Biology	2009-2013

References

Available upon request